MODELING AND ANALYSIS OF A SEMI-ACTIVE MAGNETO-RHEOLOGICAL DAMPER SUSPENSION SEAT AND CONTROLLER SYNTHESIS

Xiaoxi Huang

A Thesis

in the

Department

of

Mechanical and Industrial Engineering

Presented in Partial Fulfillment of the Requirements

For the Degree of Master of Applied Science at

Concordia University

Montreal, Quebec, Canada

September 2009

Your file Votre référence
ISBN: 978-0-494-63152-2
Our file Notre référence
ISBN: 978-0-494-63152-2

ABSTRACT

Whole body vibration in operational vehicles can cause serious musculo-skeletal disorders among the exposed workers. Consequently, considerable efforts have been made to protect vehicle operators from potentially harmful vibration. This thesis was aimed at the development of a semi-active suspension seat equipped with a magneto-rheological (MR) fluid damper. A damper controller was synthesized to minimize the vibration transmitted to the seated body and the frequency of end-stop impacts, which is known to induce high intensity vibration or shock motions to the seated occupant. A suspension seat was modeled by considering the kinematic non-linearity due to the cross-linkages and the damper link, while the cushion characteristics were linearized about the operating preload. The force-velocity properties of the MR damper were modeled by piecewise polynomial functions of applied current on the basis of the laboratory-measured data. The kineto-dynamic model of the suspension seat was thoroughly validated using the laboratory-measured responses under harmonic excitations in the *0.5 to 10Hz* range. The performance characteristics of the passive suspension seat model were evaluated under different vehicular excitations in terms of frequency-weighted *rms* acceleration, vibration dose value (VDV), seat effective amplitude transmissibility (SEAT) and VDV ratio. These performance characteristics are also evaluated under amplified vehicular excitations in order to investigate the frequency as well as the potential suppression of end-stop impacts.

The controller synthesis was realized in two stages: (1) attenuation of continuous vibration; and (2) suppression of end-stop impacts. Two different algorithms were explored in the first stage synthesis, which included a sky-hook control algorithm and a relative states feedback control algorithm. Each algorithm was further utilized in two different control current modulations. The performance potentials of each control synthesis were investigated using the

MATLAB Simulink platform under harmonic, transient, and random vehicular excitations in terms of SEAT and VDV ratio. One controller design (overall best suited for implementations) was subsequently implemented in a hardware-in-the-loop (HIL) test platform coupled with a MR-fluid damper mounted on an electro-hydraulic actuator that was linked to the HIL simulation platform. The semi-active suspension seat performance characteristics were further evaluated under different excitations using the selected control scheme. The results showed that the selected control scheme yielded SEAT and VDV ratio reductions in the *5* to *30%* range depending upon the nature of excitations. The implementation of the second-stage controller, which was tested only by simulations, entirely eliminated the occurrence of end-stop impacts at nominal vibration level and attenuated the end-stop impact severity of three times amplified excitations by up to *10%*. The results further suggested that the use of MR-fluid damper in suspension seat was most beneficial to city buses and class 1 earth moving vehicles amongst the selected inputs.

TABLE OF CONTENTS

LIST OF FIGURES

LIST OF TABLES

NOMENCLATURES

a,b,c,d	Suspension model parameters
A,B,C	MR damper third-order pre-yield model parameters
a_1,a_2,a_3	Cushion stiffness parameters
a_b,a_c	RMS accelerations of the base and cushion
α,β,γ	Suspension linkage angles
$A_{mi},B_{mi},C_{mi},D_{mi},K_m$	Vehicle excitation transfer function parameters
b_1,b_2	Cushion damping parameters
β_h,β_l	Post-yield and pre-yield damping rate
a_{wb},a_{wc}	Frequency-weighted RMS accelerations of the base and cushion
C_0,C_1	Suspension stiffness function parameters
C_c	Linear model equivalent cushion damping coefficient
C_{c1}	Passive damper damping coefficient
CF	Crest factor
d_c,d_e	End-stops impact deflections
η	Second stage controller preset limit ratio
f_3	Third order polynomial damper force
$F_A,F_B,F_C,F_D...$	Forces applied to the suspension linkage
F_b	End-stop forces
F_c	Total forces applied to the cushion mass without gravity

F'_c	Total forces applied to the cushion mass with gravity
F_d	Equivalent damper force
F_{damp}	MR damper force
F_{dampp}	Passive damper force
F_f	Friction force
F_s	Forces applied to the suspension mass without gravity
F'_s	Forces applied to the suspension mass with gravity
F_{sat}	Coulomb friction magnitude at saturation
γ_c	Passive damper post-yield to pre-yield damper coefficient ratio
γ_{c1}	Passive damper transition velocity
γ_h, γ_l	Post-yield and pre-yield rate of damping rate
δ_h, δ_l	Post-yield and pre-yield damping rate at 0 current
G	Controller proportional gain
$G(s)$	Vehicle excitation transfer function
h	Suspension instantaneous height
$h_{\max}, h_{\min}$	Suspension maximum and minimum height
h_c, h_e	End-stops transition deflections
i	Damper control current
k_c, C_{eq}	Cushion stiffness (N/mm) and damping (Ns/mm)
K_c	Linear model equivalent cushion stiffness
K_s	Linear model suspension stiffness

k_{c1}, k_{c2}	Bottom end-stop stiffness coefficients
k_{e1}, k_{e2}	Bottom end-stop stiffness coefficients
L	Suspension main linkage length
L_1, L_2, L_3	Suspension linkages lengths
L_{damp}	Instantaneous damper length
M_c	Current modulator
m_c, m_s	Apparent cushion and occupant mass, and suspension mass
p	Passive damper extension to compression damper coefficient ratio
SEAT, SEATw	seat effective acceleration transmissibility, frequency weighted
V_{damp}	Damper velocity
VDV, VDVw	vibration dose value, frequency weighted
VDVR, VDVrw	vibration dose value ratio, frequency weighted
v_f, v'_f	Nominal and altered transition velocity of the friction force function
v_t	Magneto-rheological damper transition velocity
v'_t	Altered magneto-rheological damper transition velocity
W_p	Cushion Preload
$x_b, \dot{x}_b, \ddot{x}_b$	Seat base displacement, velocity, acceleration
$x_c, \dot{x}_c, \ddot{x}_c$	Cushion mass absolute displacement, velocity, acceleration
$x_s, \dot{x}_s, \ddot{x}_s$	Suspension mass absolute displacement, velocity, acceleration
$\ddot{x}_{wb}, \ddot{x}_{wc}$	Frequency weighted acceleration of the base and cushion
$y_c, \dot{y}_c, \ddot{y}_c$	Cushion mass displacement, velocity, acceleration relative to base

$y_s, \dot{y}_s, \ddot{y}_s$	Suspension mass displacement, velocity, acceleration relative to base
Y_c	Cushion deflection (mm)
z_c	Current modulator switching function
ζ_c	Current modulator level

CHAPTER 1: INTRODUCTION AND LITERATURE REVIEW

1.1 Introduction

Whole-body vibration (WBV) and shock exposure are well known sources of discomfort, fatigue, and health disorders amongst occupational drivers. Many studies have shown an association between the drivers' exposure to WBV and its adverse effects on their musculo-skeletal, nervous, circulatory and digestive systems [1,2,3,4,5]. WBV and shocks in road and off-road vehicles arise from interactions of the vehicles tires or tracks with the terrain roughness [1,6]. The motions are subsequently transferred to the driver depending on several factors such as driving speed, vehicle load, vehicle suspension, vehicle size, seat type, tire pressure, and terrain unevenness.

The majority of the studies on driver's exposure to WBV and vibration control have been mostly directed to off-road vehicles (agricultural, mining, earth-moving, and forestry vehicles) and heavy road vehicles (trucks and buses) [1,7,8,9,10]. In an attempt to reduce the potential health and safety risks posed by exposure to WBV and shocks, several suspension system designs have been introduced to the chassis, cab, and the seat. The chassis suspension are designed to achieve a balance between conflicting measures, mainly satisfactory ride, road-holding, roll stability, and handling, with relative greater weighting imposed on the roll and directional stability measures. The suspension seat thus plays a vital role in WBV and shocks attenuation along the vertical axis, while proving comfortable and stable sitting posture.

The vibration attenuation performance characteristics of low natural frequency suspensions seats vary with the vertical vibration environment of the target vehicle [3,11,12,13]. The limited travel of such soft suspension seats causes end-stop impacts on relatively rough terrains or roads

with substantial discontinuities (e.g. potholes), which result in shock motions transferred to the occupant. Studies have shown that shock prevention or attenuation of high intensity vibration can be achieved with high suspension damping, while the effective attenuation of continuous road-induced vibration requires low suspension damping [8].

In order to enhance the suspension performance in attenuating both continuous vibration and shock motions, several variable damping concepts based upon semi-active and active control have been investigated over the past four decades. The implementations of such suspensions, however, have been severely limited due to hardware complexities, and high power demand [14,15,16,17,18]. The electro-rheological (ER) and magneto-rheological (MR) fluid dampers have been considered attractive alternatives for such applications due to their rapid response and low power requirements [19,20]. While an ER damper requires high operating voltage, the MR damper requires only small current (generally up to *2A*) at voltages ranging from *12* to *24V*. A suspension seat with an MR damper may thus be considered attractive for achieving simultaneous shock and vibration attenuation. The controller design, however, forms the most important task for extracting the full potential of a MR damper, which is a challenging task since the MR damper is highly non-linear and current switching tends to cause discontinuities in the damping force.

A number of semi-active control schemes have been proposed to achieve variable MR damping for enhanced vibration isolation or prevention of end-stop impacts in suspension seats. These include the skyhook control (with and without hysteresis), sliding-mode control, clipped semi-active control, and relative position control [21,22,23,24,25]. The practical implementations of majority of these controllers however have not been demonstrated for suspension seats due to sensor implementation difficulties and costs. Nevertheless, a few

laboratory-based studies have shown high merits of the semi-actively controlled MR dampers in suspension seats.

This dissertation research focuses on the design and development of a simple and practically implementable controller to achieve variable damping properties of a MR damper for applications in suspension seats. To accomplish the design, a MR damper model based on the bi-viscous damper model is proposed and validated. A suspension seat model comprising the cross linkage dynamics is developed and validated. Different control algorithms and current modulators are synthesized to achieve control of vibration and suppression end-stop impacts. Finally, the performance characteristics of the MR suspension seat are investigated through simulations and the hardware-in-the-loop test technique.

1.2 Review of Relevant Literature

The design of a MR damper controller for suspension seat applications requires adequate knowledge in suspension seat dynamics and modeling, damper modeling and characterization, vibration analysis, semi-active controller synthesis, characterization of vehicular vibration and shock, etc. The relevant reported studies are thus reviewed to build adequate knowledge in order to formulate the scope of the dissertation research.

1.2.1 Effects of Whole-Body Vibration (WBV) and Shocks

Occupational drivers of heavy road vehicles and off-road vehicles may be exposed to severe level of vibration and shocks caused by vehicle interactions with the terrain irregularities [1,6,9,10,26]. The severity of shocks and vibration transmitted to the seated occupant is of primary concern in many off-road vehicles employed in agriculture, construction, forestry, and mining sectors. The human body is known to be most sensitive to vertical vibration around its

fundamental resonance in the *4* to *5* Hz range [1]. The suspension seats are thus usually designed with low natural frequency in the *1.25* to *1.5Hz* range to achieve effective vibration isolation [2,8,12]. Such low frequency suspension seats yield large relative motions of the seated occupant with respect to the cab floor, particularly under high intensity vehicle vibration or when the primary suspension natural frequency lies in the vicinity of seat suspension natural frequency [27]. A city bus, with vertical mode sprung mass resonance near *1.4Hz*, is one example of the latter situation. The suspension seats are thus invariably designed with travel limiters to limit the driver motion with respect to the cabin floor or the chassis. Repeated impacts against the travel limiters (end-stops) result in shock motions.

Extended exposure to high magnitude vibration and repeated shocks of low frequency has been associated with disorders of the spine and the supporting musculo-skeletal structure [1,3,4]. Simultaneously, driver's comfort and working efficiency are deteriorated under exposure to such vehicular vibration and shocks [1,2,3,4,6]. In general, the increase in spinal injuries and lower back pain due to WBV are directly associated with three primary factors: the vibration intensity, the duration, and awkward sitting postures [1]. High magnitudes of shock motions, for example in truck accidents, can cause compressive fracture of the spine, while chronic exposures to lower level shock motions can lead to disc degeneration and lower back pain [28,29]. Furthermore, increased levels of fatigue were reported by drivers experiencing frequent impacts against the end-stops of the suspension seat [28,30], which can also cause the driver to temporarily lose control of the vehicle, leading to further safety risks.

1.2.2 Control of Whole-Body Vibration and Shock

Health and safety risks posed by occupational exposure to WBV can be reduced by decreasing the magnitudes of vibration transmitted to the seated occupant [8,31]. Considerable

efforts have thus been made in development of primary wheel suspensions and secondary suspensions at the cabin or the seat. While low natural frequency primary suspensions have been widely implemented in heavy road vehicles, their implementations in off-road vehicles have been limited for preservation of roll and tip-over stability [32]. The developments in off-road vehicles thus far have been limited to relatively stiff cab mounts suspension for control of higher frequencies vibration and noises. A suspension seat is thus considered vital for controlling the transmission of vibration to the driver. Although a few concepts in horizontal and multi-axis suspension seats have evolved [32], the vast majority of developments have been directed towards vertical suspension. This is attributed to two primary factors: (1) the magnitudes of vertical vibration and shock motions for most vehicles are known to be more severe than those in other axis; and (2) a relatively greater perception of vertical motion by the human driver, which tends to interfere with the routine tasks.

The performance characteristics of suspension seats have been extensively investigated under different types of excitations through simulations, field tests, and laboratory experiments [6,33,34,35,36]. When subject to low level vibrations, a suspension mechanism exhibits lock-up due to coulomb friction, while under the influence of higher levels of continuous vibration, a suspension seat will attenuate or amplify the vibration depending upon the nature of the disturbance. Under extreme vehicular vibration, the suspension seat could exceed its free travel limit and result in repetitive impacts against the end-stops, thereby causing shock motions [11,31]. End-stops impacts occurrence are known to be more frequent and more severe in urban buses operating on relatively rough urban roads, while off-road machine operators experience end-stops impacts on relatively rough terrains. The preservation of driver's comfort, health and

safety thus necessitates control of transmissions of shock motions due to end-stops impacts and continuous vibrations.

1.2.3 Suspension Seat System

Suspension seats for heavy road and off-road vehicles are designed with very low natural frequency to attenuate high magnitude low frequency WBV, encountered in vehicles employed in the forestry, construction, industrial, mining, and freight and passenger transportation sectors [2,26]. The maximum seat suspension travel is generally limited to *100mm* or less in off-road vehicles to ensure safe vehicle control and driver's accessibility. The suspension travel in seats employed in highway trucks and buses may be greater than *100mm*. The excessive suspension travel under severe vibration is limited by either elastic or rigid bump stops in both the compression and rebound directions. Rubber buffers are generally used in conventional seats to act as end-stops [1]. A vertical suspension seat generally comprises a cross-linkage mechanism to ensure near vertical motion of the seated driver, as shown in Figure 1.1. The figure also shows the top and bottom rubber buffers. The suspension impacts against the relatively high stiffness end-stops yield high magnitude resonant oscillations of the suspension, and high levels of shocks and vibration, causing high level of discomfort [34].

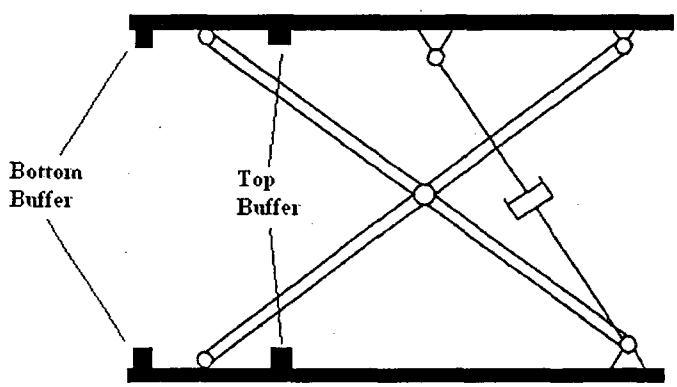

Figure 1.1: Cross linkage mechanism of a seat suspension

Suspension seats integrate either mechanical or pneumatic energy restoring element and a hydraulic damper. The suspension also consists of a weight-adjustment mechanism to ensure static equilibrium near the mid-ride height for a wide range of body masses. The height adjustment may be provided by the primary energy restoring element or by an additional mechanical or electro-mechanical preload mechanism.

The shock and vibration properties of a suspension seat strongly rely on the nature of vibration (frequency components and magnitude), seated body weight and the ride height adjustment, apart from the properties of the suspension components. Owing to complex coupling between the suspension seat and biodynamic behaviour of the seated body, the assessments of suspension seats are mostly conducted in the field or in the laboratory. The subjective and objective field assessments tend to yield greater variability in the measured data, which poses considerable difficulties in interpretations of the data [2,8,10]. Alternatively, International Standards Organization (ISO) has set forth a test procedure for assessment of suspension seats vibration isolation performance in the laboratory [37]. The standard defines the test procedure on the basis of two human subjects with body masses in the vicinity of *55* and *98 kg*. The mean vibration spectra of different classes of work vehicles have also been standardized [10,38]. The laboratory and field test methods provide measurements of shock and vibration isolation performances of a particular suspension seat design but do not directly contribute to the design and/or desired modifications, since the test results correspond to a single invariable design. Moreover, field tests are known to be time consuming and demanding in human resources, while laboratory tests require sophisticated human rated vibration synthesizers [39].

Alternatively, the design and assessment of suspension seats for a particular vehicle vibration spectrum can be evaluated through modeling and dynamic analysis. A few studies have

formulated one and two degrees-of-freedom (DOF) models of the suspension seat to assess the shock and vibration isolation performances, and to seek optimal or near optimal suspension design parameters [12,26,31,39]. Two DOF dynamic system models have been most frequently used to represent the suspension seat system with linearized suspension spring, damper and seat cushion [12,40]. These models consider human body as a rigid mass, assuming negligible contribution due to dynamics of the biological system. Moreover, the kinematics due to cross linkage is invariably ignored. Analytical models comprising nonlinearities due to damper, Coulomb friction and elastic limit stops have also been proposed in a few studies [32,34,35,41]. Boileau et al. [35] showed that consideration of end-stops impacts poses conflicting design requirements for suspension seats. Wu et al. [42] proposed an analytical model of a typical elastic buffer to encompass its nonlinear force-deflection and energy dissipation properties. The study concluded that soft and thick buffers with linear stiffness characteristics over a large range of deflection are highly desirable. Rebelle [31] developed a numerical model of a suspension seat to identify optimal design parameters for control of the end-stop impacts. The model, however, did not permit investigation of the variations in parameters of the individual components.

The vast majority of the reported models have focused on static and dynamic properties of the cushion and suspension components, while the linkage kinematics and human biodynamic are neglected. Different component models have been employed to derive the linear or nonlinear suspension seat model. The seat cushion is a highly nonlinear component of the suspension seat system. Ng et al. [43] showed that adequate support from the seat cushion results in less stress during prolonged driving activity. Tharkurta et al. [4] performed a subjective study of seat zones and driver seat interface pressure under static loads. Human perception of ride comfort was shown to be closely related to the polyurethane foam's complex mechanical properties [44,45].

The effect of composition density and thickness of the polyurethane foam on vibration transmission has also been studied [40,46]. The polyurethane foam exhibits highly nonlinear properties depending upon the excitation magnitude, the excitation frequency and the seated body weight [3]. The majority of the studies have considered lumped properties of a seat cushion, while neglecting hysteresis and dependence upon the body weight and the nature of excitation [32,35,41,47]. Rakheja et al. [39] proposed a nonlinear cushion model as function of the seated load and the deflection of the cushion.

The reported studies suggest that static and dynamic properties of the suspension system components, namely spring, damper, Coulomb friction, and end-stops buffers, are far more significant than those of the cushion [39]. Suspension seats employ either mechanical or pneumatic spring elements in conjunction with a guidance mechanism to ensure a vertical motion. The response of a suspension seat and the ride height are directly related to the stiffness characteristics of the suspension spring element, which is generally assumed to be linear [39]. The friction force, attributed to the shock absorber seals, the sliding joints and the linkage joints, is also known to affect the vibration isolation performance significantly, particularly under low levels of vibration [2]. However, the studies have employed linear relationships from mean measured data for the spring element and the friction force, while assuming negligible hysteresis.

The seated human body is also known to contribute to overall performance of the suspension seat [1,3,14,35]. The human body tends to absorb vibration power through motions of body segments and compression/extension of the muscles and tissues [48]. The energy absorption/dissipation properties of the human body, however, are quite complex. A number of lumped-parameter human body models have evolved on the basis of biodynamic responses measured with subjects seated on a rigid seat [49]. Only a few studies have implemented these

human body models to the suspension seat model to investigate the overall properties of the coupled occupant-seat system [49]. The results, however, provided poor agreements with the measured data acquired with different suspension seats coupled with the seated body [49]. The discrepancies could in-part be attributed to lack of consideration of the elastic human seat interface in the biodynamic measurement studies, and in part to wide variations in the human anthropometry and the effects of sitting posture. A recent study has suggested that the contribution of the seated body is generally small when coupled with a low natural frequency suspension seat and lower levels of vibrations [20]. The human body however altered the vibration isolation properties of the seat under higher magnitudes of vibration. Owing to the complexities associated with the human body model and lack of a generally applicable occupant model, a rigid mass representation of the body is considered to be appropriate for design and analysis of suspension seats.

1.2.4 Active and Semi-Active Suspension Systems

Various concepts in variable damping have been applied in the field of vehicle ride comfort, handling performance, and tire induced road damage [8,21]. Suspensions are classified into three types: passive, semi-active, and active suspensions. The passive suspension exhibits constant characteristics. It can only temporarily store and dissipate energy at a constant rate. The active and semi-active suspensions, on the other hand, offer variable static and dynamic characteristics using external power sources. The active suspension systems generally constitute a force generator, which can directly introduce energy into the system; such suspensions thus require considerable external energy. The most common active suspensions are based on hydraulic actuators or electro-magnetic force generators [50,51]. Semi-active suspensions also offer

variable properties but utilize only minimal energy. The vast majority of the semi-active vehicular suspensions concepts focus on variable damping mechanism [8,17,50,52].

In recent years, a number of semi-active suspension syntheses have evolved on the basis of rheological fluid dampers. The term "rheology" refers to change in shear force characteristics of a material. A rheological fluid can yield different shear force under the same amount of stress provided the required conditions, for instance the applied electro-magnetic field over the rheological fluid. The term magneto-rheology stands for change in shear force characteristics whilst under the effect of a magnetic field. Hence, its counterpart "electro-rheological" fluid exhibits variable properties under an electric field. Rabinow [19] discovered the MR fluid in 1948, which exhibits rapid, reversible, and tuneable transition from a free-flowing state to a semi-solid state under the influence of an external magnetic field. Lord Corporation [53,54,55,56] contributed to the development of MR fluids by enhancing their high yield strength, low viscosity and stable hysteretic characteristics over a broad range of temperatures. MR fluids have been applied in many devices, namely rotary brakes and various dampers. MR fluid products have been successfully applied in various vehicle suspensions and vibration control structures [54,57,58,59,60,61]. Recent developments in MR dampers have been focused on achieving variable damping in response to changing excitation and responses [57,61]. MR elastomers were also suggested for applications where stiffness or resonance performance is sought [62,63].

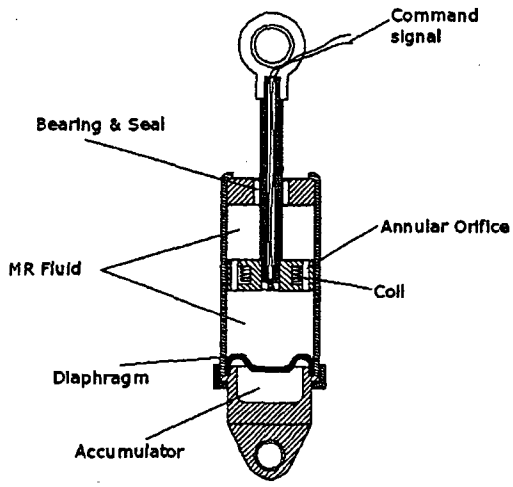

Figure 1.2: Schematic configuration of the test MR damper

Figure 1.2 shows the schematic of a MR damper developed by Lord Corporation for applications in secondary vehicle suspensions (seat suspensions). The damper comprises a nitrogen charged accumulator, two MR fluid chambers separated by a piston with an annular orifice, and electromagnetic coils embedded inside the piston. The electromagnetic coils operate with a *12V* source and current ranging from *0* to *2A*. Under the effect of the magnetic field generated by the coils, the viscous and shear properties of the fluid vary accordingly and modify the damping force.

MR dampers exhibit high viscous damping at very low velocities within the pre-yield conditions and low viscous damping at higher velocities in the post-yield conditions. The pre- and post-yield conditions are defined by a transition force according to Ma [20]. When applied to primary suspensions, MR dampers can achieve adequate ride, road holding, handling, and directional control performance of road vehicles through its variable damping using only minimal power consumption [64]. The MR dampers exhibit highly nonlinear force-velocity characteristics due to the hysteresis and force limiting properties of the MR fluid. Furthermore, the force-velocity characteristics vary with respect to the intensity of the applied magnetic field

and the magnitude of the displacement and velocity [65]. The syntheses of a controller for the MR damper with desirable variations in damping, thus requires an accurate characterization of the force-velocity properties in the pre-yield and post-yield conditions.

The reported studies have presented both the damper models and the controller designs. Since the controller design is generally based on the MR damper model, a number of MR damper models have been proposed, which may be grouped in three categories: piecewise continuous damper models, dynamic structure equivalent models, and dynamic characteristic equivalent models [66,67,68,69]. A piecewise continuous damper model characterizes the nonlinear and hysteretic properties of the damper by equivalent linear or piecewise linear viscous damping constants, namely the Bingham plastic model [70,71], the nonlinear bi-viscous model, and the nonlinear hysteretic bi-viscous model [66]. In dynamic structure equivalent models, the nonlinear components are replaced by equivalent components with known characteristics; such as the Bouc-Wen model [6,54,60,67] and the viscoelastic-plastic model [68,72,73]. Dynamic characteristic equivalent models describe the dynamic properties on the basis of regression functions such as those proposed by Choi et al. [69] and Wang et al. [65,74]. Furthermore, Leva [75] proposed an iterative and discrete method called linear-in-the-parameters NARX (nonlinear auto regressive with exogenous input) model to describe the hysteretic properties of ER and MR dampers.

Hysteresis characteristics of the MR damper continue to be a major controller design issue. The presence of hysteresis can lead to loss of stability and robustness, limit cycle oscillations, and steady-state and transient tracking errors [76,77,78]. A number of damper models incorporating damping hysteresis have also been proposed [20,65,66,67,68,69]. These models are based on fixed function structures in which the parameters are determined through

experimental measurements. Furthermore, their general validity over a wide range of operating conditions has not been demonstrated. Ma [20] tackled the hysteresis issue by proposing and validating an extended sigmoid model over a wide range of operating conditions. The results, however, showed that the consideration of hysteresis can be neglected for most applications, such as suspension seat, where the stability or tracking performance are not of concern.

Owing to the promising performance potentials of active and semi-active suspension systems, various designs of suspension seats using active and semi-active dampers have emerged. Grimm et al. [79] designed an active seat suspension for farm vehicles using a hydraulic actuator. A displacement compensator was used to control the actuator based on the relative displacement of the seat and the acceleration of either the base or the seat. The result showed an improvement in performance with respect to the passive suspension system. Stein and Ballo [80] proposed an active electro-pneumatic system to achieve improved vibration isolation performance by controlling the air flow to an air bellow. Perisse and Jezquel [15] developed an active suspension seat using an electromechanical actuator. Wu and Chen [81] applied an active vibration controller using the excitation displacement as the controller input, while the feedback error signals were defined by the seat acceleration. The performance, however, was only evaluated under a pulse excitation and low magnitude continuous vibration. Guclu [51] studied the dynamics of a nonlinear vehicle model equipped with active suspension seat employing a PID controller. The results from these studies generally show that the ride comfort can be improved by introducing a controlled actuator between the driver cab floor and the seat, while the power requirements and the associated cost are high. Consequently, investigations on semi-active suspension seat have been considered by researchers, in particular with the evolution of high operating bandwidth ER and MR dampers.

Bouazara et al. [82] presented the relative performance potentials of passive, semi-active, and active suspension seats in combination with a 3D vehicle model. Wu and Griffin [42] implemented an on-off controlled ER damper to reduce end-stop impacts; however, the high voltage requirement of the ER damper mode has been less appealing for implementation. McManus et al. [25] tackled the occurrence and severity of end-stop impacts and low frequency attenuation issues using a semi-active MR damper. However, the results did not show improvement in vibration attenuation performance. Choi et al. [57] proposed a PID semi-active controller for MR suspension seat and evaluated the performance of a full-car model equipped with a prototype MR seat using hardware-in-the-loop (HIL) simulations, while neglecting repeated shock motions caused by the end-stop impacts. Choi and Wereley [83] further developed a semi-active nonlinear optimal control algorithm for the MR suspension seat coupled with a mechanical equivalent model of the human body. The study concluded that MR suspension seats yield considerable reductions in transmitted vibration under idealized broadband excitations. Ma [20] proposed a semi-active suspension seat with sky-hook control algorithm while considering the hysteresis of the MR damper. A second stage controller was added to prevent end-stop impacts. The damper model used, however, required a sinusoidal input with known amplitude and frequency, thus limiting the implementation process.

The MR fluid dampers exhibit highly nonlinear characteristics such as hysteresis, magnetic field saturation, and transition between pre-yield and post-yield conditions. Nonlinear controller synthesis have also been proposed, which employed linearization of the nonlinear dynamic systems [84,85], nonlinear PID controllers [57,86], inverse model controllers [87], inverse compensators [85,88], adaptive control algorithms [76], and fuzzy logic and dynamic neural

network controllers [24]. Irrespective of the method used, the synthesis of the controller requires consideration of the entire occupant-seat system and the states that the controller must optimize.

Several semi-active control schemes have been synthesized for vehicle suspensions [21,22,23,24,57]. The skyhook control law proposed by Karnopp et al. [89] is the most investigated algorithm for the MR damper for vehicle suspensions. It has been shown that the sky-hook control limits the resonant oscillations of the spring mass to achieve improved vibration attenuation in the isolation frequency range. Yokoyama et al. [22] synthesized a sliding mode controller by imbedding a skyhook model as a reference model for the tracking control. The study showed that the skyhook control law could yield superior vibration isolation through the MR damper when applied in a quarter car model [90]. Liao et al. [23] used the LQG control law with acceleration feedback to realize damper force tracking. Guo et al. [24] realized the neural network control strategy, while Choi et al. [21] applied a PID controller to track the desired damping force in a full vehicle model.

The sky-hook control law requires the measurement of absolute velocity of the mass, which have been a limiting factor in a number of applications. Owing to the complexity of sky-hook control scheme implementations, several alternative control laws have been proposed. Krasnicki [91] proposed and analyzed a simplified on-off control scheme where the damper operated between the base and the sprung mass as a conventional passive damper during the vibration attenuation portion of the vibration cycle, while assuming a zero damping coefficient when a passive damper would normally accelerate the mass. The damping force was considered to be proportional to the relative velocity in the study. Rakheja and Sankar [92] proposed that the switching between the on and off states of the damper is determined by the product of the relative displacement and relative velocity of the sprung mass with respect to the base. Alanoly

and Sankar [93] further developed the control scheme based on relative position and relative velocity by making the damping coefficient continuous. Wu et al. [94] further enhanced the controller based on relative states to include a damper saturation. Decker and Schramm [95] suggested a control scheme in which the damping coefficient remains low if the absolute velocity of the sprung mass is within a certain bandwidth and is switched to high damping if two conditions are met, namely: 1) absolute velocity exceeds the bandwidth; and 2) the damper is in the rebound stage. The latter control scheme is very similar to an end-stop impact preventer.

Although a number of controller synthesis have been proposed for the MR suspension seats in the recent years, a synthesis for control of both the continuous vibration and end-stop impacts have not yet evolved for random vehicular vibration input, while being reasonably simple for implementation.

1.3 Scope and Objectives of the Dissertation Research

From the review of relevant studies, it is evident that MR dampers offer attractive potential to enhance both the shock and vibration attenuation performance of suspension seats. The reported studies thus far have focused on either continuous vibration or shock isolation, while the design compromise associated with attenuation of both, shock and vibration, has not been explored using simple and directly implementable controller design. Furthermore, the suspension seat models employed in the controller design and assessment studies, invariably, neglect the contributions due to suspension kinematics. The kinematics of the cross-linkage, and the spring and damper links can considerably alter the effective suspension properties and thus the suspension performance.

The overall goal of the dissertation research is thus formulated to contribute to the design and implementation of a controller for MR damper involving adequate compromise between continuous vibration attenuation and discontinuous shock motion prevention. The controller design is sought in consideration of the suspension kinematics, while attempts are made to design a simple and practically implementable controller. The specific objectives of the dissertation are formulated as follows:

1. Develop and validate a MR damper model for describing the mean force-velocity properties and its variation with respect to the applied current as a continuous function of the form $f = (v,i)$, and assess its effectiveness through laboratory experiments and simulations.
2. Propose and validate a two degrees-of-freedom suspension seat model including linkage kinematics and dynamics, and examine its validity through laboratory measured data for a range of vehicular spectra.
3. Synthesize simple MR damper controllers to reduce vibration transmission and to prevent end-stops impact, and assess their effectiveness through simulations and hardware-in-the-loop experiments.

1.4 Organization of the Dissertation

This dissertation work is organized into five chapters. Each chapter provides a development toward one or more stated objectives, while providing preliminaries related to the subsequent goals. Appropriate literatures are further reviewed in the introduction section of each chapter to highlight the scope and the research contributions. Chapter 2 focuses on the modeling of the MR damper model and the suspension seat model. Both models are based on existing models; although considerable modifications are systematically introduced to enhance the model prediction and to realize the semi-active MR damper seat design. The MR damper model parameters are identified through several regressive formulations, while the suspension seat model is derived using basic modeling techniques and kinematic and dynamic principles. Chapter 3 presents the validation of the suspension seat model using the available laboratory

measured data. The simulations are also performed to tune the model parameters on the basis of the target measured data. Validations are presented in terms of frequency-domain and time-domain responses. Simultaneously, the performance evaluation methods are presented in this chapter; namely root mean squared acceleration (a_{rms}), seat effective acceleration transmissibility (SEAT), vibration dose value (VDV), and VDV ratio. Chapter 4 presents the synthesis of four different controllers and their performance characteristics through simulations of the MR damper suspension seat model. The controller performances are measured under different excitations such as harmonic, transient, and random excitations due to different vehicles. The results are evaluated using *rms* acceleration, SEAT, VDV, and VDV ratio measures. Additionally, a smoothing function for the damper current and a second stage end-stops impact preventer are introduced. Chapter 5 presents the hardware-in-the-loop (HIL) test and simulation methodology along with the HIL experiments for the controller selected for implementation. The results are compared with the simulations results, and the controller performance is assessed for a range of vehicular excitation. Finally, Chapter 6 concludes the dissertation research with major highlights, major conclusions, proposals for future works and experiments related to the topic.

CHAPTER 2: FORMULATION OF MAGNETO-RHELOGICAL DAMPER AND SUSPENSION SEAT MODELS

2.1 Introduction

The design and synthesis of a system controller generally requires reasonably accurate description of the system and its components. In order to accomplish the design goal of vibration attenuation and shock prevention through a semi-active suspension seat system, comprehensive models of the suspension seat and the magneto-rheological (MR) damper are required. It has been established that the MR dampers offer considerable superior potential over the ER dampers [21,57,67,68,72,73,96]. Namely, variable damping requirements of vehicle suspensions and suspension seats can be achieved by the MR damper with minimal power consumption [21,51,59,79,97,98]. The damping property of a MR damper is characterized by high damping coefficient in the pre-yield low velocity condition and a considerable lower damping coefficient in the post-yield high velocity condition. These properties are considered desirable for achieving better compromise between the ride and handling qualities of vehicles. In case of hardware malfunctioning, the minimum damping force of the MR damper can ensure fail-safe operating conditions until necessary corrections [99].

In view of the promising performance potentials of a MR damper, effective control algorithm and MR damper dynamic models have been developed and extensively analyzed [100,101]. The Bingham plastic model was proposed assuming rigid material behaviour in the pre-yield operating conditions, while the shear flow in the post-yield operating conditions was characterized by a viscous damping coefficient [63]. Assuming plastic material behaviour in both pre-yield and post-yield conditions, Stanway et al. [66] proposed a nonlinear model where the

pre-yield force was characterized by a very high viscous damping coefficient. Based on Stanway's non linear model, Wereley et al. [96] proposed a nonlinear hysteretic bilinear model by fitting the force-velocity characteristics using four parameters: pre-yield viscous damping coefficient, post-yield viscous damping coefficient, yield force, and zero force velocity intercept. Dyke [102] proposed a damper model based on the well known Bouc-Wen hysteresis model. However, the model possesses inherent difficulties in identification of parameters and in realizations of control systems for desired tracking performance. Based on Dyke's damper model, Spencer et al. [67] derived an extended Bouc-Wen hysteresis dynamic model, which considered the effect of applied current by a linear function. Choi et al. [69] proposed a model on the basis of two polynomial functions to characterize the hysteresis nonlinearities of a MR damper. However, the model did not converge at the two extremities. The nonlinear hysteretic bi-viscous model [96], the Bouc-Wen hysteresis model [67], and the polynomial describing function model [69] characterize the damping force hysteresis to a satisfactory extent, while the effects of a continually varying control current is not considered. A generalized sigmoid hysteresis model was proposed by Wang et al. [103] in order to accurately characterize the force-velocity properties as a function of the continuously varying control current, and the excitation amplitude and frequency. Although the model could predict the force-velocity characteristics of the MR damper better than the previous models, the model required the prior knowledge of maximum velocity of a harmonic excitation, which limits the model to harmonic excitations alone. Wang [104] further provided a method for estimating peak velocity to generalize the model application. Based on the extended bi-viscous damper model, a bilinear bi-viscous model is proposed in this dissertation. The MR damper model is constructed based on the mean measured characteristics of a MR damper, developed by Lord Corporation for application in suspension seats.

Since different vehicles exhibit different dominant frequencies and magnitude of vibration, the design of a suspension seat should be based on the nature of vibration to be attenuated. However, the consideration of variations in the drivers' weights is sometime neglected, which could strongly influence the suspension performance. A seat designed for a heavy occupant would yield quite difference performance when loaded with a light-weight occupant. Furthermore, a suspension seat may amplify or attenuate vibrations from the vehicle to the driver depending on the predominant frequency of the vibration.

The modeling of a suspension seat has been mostly based on the design requirements and the standardized evaluation method. ISO–7096 [38] provides guidelines for laboratory based vibration assessment of suspension seats for different types of construction vehicles. Human subjects of fixed masses are required for the experiment. However, laboratory tests involving human exposure to high intensity vibration can cause ethical concerns, thus in certain cases, the subjects have been replaced by equivalent dead weights. A few studies have proposed linear and nonlinear analytical models of suspension seats to study the suspension performance under continuous and intermittent vibration of different intensities [2,26,31,39,105]. The reported models consider the vertical suspension seat as a two degrees-of-freedom dynamic system with linear or nonlinear components. Although a few studies have suggested that human body plays an important role in energy absorption, the human occupant is generally considered as a rigid mass [26,31,39]. Consequently, a number of biodynamic models ranging from single degrees-of-freedom (DOF) to multi-DOF have been proposed for the seated body [2,36,105]. A recent study have established that contributions due to the seated occupant are very small for low natural frequency suspensions seat but substantial for automotive seats with relatively higher natural frequency [106]. The human body could be conveniently modeled as a rigid mass, when the

natural frequency of the suspension seat is well below the human body's vertical mode natural frequency. From the laboratory-measured driving-point impedance properties of the seated body exposed to vertical vibration, it has been shown that the human body behaves like a rigid mass at frequencies below *2Hz* [107].

The majority of suspension seat models employ linear visco-elastic cushion and spring models [2,31,36]. Others have investigated the nonlinear aspect of the cushion and pan deformation under high magnitude excitations [108,109], which under extreme conditions may cause intermittent loss of body seat contact [105]. Few have characterized the cushion dynamics using regression techniques upon excitation frequency, magnitude of relative deformation, and the preload [39,105,109]. However, the prior knowledge of excitation frequency, magnitude, and preload limits the applicability of such model. The suspension system usually comprises a mechanical or air spring and a hydraulic damper. A cross linkage design is often employed to ensure vertical travel of the suspension seat. The Bouc-Wen model has been recently used to characterize the hysteretic force deflection and force velocity characteristics of the overall suspension system without the contribution of the cushion [13]. Some studies have introduced linear or nonlinear models of elastic end-stops in order to study the frequency and severity of end-stops impacts [27,31,41].

A two degrees-of-freedom suspension seat model is derived in this chapter incorporating the geometry of the suspension linkages and the damper. The modeling and performance test of the suspension seat model is performed with the passive damper, which is subsequently replaced by a MR damper for controller design purpose.

2.2 Characteristics of the Magneto-Rheological Damper

A MR damper (Lord Corporation, model RD-1005-3) is considered for the development of the damper model and the design of the semi-active controller. The MR damper is composed of a nitrogen charged accumulator and two MR fluid chambers separated by a piston that houses orifices and electromagnetic coils. A direct current, up to *2A*, controls the magnitude of the magnetic field generated by the coils, and thus the rheological properties of the fluid. The MR damper considered in the study has a travel of *5cm* and requires a *12V* supply to operate. The force-velocity characteristics of the MR damper have been experimentally verified through a wide range of excitation conditions by Ma [20] and Wang [104].

2.2.1 Experimental Methodology

The force-velocity and force displacement characteristics of the MR damper were measured in the laboratory by Ma [20] in order to characterize the damper hysteresis over a wide range of excitations. The damper was installed on an electro-hydraulic shaker wedged between a moving hydraulic cylinder and a fixed load cell. A linear velocity transducer (LVT) and a linear variable differential transformer (LVDT) sensor were used to measure the velocity and the displacement of the damper, respectively. The MR damper was subjected to harmonic displacement excitations of different constant amplitudes at selected discrete frequencies, and further combined with discrete current settings. The collected data were directly acquired in Excel spreadsheets for post processing. A thermocouple was attached to the MR damper body to monitor the damper temperature, which was held near 30°C±10 to prevent characteristic variation due to temperature. Figure 2.1 shows the schematics of the experimental setup.

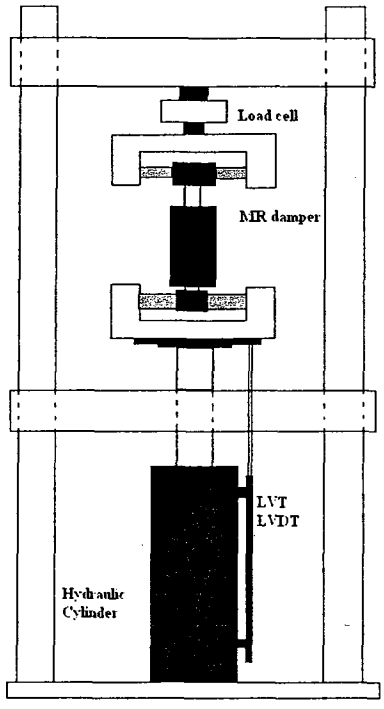

Figure 2.1: MR damper test bench schematics

The characteristics of the MR damper were measured from *0* to *15Hz*, which is the frequency range of predominant vehicular vibration along the vertical axis [110]. The displacement amplitude ranged from *2.5mm* to *18.75mm*, while the constant current ranged from *0* to *1.5A*. Initial tests were performed at a low frequency of *0.1Hz* to identify the static seal friction. The experiments were performed under *203* different combinations of discrete frequencies, amplitudes, and current (Table 2.1). The magnitude of displacements at high frequencies was limited to ensure damper operations within a safe velocity range. The collected data were displayed in the form of time history, force velocity, and force-displacement curves.

2.2.2 Force-Displacement and Force-Velocity Characteristics

As an example of the damper characterization data, Figure 2.2 shows the time histories of the damper displacement, damper velocity, and damper force under a harmonic excitation of *6.25mm*

Table 2.1: MR damper characterization test matrix [20]

Amplitude (A_i)	Current (i)	Frequency f_i (Hz)								
		0.1	0.5	1.5	2.5	5.0	7.5	10	12.5	15
2.5 mm	0	×	×	×	×	×	×	×	×	×
	0.25 A	×	×	×	×	×	×	×	×	×
	0.50 A	×	×	×	×	×	×	×	×	×
	0.75 A	×	×	×	×	×	×	×	×	×
	1.00 A	×	×	×	×	×	×	×	×	×
	1.25 A	×	×	×	×	×	×	×	×	×
	1.50 A	×	×	×	×	×	×	×	×	×
6.35 mm	0	×	×	×	×	×	×	×	×	×
	0.25 A	×	×	×	×	×	×	×	×	×
	0.50 A	×	×	×	×	×	×	×	×	×
	0.75 A	×	×	×	×	×	×	×	×	×
	1.00 A	×	×	×	×	×	×	×	×	×
	1.25 A	×	×	×	×	×	×	×	×	×
	1.50 A	×	×	×	×	×	×	×	×	×
12.5 mm	0	×	×	×	×	×	×			
	0.25 A	×	×	×	×	×	×			
	0.50 A	×	×	×	×	×	×			
	0.75 A	×	×	×	×	×	×			
	1.00 A	×	×	×	×	×	×			
	1.25 A	×	×	×	×	×	×			
	1.50 A	×	×	×	×	×	×			
18.75 mm	0	×	×	×	×	×				
	0.25 A	×	×	×	×	×				
	0.50 A	×	×	×	×	×				
	0.75 A	×	×	×	×	×				
	1.00 A	×	×	×	×	×				
	1.25 A	×	×	×	×	×				
	1.50 A	×	×	×	×	×				

amplitude at *2.5Hz*. Figure 2.3 shows the corresponding force-displacement and force-velocity characteristics of the MR damper under different currents. It should be noted that the curves are clockwise with increasing time in Figure 2.3 (a) and counter clockwise with increasing time in Figure 2.3 (b, c, d). The nonlinear characteristics of the MR damper can be observed in the time history of the force magnitude as well as from the force-velocity characteristics shown in Figure 2.3. Based upon the measured data, the characteristics of the MR damper can be summarized by the following features:

1. *Incremental features*: The force velocity characteristics of the MR dampers can be generally represented as symmetric bi-nonlinear curves with hysteresis at lower velocities (pre-yield conditions), followed by linearly increasing force at higher velocities (post-yield). A force-limiting behaviour is also evident during transition between low and high velocity responses. This behaviour is also evident in the force velocity characteristics of typical hydraulic dampers with low-speed bleed flows and high speed blow-off valves [105]. The damping force may thus be characterized as an incremental function of velocity in the pre-yield and post-yield conditions.
2. *Passive behaviour*: The MR damper exhibits almost viscous property when zero control current is applied (passive property), as evident from the near elliptical force-displacement curve and nearly linear force-velocity curve with relatively small hysteresis (Figures 2.3 (a) and (b)).
3. *Controllability*: The damping force increases considerably with magnitude of control current. The measured yield force (force developed at the onset of post-yield saturation corresponding to either $dv/dt < 0$ (upper force-velocity curve) or $dv/dt > 0$ (lower force velocity curve) can be observed with increasing control currents. The rate of increase in force magnitude is approximately linear under lower current levels ($i < 0.5A$), which tends to gradually decrease under higher values of applied current ($i = 0.5 \sim 1.25A$). A further increase in current ($i > 1.25A$) yields saturation of the damping force.
4. *Hysteresis Phenomenon*: The damper hysteresis progresses along counter clockwise path with increasing time (Figure 2.3 (c)). The upper curve in the force velocity characteristics reflects force variation with decreasing velocities ($dv/dt < 0$), while the lower curve corresponds to force with increasing velocities ($dv/dt > 0$). The mean slope of hysteretic loop, referred to as the viscous damping coefficient, is dependent upon both the control current and excitation conditions (frequency and stroke).

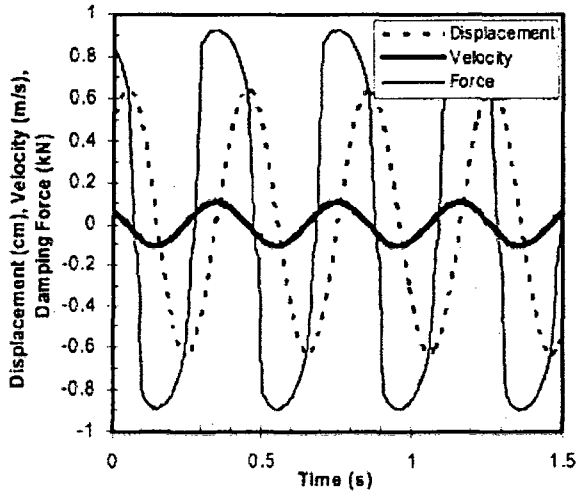

Figure 2.2: Time history of MR damper response and excitation under harmonic inputs (amplitude = *6.25mm*, frequency = *2.5Hz*, current = *0.5A*) [20]

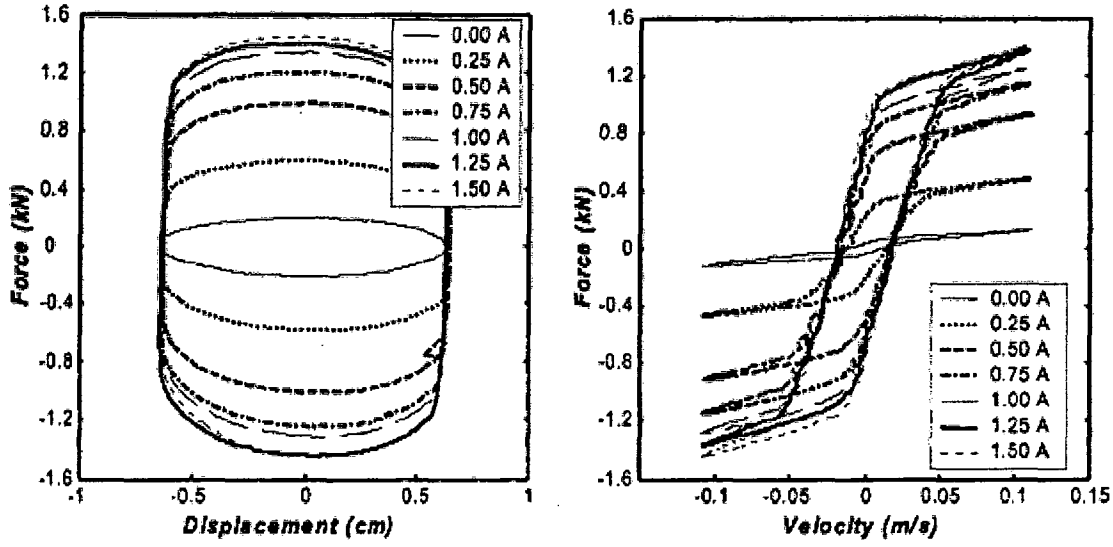

(a) (b)

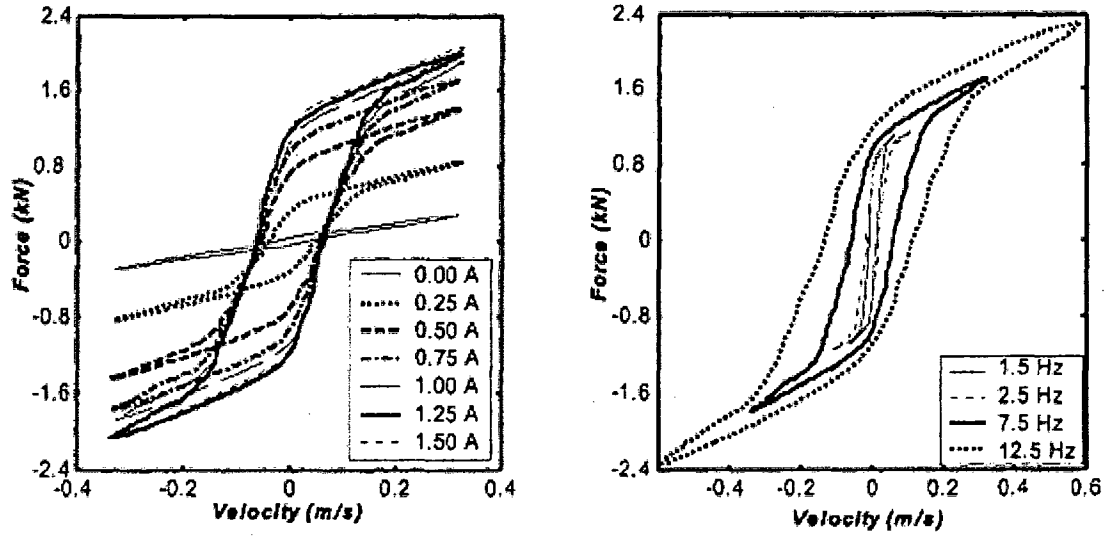

(c) (d)

Figure 2.3: Measured damper (a) force-displacement characteristics (amplitude = *6.25mm*, frequency = *2.5Hz*), force-velocity characteristics as a function of current (b) (amplitude = 6.25mm, frequency = *2.5Hz*), (c) (amplitude = *6.35mm*, frequency = *7.5Hz*), and (d) as a function of frequency (amplitude = *6.35mm*, current = *0.75A*) [20]

5. *Viscous Characteristics*: Given a control current, the MR damper yields nearly identical force velocity curves under same excitation velocity that may be realized from different combinations of frequency and stroke. The damping force can therefore be expressed as a function of piston velocity and control current, with appropriate consideration of the force-limiting behaviour.

2.3 Synthesis of a Generalized Bi-Linear Bi-Viscous Model

Numerous vehicle suspension damper models, which generally focus on the characterization of force-displacement and force-velocity properties, have been proposed in the reported literature. A number of MR damper models have also evolved over the past many years to characterize the damping properties as a function of the applied current and the velocity. These models, with and without hysteresis characteristics have been critically reviewed in a recent study [20]. A generalized bilinear bi-viscous model is proposed in this section with the objective of describing the force-velocity characteristics of the MR damper considered in the study. The variability in the force-velocity characteristics of the MR damper for a given current (Figure 2.3) can be built upon a basic bi-viscous model. Neglecting the hysteresis characteristics, force-velocity properties, in general, can be represented by a bilinear function of damper velocity (V_{damp}) and damper current (i). The measured data acquired under different velocities and currents are analyzed to identify the characteristic model parameters through linear regression.

2.3.1 Generalized Characteristic Parameters

A typical MR damper force-velocity characteristic corresponding to constant magnitudes of velocity and control current can be approximated by a general piecewise-affine function, as shown in Figure 2.4, while neglecting the hysteresis. Since the model is symmetric in compression and extension, the essential parameters of the functions are described in Figure 2.4, in compression ($V_{damp} > 0$) only.

1. *Transition Velocity* ($v_t, m/s$): Piston velocity corresponding to onset of force limiting property (post-yield condition). The transition velocity is obtained from the intersection of the pre-yield and post-yield characteristic curves.

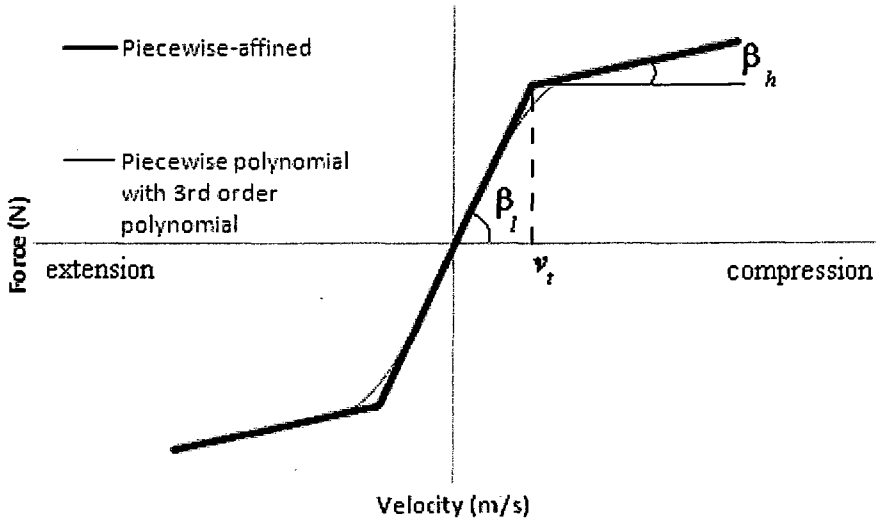

Figure 2.4: Bi-viscous damper force velocity characteristics

2. *Low Velocity Slope* ($\beta_l, Ns/m$): Slope of the force-velocity curve at $V_{damp} = 0$ representing low speed viscous damping coefficient.
3. *High Velocity Slope* ($\beta_h, Ns/m$): Slope of the force-velocity curve at v_t representing high speed viscous damping coefficient.

2.3.2 Synthesis of the Damping Coefficients and Transition Velocity

The damping coefficients corresponding to the pre-yield and post-yield conditions are characterized by constants for each corresponding input current. Thus, the damping function can be characterized by three first order polynomials: the pre-yield polynomial, the compression post-yield polynomial and the extension post-yield polynomial. Consequently, the transition velocity is determined by the intersection of the pre-yield polynomial with respect to any post-yield polynomials. The MR damper curves, however, exhibits different slopes under different combination of excitation amplitudes and frequencies. The changes in the force velocity characteristics with increasing frequency can be seen in Figure 2.3. It can be further observed that combinations of different amplitudes and frequencies yielding the same maximum velocity would yield the same damping coefficients for both pre- and post-yield conditions.

The data sets acquired corresponds to each test condition were analyzed to identify mean damping coefficients. The data points near the transition velocity, however, were rejected due to their non-linear properties. The criteria of data points' selection were determined on the basis of percentage of the total range of the data set. The first order polynomial in pre-yield was estimated by considering the data in the *-10%* to *10%* of the total range, where the zero intercept was set to zero to yield a linear function. The data in the *-50%* to *-40%* and *40%* to *50%* of the total range were used for linear regressions to obtain the extension and compression post-yield first order polynomials, respectively. Two affined functions were obtained through this process. Furthermore, an average value of the two post-yield coefficients was taken by assuming symmetric damper operation. Finally, the intersection point of the pre-yield and the post-yield polynomials would yield the transition velocity. The linear regressions were applied to all data sets obtained through damper characterization, while the averages pre-yield and post-yield damping coefficients were obtained for each discrete value of current.

2.3.3 Influence of the Control Current

The mean damping coefficients corresponding to pre- and post-yield conditions reveals nonlinear variations with the control current. Although the candidate MR damper is designed to operate between *0* and *2A*, the most significant variations due to current were observed in the *0* to *0.75A* range. The damping coefficients increase with the current but at a diminishing rate with increasing current. Within the *0* to *0.75A* current bandwidth, however, the damping coefficient variations could be approximated by a first order polynomial without major loss in precision. Again, using linear regression, the rate of change of the damping coefficients are evaluated as first order polynomials in the pre-yield and the post-yield conditions.

2.3.4 Synthesis of the Overall MR Damper Model

The effects of velocity and input current on the bi-viscous force-velocity characteristic canbe described by the piecewise-affine functions, such that:

$$\begin{cases} F_{damp} = \beta_l V_{damp}; & -v_t \le V_{damp} \le v_t \\ F_{damp} = \beta_h (V_{damp} - v_t) + \beta_l v_t; & v_t < V_{damp} \\ F_{damp} = \beta_h (V_{damp} + v_t) - \beta_l v_t; & -v_t > V_{damp} \end{cases} \quad (2.1)$$

where F_{damp} is the damper force, V_{damp} is the damper velocity, β_l and β_h are the pre-yield and post-yield damping coefficients, respectively, and v_t is the transition velocity. The pre- and post-yield damping coefficients, β_l and β_h, are replaced by first order polynomial functions in current, $\beta_l(i)$ and $\beta_h(i)$, respectively, to reflect their dependence on the current i, such that:

$$\beta_l(i) = \gamma_l i + \delta_l; \quad \text{and} \quad \beta_h(i) = \gamma_h i + \delta_h \quad (2.2)$$

where $\gamma_l, \delta_l, \gamma_h$, and δ_h are the constant coefficients, which were estimated from the measured data. Table 2.2 summarizes the values of these damping coefficients together with the transition velocity v_t. Substituting Eq. (2.2) into Eq. (2.1) yields the damping force by the following piecewise affine functions in damper current and velocity:

$$\begin{cases} F_{damp} = (\gamma_l i + \delta_l) V_{damp}; & -v_t \le V_{damp} \le v_t \\ F_{damp} = (\gamma_h i + \delta_h)(V_{damp} - v_t) + (\gamma_l i + \delta_l) v_t; & v_t < V_{damp} \\ F_{damp} = (\gamma_h i + \delta_h)(V_{damp} + v_t) - (\gamma_l i + \delta_l) v_t; & -v_t > V_{damp} \end{cases} \quad (2.3)$$

Table 2.2: Parameter values of Lord Corporation RD-1005-3 MR damper

γ_l(kg/sA)	γ_h(kg/sA)	δ_l(kg/s)	δ_h(kg/s)	v_t(m/s)
24644	2379.25	4249	767.5	0.027

Although the MR damper model described by Eq. (2.3) is continuous, the non-smooth characteristics at the compression and extension transition velocities cause considerable oscillations in the system response. The pre-yield damping function was thus characterized by a third order polynomial to achieve a smooth transition. To maintain the same pre-yield damping coefficient and to create a smooth transition at the transition velocity, an overlap of up to *0.01m/s* beyond the transition velocity was introduced in the post-yield functions, as illustrated in Figure 2.4. A third-order polynomial function f_3 is considered to describe the damper force in pre-yield. Let f_3 be a third-order polynomial function with only odd power terms. The substitution of the third-order polynomial function as the pre-yield damper function, at a given current value, involves the following four conditions:

1. $\left.\frac{df_3}{dV_{damp}}\right|_{v_{damp}=0} = \beta_l(i)$

2. $\left.\frac{df_3}{dV_{damp}}\right|_{v_{damp}=0.04} = \beta_h(i)$

3. $f_3(0.04) = F_{damp}(0.04)$

4. $f_3(0) = F_{damp}(0) = 0$ (2.4)

The consideration of the pre-yield function f_3 of the form

$$f_3(V_{damp}) = AV_{damp}^3 + CV_{damp} \tag{2.5}$$

yields following expressions for the coefficients A, and C.

$$A = \frac{\beta_h(i) - \beta_l(i)}{0.0048}$$

$$C = \beta_l(i) \tag{2.6}$$

where condition 3 can be verified using Eq. (2.6) and condition 4 is satisfied by considering only odd terms of the polynomial. Using Eqs. (2.5) and (2.6), the damper model can be expressed by the following piecewise smooth functions:

$$\begin{cases} F_{damp} = \dfrac{[(\gamma_h - \gamma_l)i + \delta_h - \delta_l]}{0.0048} V_{damp}^3 + (\gamma_l i + \delta_l) V_{damp}; & -v'_t \le V_{damp} \le v'_t \\ F_{damp} = (\gamma_h i + \delta_h)(V_{damp} - v_t) + (\gamma_l i + \delta_l) v_t; & v'_t < V_{damp} \\ F_{damp} = (\gamma_h i + \delta_h)(V_{damp} + v_t) - (\gamma_l i + \delta_l) v_t; & -v'_t > V_{damp} \end{cases} \tag{2.7}$$

where $v'_t = 0.04 m/s$ is the altered transition velocity, incorporating the chosen overlap.

2.3.5 Validation of the Generalized MR Damper Model

The piecewise smooth MR damper model is evaluated for wide ranges of currents and velocities and the results are compared with experimental data to demonstrate its validity. The model, in general, resulted in an acceptable estimation of the mean damping force over considered range of velocity and current. Figures 2.5(a) to 2.5(g) illustrate comparisons of the measured force-velocity characteristics with the model results corresponding to different damper currents. The results suggest that the model yields reasonably good estimations of the mean damping force at lower currents. The model, however, tends to underestimate the post-yield damping in the mid current range (*0.5 – 0.75A*), which is mostly attributable to the use of the first-order polynomial in current. The results further show large increments in damping coefficients with current, which tends to diminish with further increase in the current. An overestimation in the post-yield can also be observed at high currents in excess of *1A*. The prediction error could be considered

negligible since it mostly occurs at higher currents and that the damper exhibits larger changes in damping only in the $0 - 0.75A$ range.

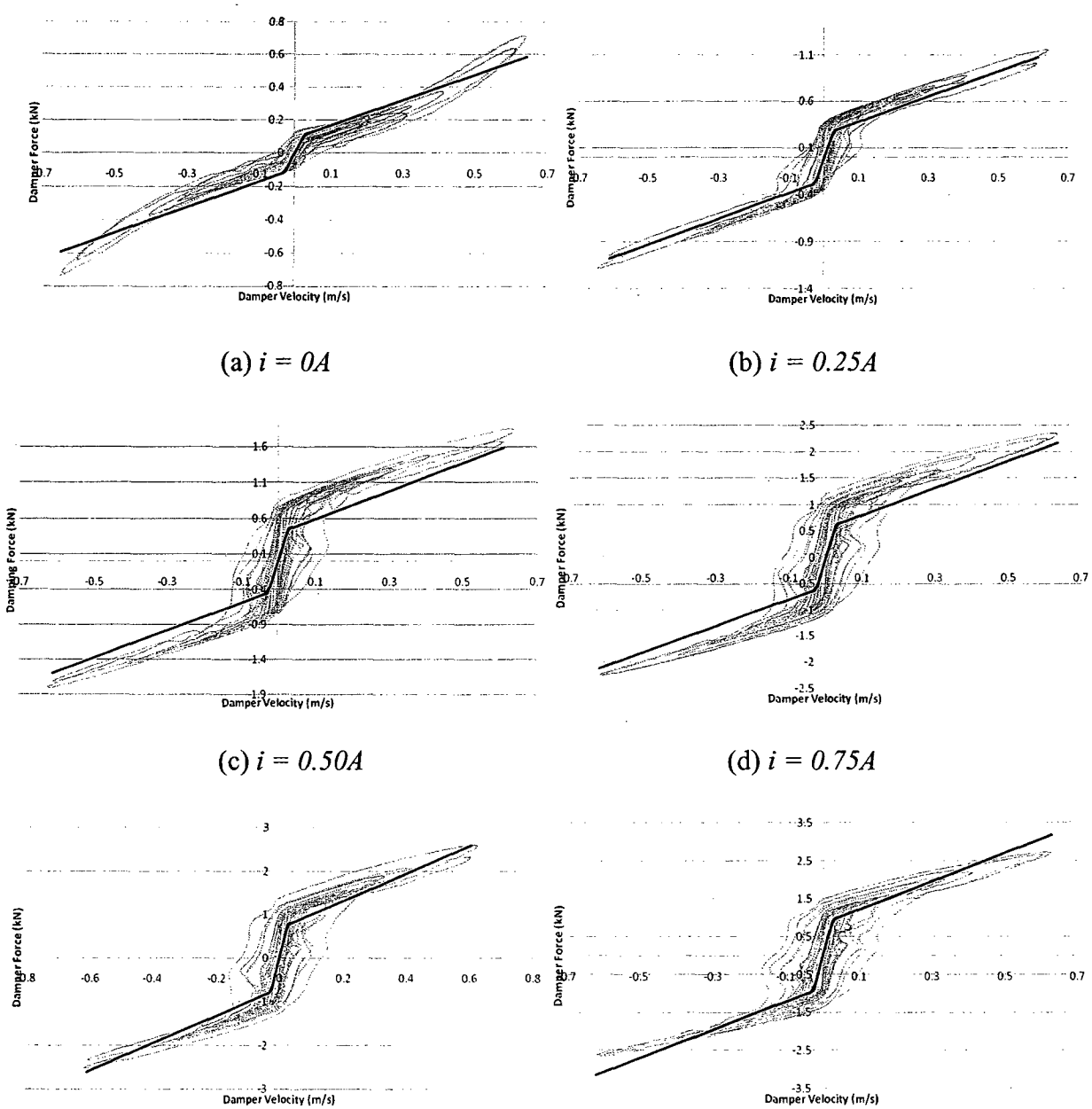

Figure 2.5: Comparisons of measured damper force-velocity characteristics with that of the bilinear bi-viscous damper model under different constant current (continued) [20]

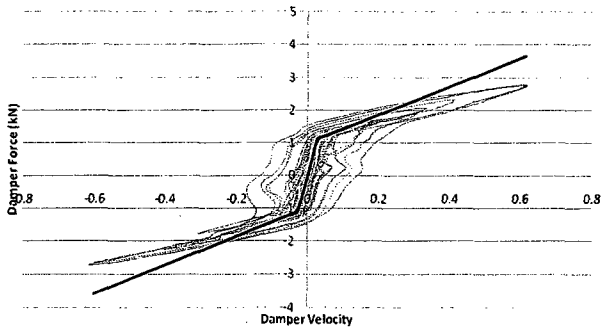

(g) $i = 1.50A$

Figure 2.5: Comparisons of measured damper force-velocity characteristics with that of the bilinear bi-viscous damper model under different constant current [20]

2.4 Characteristics of the Suspension Seat System

Suspension seats used in heavy road and off-road vehicles are designed to provide vibration attenuation along the predominant vertical axis. The seat comprises a suspension system with cross linkages that support a nearly vertical motion of the cushion. The suspension seat is designed with a very low natural frequency due to the predominant low frequency vertical vibration induced from road roughness or off-road obstacles. Considering that the primary resonance frequency of the human body lies in the *4* to *5Hz* range, a low natural frequency suspension seat can effectively attenuate vibrations in this range. The low natural frequency design, however, yields greater dynamic deflection and often exceeds the limited travel. The suspension seat may thus transmit high intensity vibration shock to the occupant due to end-stop impacts under excitations arising from pot-holes and off-road unevenness. Elastomeric end-stops are thus installed near the ends of the limited suspension travel to cushion the impact. The end-stop impacts may also cause loss of occupant's contact with the seat.

2.4.1 Development of the Passive Suspension Seat Model

Since the study focuses on the damper as a key element to provide improved attenuations of shock motions and continuous vibrations, a model of the passive suspension seat is initially developed. The passive damper is subsequently replaced by the MR damper model for semi-active control synthesis. The suspension seat considered is constructed with a relatively soft poly-urethane foam cushion supported by the suspension platform. The platform is supported by a cross-linkage mechanism to ensure nearly vertical motion. A pneumatic spring and a hydraulic damper are installed between the platform and the suspension base through complex configurations within the cross-linkage. The rebound and compression elastic end-stops are installed to limit the free travel to approximately *140mm*. The rebound end-stop, installed within the roller guide can be adjusted to achieve different suspension travel, while the height adjustment is achieved by controlling the air pressure within the pneumatic spring. The natural frequency of the suspension seat was measured to be in the order of *1.25Hz* when set to mid-ride position under a passive mass of *77kg* [39]. The static and dynamic characteristics of suspension components were measured in the laboratory in terms of instantaneous force, displacement, and velocity responses under different preloads and excitation levels [39].

Generally, the suspension seat systems are represented as a two degrees-of-freedom (DOF) model with the occupant considered as a rigid mass [27,31,39,108]. The kinematics of the cross-linkage suspension and the damper link are invariably ignored. It is hypothesized that the kinematics of the linkage suspension tends to alter the effective suspension and damping rates, and thus the shock and vibration isolation performance. A suspension seat model incorporating the kinematics due to suspension links is thus developed subject to the following simplifying assumptions:

1. *Cushion Body Contact*: The contact between the seat cushion and the apparent human body mass is always maintained. The occupant is thus considered as a mass attached to the visco-elastic cushion.
2. *Linear Cushion Characteristics*: Although it has been shown that cushion exhibits nonlinear characteristics, especially under high loading or high frequency excitations, the cushion is characterized by effective linear stiffness and viscous damping.
3. *Linear Suspension Air Spring*: The force displacement characteristic of the air bag is considered to be linear.
4. *Rigid Seated Occupant*: The human body mass is considered as a rigid mass neglecting the contributions due to the visco-elastic biological system.

Based on the above assumptions, the suspension seat system is modeled as a two-DOF system as shown in Figure 2.6. Let m_c and m_s represent the seated body mass and the suspension mass, respectively. The suspension system is characterized by: (1) F_c, the force developed by the cushion due to its stiffness and damping; (2) F_s, the equivalent suspension spring force; (3) F_f, the effective linkage and joint friction force; (4) F_d, the effective suspension damping force; and (5) F_b, the force due to end-stops. The equations of motion for the model can be written as:

$$\begin{cases} m_c\ddot{x}_c = -F'_c + m_c g \\ m_s\ddot{x}_s = -F'_s - F_f - F_d - F_b + F_c + m_s g \end{cases}, \tag{2.8}$$

where the terms F'_c and F'_s include the static components of the cushion and spring forces, respectively. By setting the system to the equilibrium position (mid-ride height) and assigning the equilibrium position to be zero allows the removal of the terms $m_c g$ and $m_s g$. Thus the equation of motion at the equilibrium point may be written as:

$$\begin{cases} m_c\ddot{x}_c = -F_c \\ m_s\ddot{x}_s = -F_s - F_f - F_d - F_b + F_c \end{cases} \tag{2.9}$$

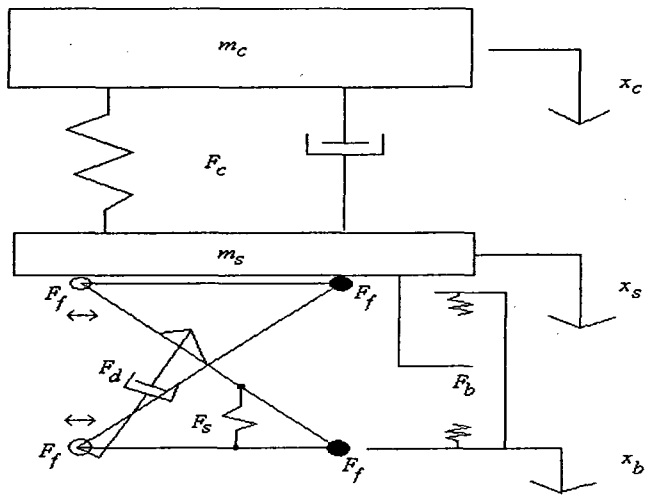

Figure 2.6: Schematic of the two degrees-of-freedom model of the suspension seat

2.4.2 Linearization of the Cushion Characteristics

The stiffness and damping characteristics of the poly-urethane foam (PUF) cushion have been established to be nonlinear functions of the preload and excitation [39]. Furthermore, the pan supporting the PUF may deform under high loads and may contribute to a considerable change in the force-deflection characteristics. The nonlinearity due to the PUF cushion, however, may be considered negligible due to its small contribution to the overall performance of the suspension seat, particularly under small cushion deformation.

The PUF cushion of the suspension seat considered in this study has been characterized in the laboratory under different loads applied through *20cm* diameter indenter, as recommended in SAE J1051 [39,111]. Figures 2.7 to 2.9 illustrate the static and dynamic stiffness properties and the equivalent viscous damping coefficient of the cushion as a function of the excitation frequency, respectively. The measured data are presented for three different loads, denoted as "L", "M", and "H", which correspond to light (*40kg*), medium (*55kg*) and heavy (*66kg*) preloads, respectively, and three different deflections (*6.35mm*, *12.7mm*, *19.05mm*). The measured properties in Figures 2.8 and 2.9 are denoted by the preload followed by the deflection

amplitude. The measured data are used to identify the constant damping and stiffness coefficients corresponding to representative preload and frequency values. It has been suggested that the cushion stiffness and damping coefficients can be expressed as a function of preload and frequency, it is evident from Figures 2.8 and 2.9, such that [39]:

$$k_c = W_p \cdot (a_1 \cdot f + a_2 \cdot Y_c + a_3) \tag{2.10}$$

$$C_{eq} = b_1 \cdot W_p \cdot f^{-b_2};\ f \succ 0. \tag{2.11}$$

where k_c is the stiffness coefficient in *N/mm*, C_{eq} is the equivalent damping coefficient in *Ns/mm*, W_p is the preload in *N*, f is the frequency in *Hz*, Y_c is the cushion deflection amplitude in *mm*, and a_1, a_2, a_3, b_1, and b_2 are constant coefficients. Table 2.3 shows the constant coefficients identified from the measured data through minimization of the squared error between the measured and predicted coefficients.

Table 2.3: Cushion model parameters (modified from Rakheja et al. [39])

a_1	a_2	a_3	b_1	b_2
0.0018	-0.0011	0.0601	0.0019	0.67

The seated mass of the human body considered for the suspension seat model is *66kg*, which also serves as the preload for the cushion model. The frequency parameter is selected as *1.5Hz*, since it is close to the vertical mode natural frequency of the suspension seat. An equivalent value of the stiffness is derived assuming *15mm* cushion deformation. A linear stiffness coefficient K_c is thus evaluated using Eq. (2.10) as *29.977N/mm*. The corresponding cushion damping coefficient C_c is subsequently evaluated using Eq. (2.11) as *0.938Ns/m*. The total cushion force can then be written as

$$F_c = K_c(x_c - x_s) + C_c(\dot{x}_c - \dot{x}_s) \tag{2.16}$$

where K_c = *29977N/m* is the equivalent cushion stiffness and C_c = *938Ns/m* is the equivalent cushion damping coefficient.

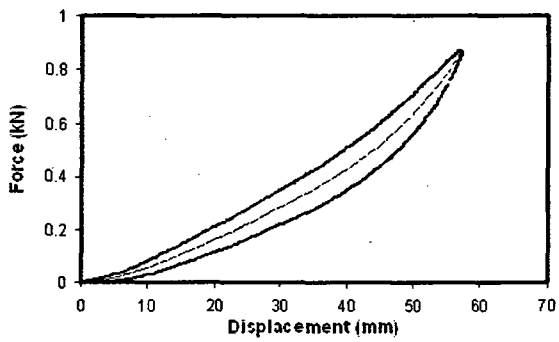

Figure 2.7: Static force-deflection characteristics of the cushion [39]

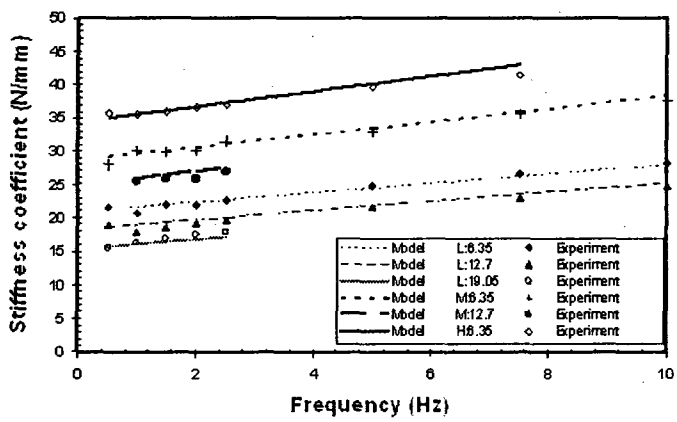

Figure 2.8: Dynamic stiffness characteristics of the cushion [39]

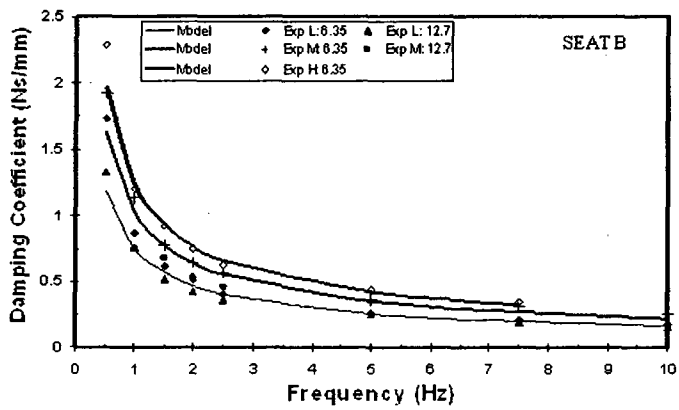

Figure 2.9: Equivalent damping coefficients as a function of the excitation frequency [39]

2.4.3 Equivalent Suspension Stiffness

Similar to the cushion characteristics, the suspension characteristics have also been thoroughly investigated characterized in the laboratory under different preloads [39]. The air spring force of the seat suspension can be represented as a function of the preload and the suspension deflection, such that:

$$f_s = W_p \cdot (c_0 + c_1 y_s) \tag{2.13}$$

where $c_0 = 0.41$, $c_1 = 7.7mm^{-1}$, and $y_s = x_s - x_b$. Figure 2.10 illustrates comparisons of the measured force-deflection characteristics of the seat suspension with those derived from Eq. (2.13). The results are presented for different preloads, ranging from *789* to *1112N*. The suspension stiffness corresponding to a preload of *789N* is evaluated as $K_s = 6075N/m$, while the spring force may be defined as $F_s = K_s y_s$.

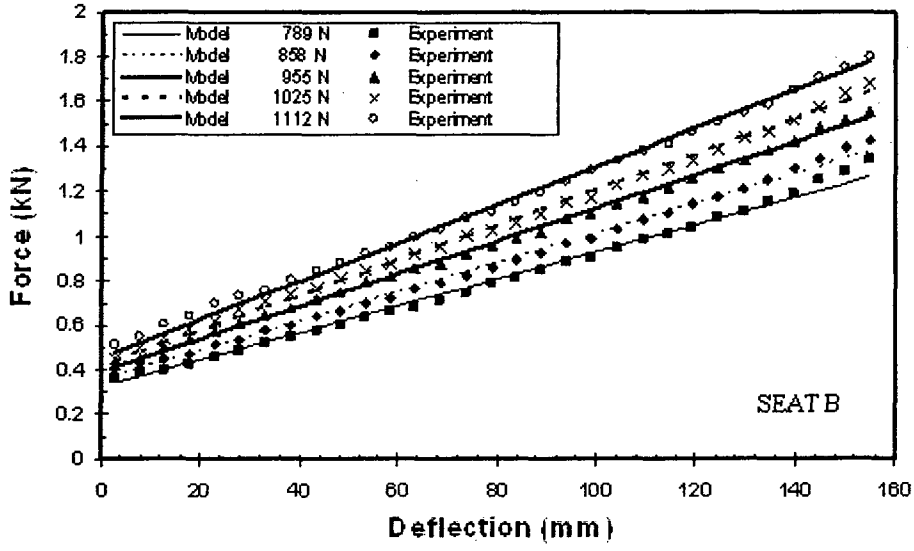

Figure 2.10: Suspension force deflection characteristics [39]

2.4.4 Damper Kinematics Model

The seat suspension linkages are designed using various constraints to ensure a vertical travel of the seat. The cross-linkage suspension integrates a *15cm* (eye-to-eye) damper within the confined space and utilizes the entire damper travel over the permissible suspension travel. The effective damper force thus depends not only on the relative velocity but also on the relative displacement. Figure 2.11 shows the schematics of the suspension linkage under an inclination angle α and the damper link EF ($L_{damp} = EF$). While the instantaneous suspension height is designated as h, the angles β and γ are constants. The linkage schematic shows that the effective damping force is at its lowest when the suspension is fully compressed and at its highest when the suspension is fully extended.

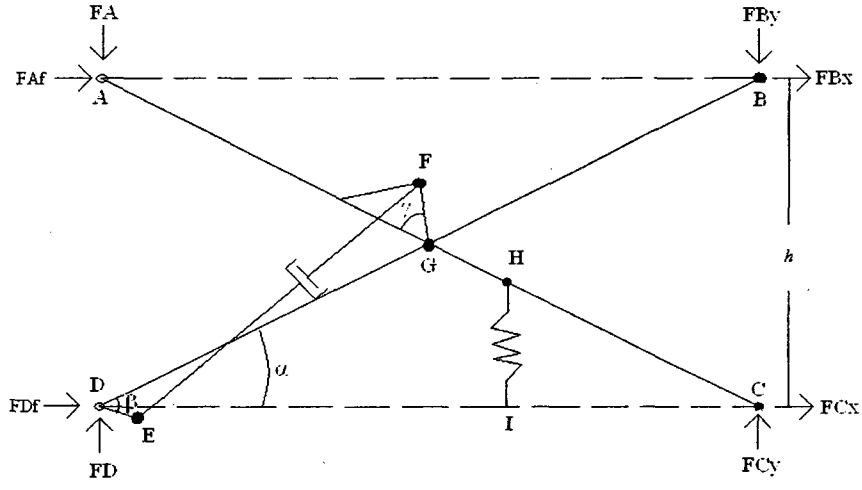

Figure 2.11: Suspension linkage schematics

Let the maximum and minimum suspension heights be h_{max} and h_{min}, respectively, corresponding to full extension and compression, the instantaneous height is determined from the mid-ride height and the suspension deflection as:

$$h = \frac{h_{\max} - h_{\min}}{2} + h_{\min} - y_s \tag{2.14}$$

Let L be the length of the cross linkage AC or BD. The instantaneous angle α can thus be expressed as:

$$\alpha = \arcsin\left(\frac{h}{L}\right) \tag{2.15}$$

The instantaneous length (L_{damp}) and velocity (V_{damp}) across the damper are determined from the suspension geometry and kinematics, such that:

$$L_{damp} = \sqrt{(a\cos\alpha + b\sin\alpha)^2 + (c\cos\alpha + d\sin\alpha)^2}$$

$$V_{damp} = \frac{(a\cos\alpha + b\sin\alpha)(-a\sin\alpha + b\cos\alpha) + (c\cos\alpha + d\sin\alpha)(-c\sin\alpha + d\cos\alpha)}{L\sqrt{\left[(a\cos\alpha + b\sin\alpha)^2 + (c\cos\alpha + d\sin\alpha)^2\right]\left[1 - \left(\frac{h}{L}\right)^2\right]}}\dot{y}_s \tag{2.16}$$

where

$$a = -L_1\cos\beta + L2 - L_3\cos\gamma$$

$$b = -L_1\sin\beta + L_3\sin\gamma$$

$$c = L_1\sin\beta + L_3\sin\gamma$$

$$d = -L_1\cos\beta + L_2 + L_3\cos\gamma$$

2.4.5 Suspension Friction Force Model

The friction force due to sliding rollers and bushings is modeled as a Coulomb friction function with a narrow viscous band (*0.002m/s*). Let F_{Af}, and F_{Df} represent the friction forces developed at the sliding joints A and D, respectively, and F_f be the sum of the two friction force, the friction force function can be expressed as:

$$F_f = \begin{cases} F_{sat} & \dot{y}_s > v_f \\ \dfrac{F_{sat}}{v_f}\dot{y}_s & -v_f \le \dot{y}_s \le v_f \\ -F_{sat} & \dot{y}_s < -v_f \end{cases} \tag{2.17}$$

where F_{sat} is the saturation value of the Coulomb friction force and v_f is the magnitude of the viscous range. Similarly to the MR damper model, the non-smooth properties of the friction force model may cause transient behaviour during simulations. For that matter, the viscous band is replaced by a third order polynomial function, which overlaps the Coulomb force at saturation by *50%* of the range of the viscous band. The viscous band is defined from $v_f = 0.01m/s$, therefore, the overlap of *50%* is created by the modified transition velocity $v'_f = 0.015m/s$. The friction force function can thus be expressed as:

$$F_f = \begin{cases} F_{sat} & \dot{y}_s > v'_f \\ -\dfrac{F_{sat}}{3v_f\left(v'_f\right)^2}\dot{y}_s^3 + \dfrac{F_{sat}}{v_f}\dot{y}_s & -v'_f \le \dot{y}_s \le v'_f \\ -F_{sat} & \dot{y}_s < -v'_f \end{cases} \tag{2.18}$$

by evaluating the first derivative of the polynomial: (i) equal to the viscous damping rate at zero velocity, and (ii) equal to the saturation force at the modified transition velocity. The saturation force is determined using a trial and error approach involving comparisons of frequency response of the suspension seat model with passive damping and laboratory measured responses of the suspension seat with passive damping. The identified parameters and the methodology are further described in Chapter 3.

2.4.6 Equivalent Damping Force

The effective damping force due to the suspension is computed from the static equilibrium in the absence of spring and friction components of the suspension model shown in Figure 2.12. It is further assumed that the vertical forces developed at joints *A*, *B*, *C*, and *D* are equal in

magnitude. The contribution due to horizontal forces at joints B and C are thus considered negligible. Let F_A, F_{By}, F_{Cy}, and F_D be the normal forces acting at the joints A, B, C, and D of the cross-linkages, and F_{Bx} and F_{Cx} be the horizontal forces acting at the fixed bushings B and C. The moment equation for the link AC is derived as:

$$F_A \frac{L}{2}\cos\alpha + F_{Cy}\frac{L}{2}\cos\alpha - F_{Fx}L_3\sin(\alpha+\gamma) - F_{Fy}L_3\cos(\alpha+\gamma) = 0 \tag{2.18}$$

The force components at the damper joints F (F_{Fx}, F_{Fy}) and E (F_{Ex}, F_{Ey}) can be related to the damper force F_{damp} and the damper inclination angle. These force components can be expressed as:

$$F_{Fx} = F_{Ex} = \frac{a\cos\alpha + b\sin\alpha}{L_{damp}}F_{damp}; \quad F_{Fy} = F_{Ey} = \frac{c\cos\alpha + d\sin\alpha}{L_{damp}}F_{damp} \tag{2.19}$$

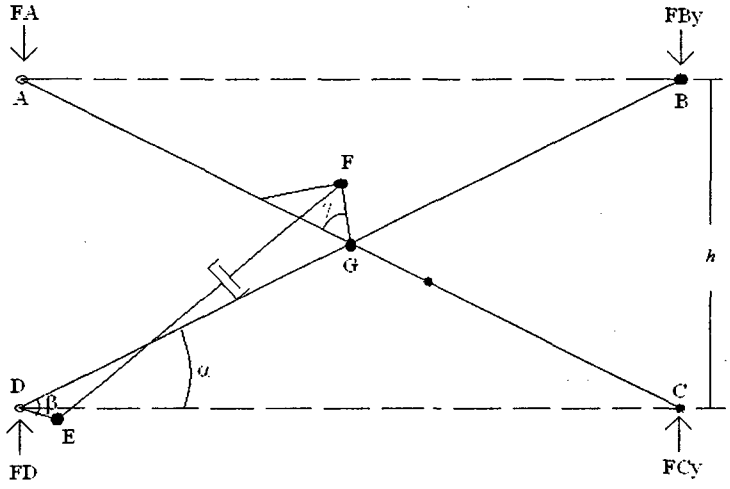

Figure 2.12: Suspension schematics without friction and spring

Eqs. 2.18 and 2.19 yield following relation between the suspension force at the joints and the damper force:

$$F_A = \frac{a\cos\alpha + b\sin\alpha}{L_{damp}L\cos\alpha}F_{damp}L_3\sin(\alpha+\gamma) + \frac{c\cos\alpha + d\sin\alpha}{L_{damp}L\cos\alpha}F_{damp}L_3\cos(\alpha+\gamma) \tag{2.20}$$

The total damping force applied to the suspension mass in the absence of the suspension spring and the friction force is twice the magnitude of F_A, attributed to forces developed at joints A (F_A) and B (F_{By}). The effective vertical damping force F_d is thus expressed as:

$$F_d = 2F_A = 2\left(\frac{a\cos\alpha + b\sin\alpha}{L_{damp} L\cos\alpha} F_{damp} L_3 \sin(\alpha+\gamma) + \frac{c\cos\alpha + d\sin\alpha}{L_{damp} L\cos\alpha} F_{damp} L_3 \cos(\alpha+\gamma) \right) \quad (2.21)$$

The above formulation illustrates the contribution due to kinematics of the suspension links and the damper link to the effective damping force along the vertical axis. The force-velocity characteristics of the passive damper employed in the candidate suspension have been evaluated in the laboratory. The force-velocity characteristics of the damper were determined from the measured peak force and peak velocity data, which suggested higher compression damping coefficient than that in extension. The data further showed two-stage damping characteristics in compression. The damper force is thus expressed by a piece-wise affine model (Figure 2.13), such that:

$$F_{dampp} = \begin{cases} C_{c1} V_{damp} & 0 \le V_{damp} \le v_{c1} \\ C_{c1}\left[v_{c1} + \gamma_c (V_{damp} - v_{c1})\right] & V_{damp} > v_{c1} \\ pC_{c1} V_{damp} & V_{damp} < 0 \end{cases} \quad (2.22)$$

where C_{c1} is the low speed compression mode damping coefficient, $\gamma_c = C_{c2}/C_{c1}$ is the compression mode damping reduction factor at higher speeds, v_{c1} is the transition velocity between the low- and high-speed damping characteristics, and $p = C_e/C_{c1}$ is the damping asymmetry factor that relates the extension damping coefficient (C_e) to the low speed compression mode coefficient. This passive damper model was employed in the suspension model to examine the validity of the suspension model, which is described in Chapter 3.

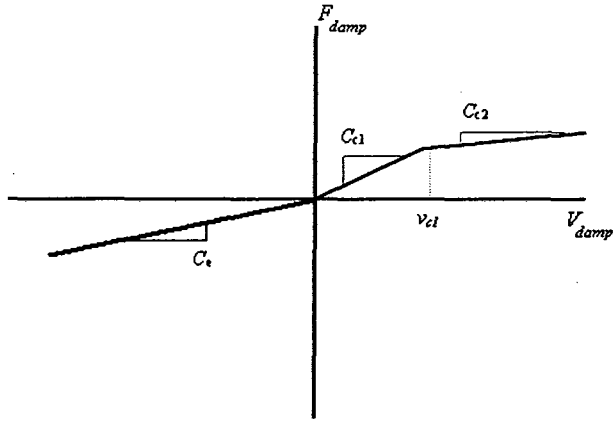

Figure 2.13: Passive damper model

2.4.7 Elastic End-Stops

The elastic motion limiting end-stops are modeled as clearance springs. The end-stops are generally designed as conical rubber elements, which yield relatively lower stiffness under light impacts. The spring rate, however, increases significantly under higher deformations cause by more severe impacts. A two stage piecewise affined model, proposed by Rakheja et al. [39], is employed in the suspension seat model for deriving the force developed during end-stop impacts. The model comprises a clearance spring designating the suspension travel and a relatively high stiffness coefficient near the end of the travel followed by an even higher stiffness coefficient, as shown in Figure 2.14. The function is presented through five intervals:

$$F_b = \begin{cases} 0 & -d_e \le y_s \le d_c \\ k_{c1}(y_s - d_c) & d_c < y_s \le h_{c1} \\ k_{c1}(h_{c1} - d_c) + k_{c2}(y_s - h_{c1}) & h_{c1} < y_s \\ k_{e1}(y_s + d_e) & -h_{e1} \le y_s < -d_e \\ -k_{e1}(h_{e1} - d_e) + k_{e2}(y_s + h_{e1}) & y_s < -h_{e1} \end{cases} \tag{2.34}$$

where k_{c1} and k_{c2} are the linear stiffness coefficients of the compression buffer, k_{e1} and k_{e2} are the corresponding coefficients of the extension buffer, and h_{c1} and h_{e1} are the transition positions for the compression and extension buffers, respectively.

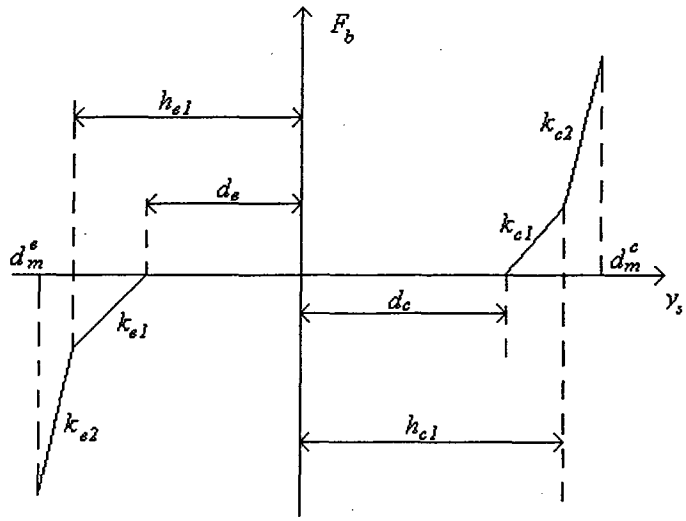

Figure 2.14: End-stops model

2.4.8 Summary of the Passive Suspension Seat Model

The proposed kineto-dynamic model of the passive suspension seat employs the forces developed by various suspension components together with the suspension kinematics described in sections 2.4.2 to 2.4.7. These include (1) the cushion force due to the equivalent cushion stiffness K_c and cushion damping C_c coefficient; (2) suspension spring force F_s related to equivalent suspension stiffness K_s; (3) friction force generated by the suspension linkages F_f; (4) equivalent vertical damping force F_d related to suspension geometry and instantaneous damper velocity V_{damp}; and (5) the elastic end-stop forces F_b. Table 2.4 summarizes the parameters of the suspension seat model. The friction function parameters, however, are determined in the subsequent chapter.

2.5 Summary

In chapter 2, a model describing the force-velocity characteristics of the MR damper was described as a function of the applied current on the basis of measured properties. The proposed MR damper model is based on the bi-viscous model, while the current dependency was

Table 2.4: Suspension seat model parameters

	Parameters	Values	Parameters	Values
Cushion	K_c	*29977N/m*	C_c	*938Ns/m*
Suspension	K_s	*6075N/m*	L	*0.4318m*
	h_{max}	*0.1905m*	h_{min}	*0.0381*
	β	*0.4924*	γ	*0.9826*
	a	*0.1293*	b	*0.0290*
	c	*0.047*	d	*0.180*
Elastic End-Stops	k_{c1}	*12500N/m*	k_{c2}	*93800N/m*
	k_{e1}	*10800N/m*	k_{e2}	*60000N/m*
	h_{c1}	*0.0865m*	h_{e1}	*0.0806m*
	d	*0.07m*		
Passive Damper	C_{c1}	*6130Ns/m*	γ_c	*0.40*
	v_{c1}	*0.115m/s*	p	*0.79*

introduced by a first order polynomial function in the current. The coefficients of the damper model were determined through least square regression, and its validity was demonstrated using the measured data over wide ranges of current and excitations. An analytical model of the seat suspension system was developed incorporating the kinematics due to suspension linkages, the damper kinematics, the cushion's equivalent linear characteristics, and the end-stops properties. The model validity is explored in the following chapter under different inputs. The suspension seat model is mainly based on laboratory measured data.

CHAPTER 3: MODEL VALIDATION AND PERFORMANCE MEASURES

3.1 Introduction

A suspension seat is generally designed for a wide range of vehicles. The suspension may thus be required to perform under varying excitations arising from different target vehicles. Owing to the nonlinear properties of the suspension, a suspension may either attenuate or amplify the vehicle vibration depending upon the nature of vibration of the target vehicle. The design and performance assessments of the seat suspension are thus generally carried out under excitations arising from different vehicles [20]. The frequency response characteristics and end-stop impact performances, on the other hand, can be best evaluated under swept harmonic and transient inputs, respectively. While several studies have employed sinusoidal inputs for model validations or part of their experimental work [20,39,104], only a few studies have employed intensity transient inputs to investigate occurrence of end-stop impacts under road induced shock motions arising from potholes or extreme unevenness in off-road conditions [25,90,105]. The vibration characteristics of different classes of vehicles have been defined by their acceleration spectra. These are based on extensive field measurements under representation work conditions, and have been defined for city buses, side walk snowploughs, industrial trucks and various wheeled and tracked earthmoving vehicles [37,38]. The vibration spectra of such vehicles have been defined by transfer functions, which may be conveniently applied in the laboratory for experimental assessments of suspension seats, and to the suspension seat models to identify vehicle specific suspension design.

In this chapter, the vibration spectra of selected classes of vehicles and transient excitations are synthesized and applied to examine validity of the suspension seat model coupled with a passive hydraulic damper. The model validity is demonstrated using the reported measured data for a suspension seat. The suspension model with the MR damper is further evaluated under defined inputs. The performance characteristics of the suspension seat are evaluated using the seat effective acceleration transmissibility (SEAT), and vibration dose value (VDV) measures based upon both unweighted and frequency-weighted acceleration inputs and responses, as defined in ISO – 2631 – 1 [38].

3.2 Description of Inputs

In vibration studies, the types of inputs as well as their amplitude are important factor towards the evaluation of the system response. Often, a single type of input and amplitude combination is insufficient to test the various properties and characteristics of the system. The International Standards Organization (ISO-7096) has provided input spectra, of different categories of earth moving machineries [38]. Boileau et al. [10] defined vibration spectra of urban buses and sidewalk snowploughs on the basis of several field measurements. The study also defined transfer functions to derive vibration spectra of such vehicles for assessment of suspension seats. The inputs provided by the two cited works, coupled with harmonic and transient inputs are considered to suffice the ranges of excitations for evaluation of performance of suspension seats.

3.2.1 Harmonic Input

A harmonic input serves as the basic input to characterize the system's frequency response characteristics. A swept harmonic input at the suspension base is employed to examine the model

validity using the reported data for a passive suspension seat system [39]. The reported data was acquired under constant displacement harmonic input (amplitude = *0.025m*) in the *0.5* to *2Hz* frequency range, while a constant acceleration amplitude of $3.95m/s^2$ was imposed in the *2* to *10Hz* range. Such an input permits high displacement excitation at lower frequencies and limits acceleration magnitude at higher frequencies, and thereby ensures safety of the test system and human subjects, if involved, in the laboratory tests.

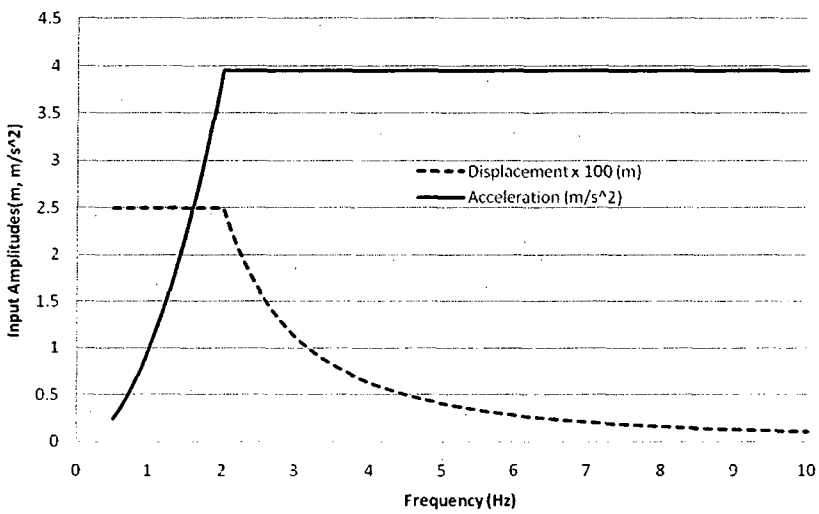

Figure 3.1: Harmonic Input Amplitudes

3.2.2 Random Vehicular Inputs

Random vibration spectra of three different vehicles are considered for evaluations of the suspension seat model and for synthesis of the MR damper semi-active control laws. These include a city bus, an earthmoving vehicle, and a sidewalk snowplough. The spectra of mean vibration measured at the seat base of vehicles have been defined via transfer functions [10,38]. The convolution of the given transfer function with white noise random vibration can yield a synthesis of time histories of seat base vibration of the selected vehicles under representative operating conditions. An arbitrary gain ($k > 1$) may further be applied to achieve high intensity vibration of such vehicles subject to more severe terrain conditions.

Boileau et al. [10] has defined a transfer function for characterizing the vertical ride vibration of a city bus, referred to as 'BUS'. The vibration spectrum reveals vertical mode resonant frequency near *1.3Hz*. The implementation of a suspension seat with natural frequency in the order of *1.25Hz* may cause repetitive end-stop impacts leading to high intensity vibration at the driver seat. The transfer function describing the bus vibration is given by:

$$G(s)=\left\{K_m \frac{s\left(s^2+A_{m1}s+B_{m1}\right)}{\prod_{i=1}^{2}\left(s^2C_{mi}s+D_{mi}\right)}\right\} \tag{3.1}$$

where the constants K_m, A_{mi}, B_{mi}, C_{mi}, and D_{mi} are defined in Table 3.1.

The vertical vibration characteristics of side-walk snowplough, referred to as 'SNOW', were also defined by the same transfer function in Eq. (3.1). The values of the corresponding constants are summarized in Table 3.1. The vibration spectrum reveals predominant vibration around the vertical mode resonance of the tracked snowplough near *4Hz*.

The vibration characteristics of a class one earthmoving vehicle, denoted as 'EM1' has been defined in ISO-7096 [38] through the following transfer function:

$$G(s)=\left\{K_m \frac{s^4}{\prod_{i=1}^{2}\left(s^4+A_{mi}s^3+B_{mi}s^2+C_{mi}s+D_{mi}\right)}\right\} \tag{3.2}$$

where the constants K_m, A_{mi}, B_{mi}, C_{mi}, and D_{mi} are listed in Table 3.1.

The earthmoving vehicle vibration spectrum reveals its vertical mode resonance near 2Hz, while the peak acceleration power spectral density was significantly higher than the city bus. This was attributed to the absence of primary suspension and large diameter soft tires.

Table 3.1 Vehicle vertical vibration transfer function coefficients (bus: BUS, snowplough: SNOW, class one construction vehicle: EM1)

Vehicle	Coefficients									
	K_m	K_m(severe)	A_{m1}	B_{m1}	C_{m1}	D_{m1}	A_{m2}	B_{m2}	C_{m2}	D_{m2}
BUS	*9.99*	*13.35*	*13.13*	*1405.83*	*31.98*	*4352.5*	-	-	*4.62*	*82.9*
SNOW	*18.6*	*29.76*	*8.48*	*476.11*	*7.29*	*712.98*	-	-	*10.12*	*157.91*
EM1	*10200*	*14280*	*24.8*	*303.25*	*2200*	*7890*	*41.33*	*842.37*	*10200*	*60900*

The study also considered amplified vibration spectra of selected vehicles to study the responses to high intensity vibration leading to potential end-stop impacts. Those spectra are designed by 'BUSA', 'SNOWA', and 'EM1A', respectively, and were obtained by multiplying K_m by a factor of *1.5*. Furthermore, due to the low intensity of the 'BUS' input, a 'BUS2A' input, representing 200% of the 'BUS' input, is also considered. The vehicular excitations were synthesized using a white noise vibration signal filtered through the transfer functions defined in Eqs. (3.1) and (3.2). The synthesized time-histories were sampled at a frequency of *1024Hz* over *128s*. A total of *131072* data points were thus used to estimate the power spectral density (PSD) of the acceleration signals. The acceleration PSD of the synthesized vehicle excitations time histories selected vehicles are presented in Figure 3.2 together with their PSD of the amplified vibration. The spectra clearly show predominant vibration of the bus and the earthmoving vehicle near *1.3* and *2Hz*, respectively. The vibration spectra of the snowplough reveal peaks near *2.1* and *4.1Hz*.

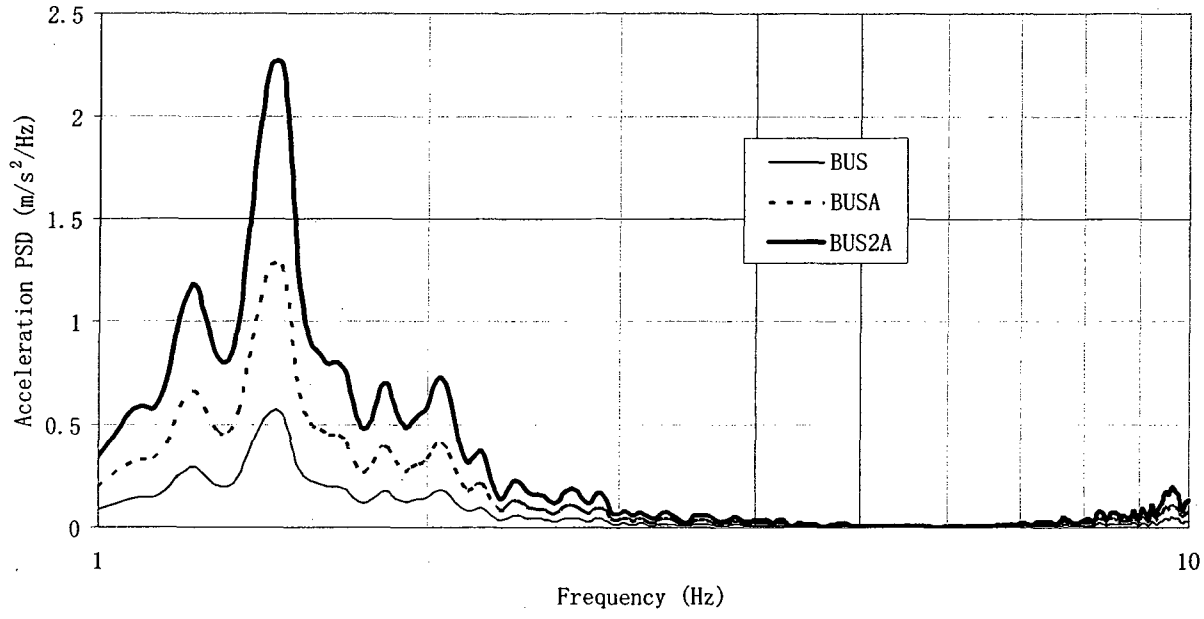

(a)

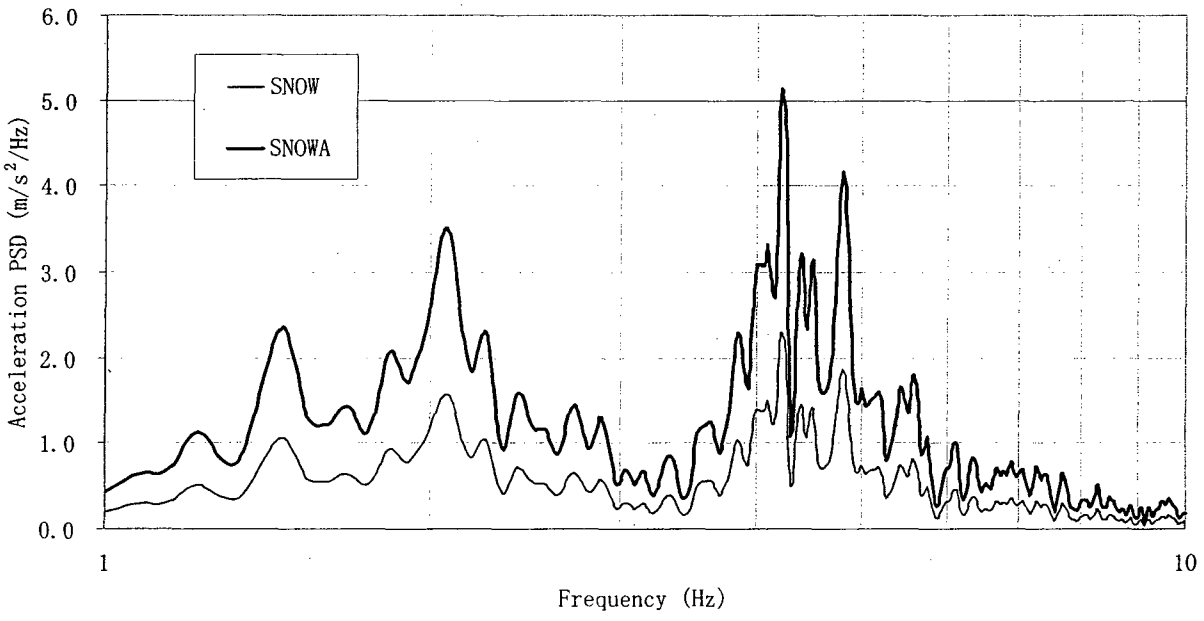

(b)

Figure 3.2: Power spectral density of vertical accelerations measured at the seat base of selected vehicles together with their amplified vibration: (a) BUS; (b) SNOW; and (c) EM1 (Continued)

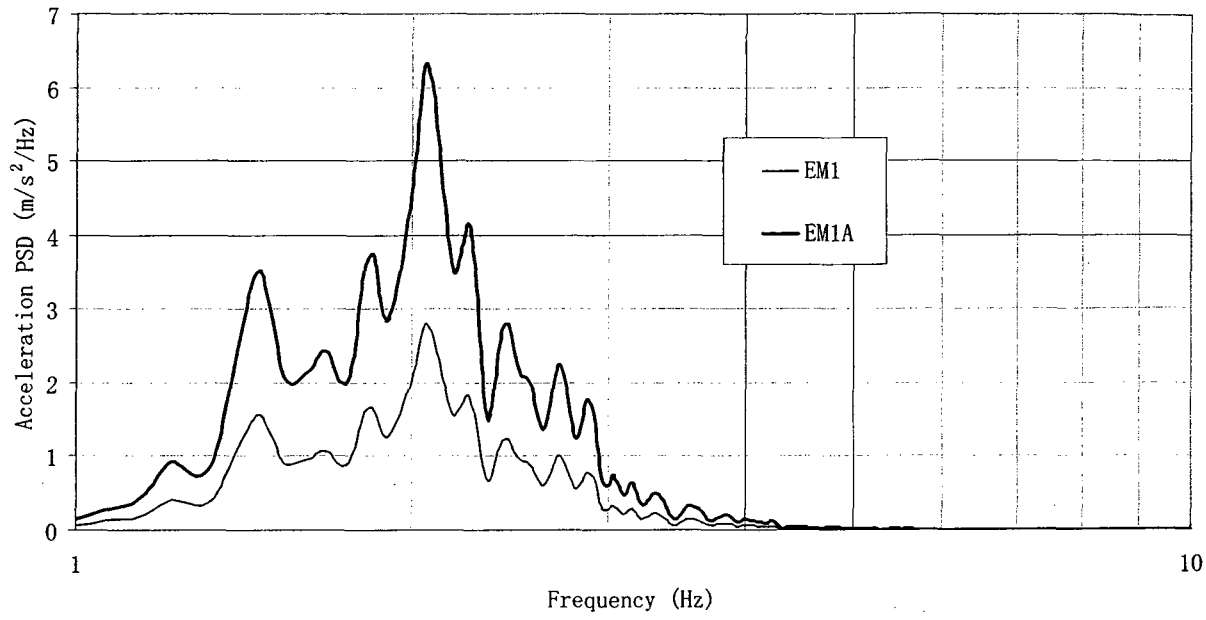

(c)

Figure 3.2: Power spectral density of vertical accelerations measured at the seat base of selected vehicles together with their amplified vibration (a) BUS, (b) SNOW, and (c) EM1

3.2.3 Transient Input

A vehicle's interactions with an abrupt discontinuity in the terrain profile causes exponentially decaying oscillations of the vehicle mass at the vertical mode resonant frequency [9]. Such oscillations may exhibit large magnitude and induce end-stop impacts of the suspension seat. A transient excitation with oscillations at the natural frequency of the candidate suspension seat (*1.25Hz*) is thus synthesized to study the end-stop impact performance of the suspension seat. A transient oscillation waveform is illustrated in Figure 3.3. The magnitude of the transient excitation can be adjusted to (reduced or augmented) achieve end-stop impact. Figure 3.4 shows the transient input function in terms of base acceleration since acceleration input is required for the suspension seat model developed in Chapter 2.

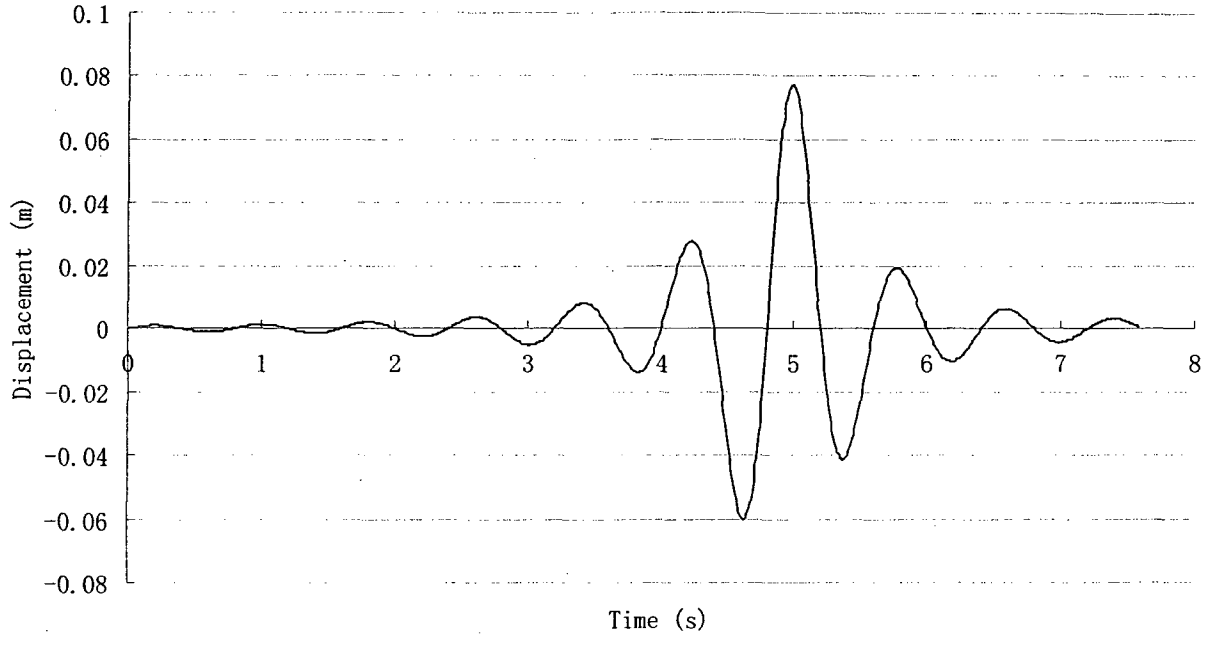

Figure 3.3: Transient input displacement function

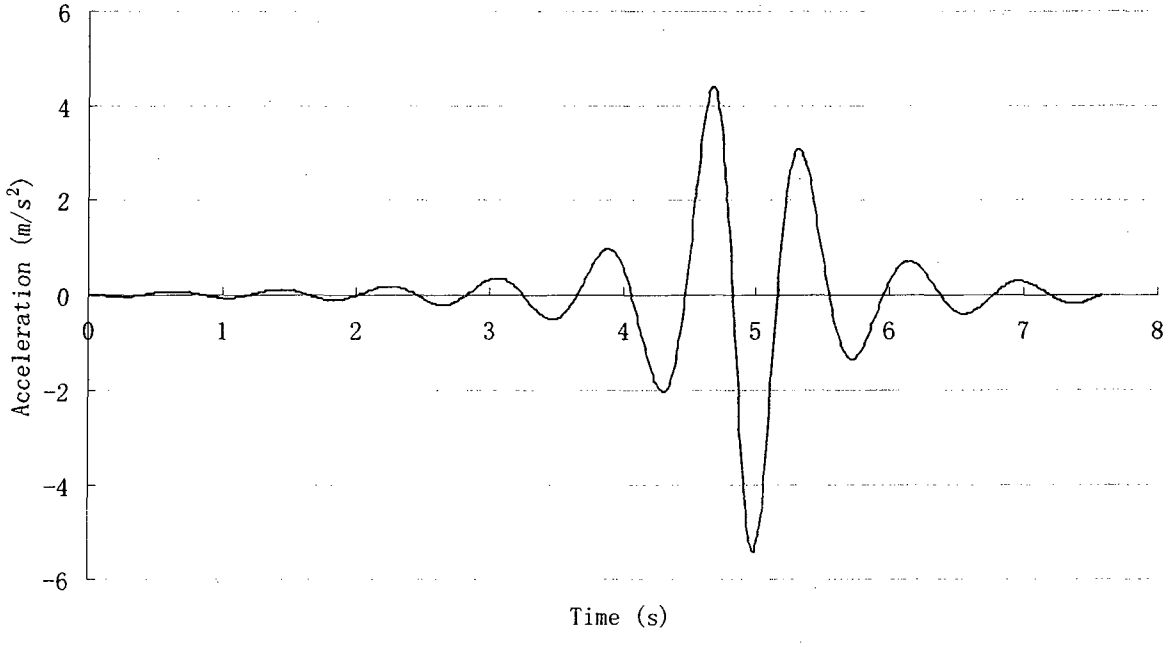

Figure 3.4: Transient input acceleration function

3.3 Performance Measures

The vibration isolation performance characteristics of suspension seats have been evaluated using different measures, which are invariably based on the acceleration response at the occupant-seat interface [37,38]. The suspension seat performance in this study is evaluated using five different performance measures: (1) the root-mean square acceleration (*rms*) at the seat cushion, which describes the occupant exposure to vibration; (2) the crest factor of response acceleration, which evaluate end-stop impacts power; (3) the seat effective amplitude transmissibility, which describes the isolation effectiveness of the seat; (4) the vibration dose value; and (5) the vibration dose value ratio, which take into account the shock content of the exposure. Each of these five performance measures can be evaluated using unweighted or frequency-weighted accelerations in accordance with weighting defined in ISO-2631-1 [37], which accounts for human susceptibility to vibration. The methods of analysis of the selected measures are described below.

3.3.1 Root-Mean Square Acceleration

The root-mean square (*rms*) acceleration is a positive value representing the level of energy over defined exposure duration. The *rms* acceleration and the frequency-weighted rms acceleration are computed from:

$$a_c = \sqrt{\frac{1}{T}\int_0^T \ddot{x}_c^2(t)dt}\ ;\ a_b = \sqrt{\frac{1}{T}\int_0^T \ddot{x}_b^2(t)dt}\ ;\ a_{wc} = \sqrt{\frac{1}{T}\int_0^T \ddot{x}_{wc}^2(t)dt}\ ;\ a_{wb} = \sqrt{\frac{1}{T}\int_0^T \ddot{x}_{wb}^2(t)dt} \qquad (3.3)$$

where a_c and a_b are the *rms* accelerations at the seat cushion and the base, and a_{wc} and a_{wb} are the corresponding frequency weighted accelerations, respectively. $\ddot{x}_c(t)$ and $\ddot{x}_b(t)$ are the instantaneous accelerations at the seat cushion and the seat base, respectively, and $\ddot{x}_{wc}(t)$, and

$\ddot{x}_{wb}(t)$ are the respective frequency-weighted instantaneous accelerations. T is the exposure duration.

3.3.2 Crest Factor

The crest factor is the ratio of the maximum absolute acceleration of the seated mass to the *rms* acceleration of the seated mass. The crest factor represents the severity of the maximum impact with respect to the average vibration. A high crest factor implies that there is at least a single severe impact motion. The crest factors associated with base and response acceleration are computed from:

$$CF_c = \frac{\max|\ddot{x}_c|}{a_c};\ CF_b = \frac{\max|\ddot{x}_b|}{a_b};\ CF_{wc} = \frac{\max|\ddot{x}_{wc}|}{a_{wc}};\ CF_{wb} = \frac{\max|\ddot{x}_{wb}|}{a_{wb}} \tag{3.4}$$

where CF_c and CF_b are the crest factors associated with the cushion and base acceleration signals, respectively, and CF_{wc}, and CF_{wb} are the respective values of the frequency-weighted cushion and base acceleration.

3.3.3 Seat Effective Amplitude Transmissibility Value

The seat effective amplitude transmissibility (*SEAT*) value is the ratio of *rms* frequency-weighted and unweighted acceleration measured at the seat to that at the base, such that [37]:

$$SEAT_{wc} = \frac{a_{wc}}{a_{wb}} \tag{3.5}$$

where $SEAT_{wc}$ is the frequency weighted *SEAT* value. The *SEAT* value represents the overall vibration transmissibility of the suspension over the frequency range of interest. A higher *SEAT* value implies the transmission, of greater base vibration to the seated occupant. The suspension

seats are thus designed to attain a lower *SEAT* value. The overall vibration isolation effectiveness of a suspension seat could also be defined on the basis of unweighted accelerations, such that:

$$SEAT_c = \frac{a_c}{a_b} \tag{3.6}$$

where $SEAT_c$ defines the unweighted *SEAT* value. Although the *SEAT* measure provides isolation effectiveness of the seat by a simple number, it lacks the emphasis of the frequency response behaviour of the suspension. Furthermore, the contributions due to shock motions tend to be relatively small due to considerations of the *rms* accelerations.

3.3.4 Vibration Dose Value

In order to account for the effect of shock motions of a seat suspension, a measure based on fourth power performance has been recommended [37,38]. The measure is referred to as the vibration dose value (*VDV*). The *VDV* due to accelerations at the seat and the base are computed from either the frequency-weighted or unweighted accelerations, such that:

$$VDV_c = \sqrt[4]{\int_0^T \ddot{x}_c^4(t)dt}\,; \qquad VDV_{wc} = \sqrt[4]{\int_0^T \ddot{x}_{wc}^4(t)dt}\,;$$

$$VDV_b = \sqrt[4]{\int_0^T \ddot{x}_b^4(t)dt}\,; \qquad VDV_{wb} = \sqrt[4]{\int_0^T \ddot{x}_{wb}^4(t)dt} \tag{3.7}$$

where VDV_c and VDV_b are the *VDV* values for the seat response and base input, respectively, and VDV_{wc} and VDV_{wb} are the respected frequency-weighted *VDV* values based on the accelerations.

Similar to the *SEAT* measure, the *VDV* ratio is defined as the measure of effectiveness of a suspension seat in attenuating high intensity vibration shock motions. The *VDV* ratio based upon frequency-weighted and unweighted *VDV*, are defined as:

$$VDVr_c = \frac{VDV_c}{VDV_b}; \qquad VDVr_{wc} = \frac{VDV_{wc}}{VDV_{wb}} \tag{3.8}$$

The *VDV* ratios approach the respective *SEAT* values when the base vibration is free from shock motions and in the absence of suspension end-stop impacts [37].

3.4 Validation of the Passive Suspension Seat Model

The suspension seat model, presented in Chapter 2, was initially validated considering the passive damper. The model simulations were performed using the measured component characteristics reported by laboratory experiments [39]. The reported data included the damper force-velocity characteristics along the damper axis, assuming two-stage compression damping and single-stage rebound damping, equivalent vertical stiffness due to air spring, cushion properties, and the equivalent vertical static friction. The parameters of the kineto-dynamic suspension seat model have been summarized in table 2.4.

The reported suspension parameters [39], particularly the friction force and the suspension stiffness, were measured along a vertical-axis, while the kinematics due to the suspension was not considered. The application of this data to the proposed suspension model was thus expected to yield some errors. Furthermore, the suspension mass had not been characterized in the previous studies, possibly due to its relatively small effect, its large variations in different designs, and difficulties associated with its measurement. However, a mass value ranging from *5* to *20kg* has been generally considered acceptable [20,39,112,113].

The coulomb friction force is generally defined as the lumped vertical force due to roller-guides, bushings, and damper seal friction, eventhough the roller-guide friction force acts along a horizontal axis. Moreover, the reported studies have measured only static force, which would be

considerably larger than the dynamic friction force. A better estimate of Coulomb friction could be attained through comparison of the low frequency vibration response of the suspension seat with the measured data followed by an iterative parameter identification process.

For this purpose, the F_{sat} was initially assumed as *35N*, while the suspension mass was considered as *5kg*. Simulations were performed to derive the frequency response characteristics of the suspension model under harmonic excitation defined in Figure 3.1. It should be noted that the same excitation was used in the measurement of the frequency response characteristics in the laboratory. The responses were obtained for a seated rigid mass of *77kg*. The simulation results are compared with the measured acceleration transmissibility in Figure 3.5. The comparison reveals discrepancies between the model results and the measured data.

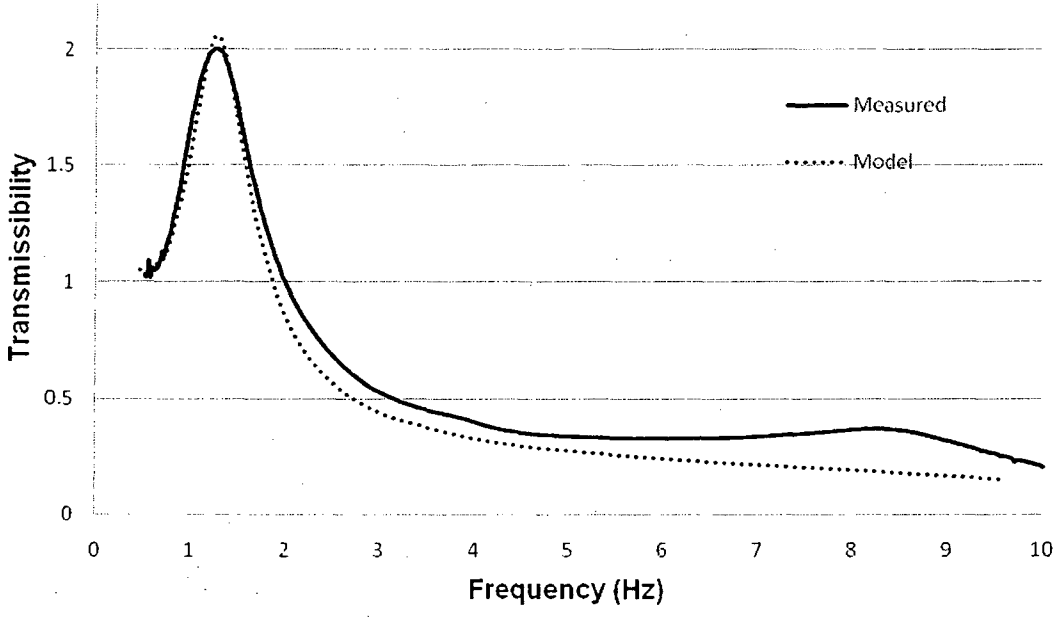

Figure 3.5: Comparison of the suspension seat model transmissibility response and the laboratory measured seat transmissibility response

The natural frequency of the model was observed to be slightly higher than the measure value by only *0.03Hz*, while the peak transmissibility of the model was only slightly higher by

0.06. Considerable differences, however, are evident at frequencies above *2Hz*. These discrepancies were believed to be caused by lack of consideration of the linkage kinematics and possible jumping of the rigid mass from the seat surface, particularly at higher frequencies during laboratory experiment. This is evident from the model response, which does not exhibit secondary peak near *8.25Hz*. The suspension mass and Coulomb friction force parameters were subsequently adjusted to achieve better agreement in the suspension resonance frequency and peak transmissibility. The results suggested that an increase in the suspension mass (m_s = *10kg*) and Coulomb friction force (F_{sat} = *40N*) would yield better match with the experimental data. These adjustments resulted in better agreements in the natural frequency and peak transmissibility, but also showed lesser discrepancies at higher frequencies, as shown in Figure 3.6. Due to the linearization of several components, it is impossible to obtain a perfect match between the measured data and the model, however the error from *1* to *5Hz* varies from *0.01%* to *20%*. These extremes correspond to the resonance frequency of *1.25Hz* and *2Hz* respectively.

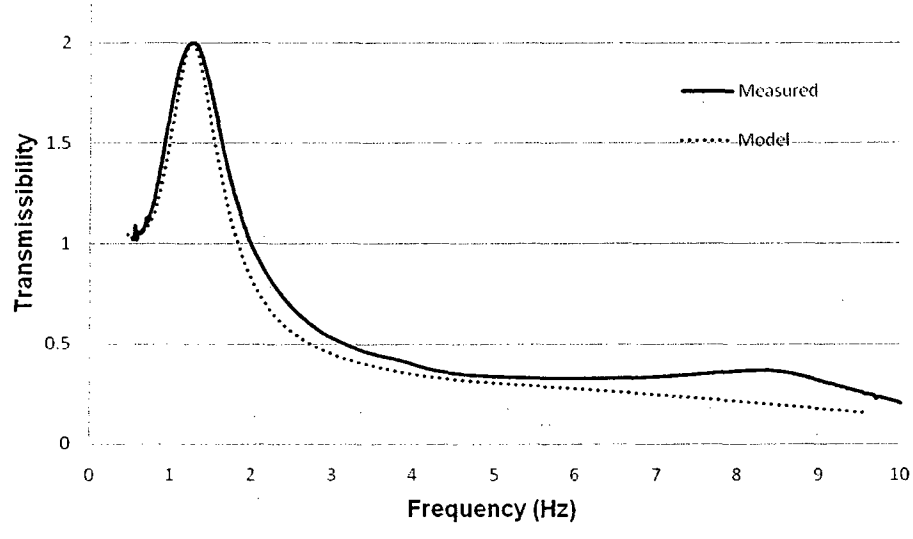

Figure 3.6: Comparison of model acceleration transmissibility with the measure response (refined parameters: m_s = *10kg*; F_{sat} = *40N*) [39]

3.4.1 MR Damper Suspension Seat Response in Passive Mode

The MR damper is considered to operate in the passive mode under the application of a constant current. The response characteristics of the suspension seat model with the MR damper replacing the passive hydraulic damper are evaluated under the same harmonic excitation at discrete frequencies in the *0.5* to *10Hz* range. The simulations are performed for different current settings, namely 0A, 0.1A, 0.15A, 0.20A, 0.30A, 0.5A, and 0.75A, and the responses are evaluated in terms of the acceleration transmissibility. Figure 3.7 presents comparisons of the acceleration transmissibility responses of the MR damper suspension seat corresponding to different constant currents in the *0* to *2A* range.

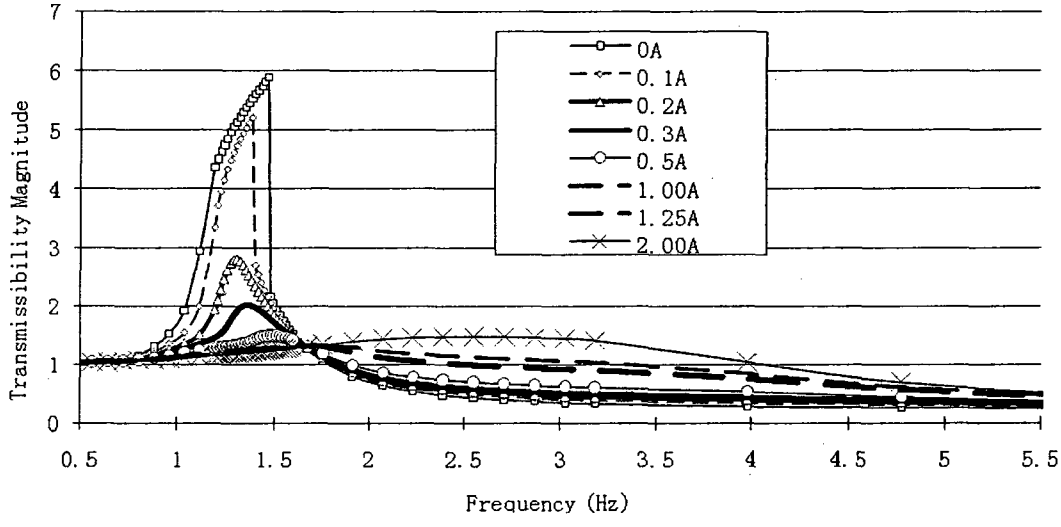

Figure 3.7: Comparisons of acceleration transmissibility responses of the suspension seat model with a MR damper subject to different constant currents

The results shows occurrence of end-stop impacts for damper currents at *0.1A* or lower current settings, which is shown by the unusual shape of the resonance peak comprising a sharp drop in transmissibility in the *1.4* to *1.5Hz* range. During simulations, end-stop impacts were recorded near the resonance frequency of the suspension seat. Due to the end-stop impacts, the

resonance frequency at low current settings cannot be determined through the transmissibility response. Nevertheless, the transmissibility response at *0.2A* gives a fair estimate of the suspension seat's natural frequency (*1.3Hz*). The occurrence of end-stop impacts suggests that the operation of the suspension seat featuring MR damper may cause serious shock motion to the occupant when the damper current can no longer be maintained or controlled such as: coil failure, controller failure, or power supply failures. The problem can be remedied by adjusting the angle of the MR damper in order to increase its effective damping force or by employing an MR damper with higher damping force at idle condition.

The results in Figure 3.7 further demonstrate that an increase in the damper currents yields considerably higher damper force, which causes the resonant transmissibility to decrease. The natural frequency of the suspension also increases with the applied current, as seen in Figure 3.7. This was attributed to greater coupling between the cushion and the suspension modes under higher suspension damping. An Eigen-value analysis of a linear two-DOF suspension seat model was conducted to verify the damping effect on the primary resonant frequencies. The results confirmed that an increase in suspension damping yields higher primary resonance and an overdamped suspension mass mode. The simulation results also show poor vibration isolation performance of the suspension seat under higher damper currents. For instance, application of *1A* current yields attenuation of vibration only at frequencies above *2.5Hz*, and damping does not occur until *4Hz* for current setting of *2A*.

The acceleration transmissibility responses of the MR damper suspension seat model were also compared with those of the passive damper seat model. The results were compared in an attempt to identify a MR damper current that yields response comparable to the passive suspension seat. It was concluded that a current setting of *0.31A* would yield acceleration

transmissibility close to that of the passive suspension seat model. Figure 3.8 illustrates comparison of the acceleration transmissibility of the passive and MR damper (*0.31A*) suspension seat models. The results show slightly higher frequency of the MR damper seat model, which is attributed to the small pre-yield range of the MR damper (v_t = *0.027m/s*). As the response increase toward its resonance peak magnitude, an increase in the slope can be observed in Figure 3.8. The sudden change in slope represents the frequency at which the damper starts operating in both pre- and post-yield conditions, thus yielding a higher peak at a slightly higher frequency. The low frequency response of the MR damper suspension is lower than the passive damper suspension, which is most likely caused by the high pre-yield damping coefficient of the MR damper. The results also reveal that the MR damper equivalent harmonic response corresponds perfectly with the passive hydraulic response in the *1.35Hz* to *2.1Hz* range. A small increase in amplitude of the MR damper can be observed from *2.1Hz* to *8Hz*, within which the second peak of the MR damper constant current harmonic response shows its second peak under high current input (Figure 3.8).

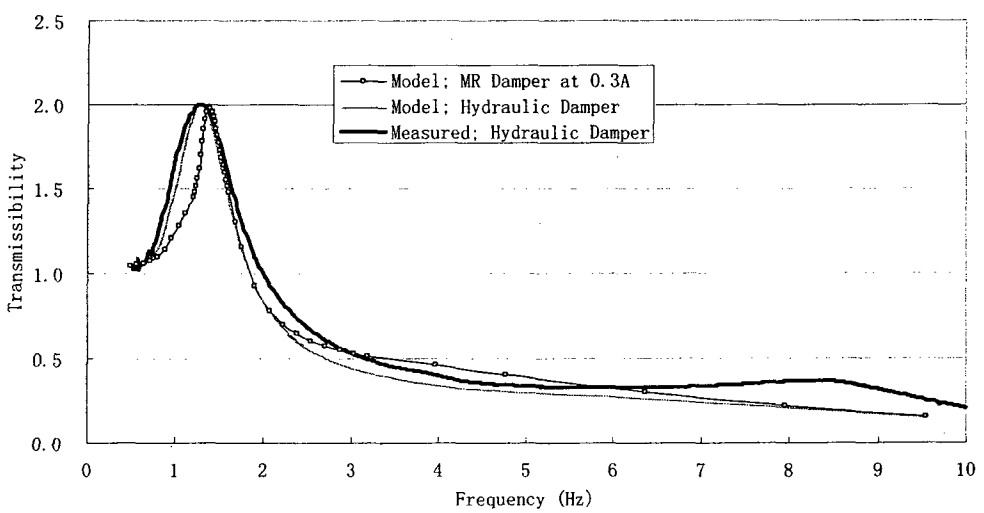

Figure 3.8: Comparison of MR damper suspension seat model (*i =0.31A*) response with the passive suspension model [39]

3.4.2 Passive Suspension Seat Response to Random Vehicular Excitations

The vibration attenuation performance of the suspension seat model are further investigated under random vibration excitations of selected vehicles, namely, 'BUS', 'SNOW', and 'EM1', as described in section 3.2.2. The responses are also evaluated under the amplified vibration spectra ('BUSA', 'SNOWA', 'EM1A', and 'BUS2A').

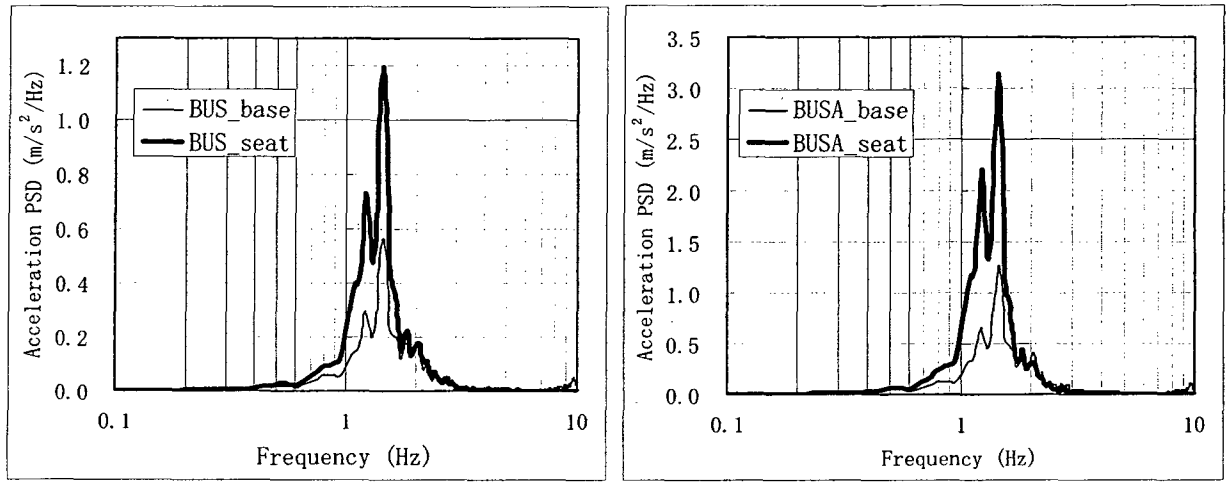

(a) (b)

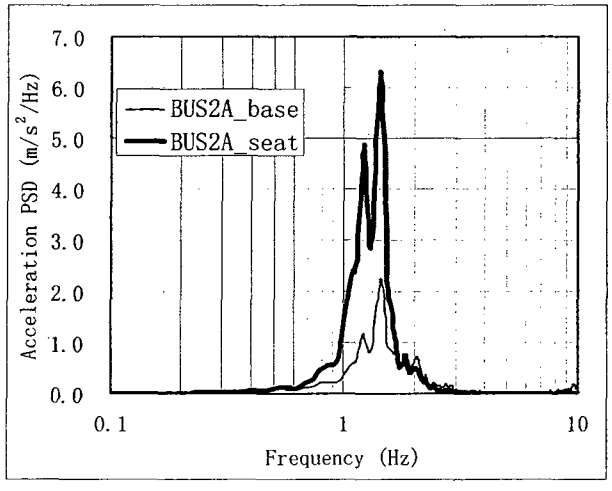

(c)

Figure 3.9: Comparison of response acceleration PSD and excitation acceleration PSD: (a) BUS, (b) BUSA, (c) BUS2A

Figure 3.9 presents comparisons of acceleration PSD of the passive suspension seat to BUS, BUSA, and BUS2A excitations with the input acceleration PSD. The acceleration PSD reveal suspension model resonance in the vicinity of *1.3Hz*. The results clearly show that the passive suspension would amplify the bus floor vibration due to its very low frequency components. The model responses, however, exhibited only slight end-stop impacts under 'BUS2A' input. The increase in transmissibility with higher amplitude inputs can also be partially attributed to the large variability of the damper angle, which in turn varies greatly the effective damping force and the damper speed. The end-stop impacts, however, were clearly observed under SNOWA and EM1A excitations, which resulted very large resonant acceleration PSD, as seen in Figure 3.10. Slight amount of end-stop impacts were also observed during simulations. The acceleration PSD responses to BUS and SNOW excitations were comparable with those reported in the IRSST report on bus floor and snowplough vibrations [10]. The EM1A excitation, with its predominance around *2Hz*, resulted in slightly more frequent and severe impacts compared to those occurring under SNOWA excitation with predominant frequencies around *2Hz* and *4.5Hz*. Furthermore, the magnitude acceleration PSD due to SNOW excitation around *2Hz* are significantly lower than those of EM1 excitations. The suspension seat effectively suppress the SNOW excitation peak near *4.5Hz*.

The acceleration responses to vehicular excitation were further analyzed using performance measures to assess the suspension performance. The responses were thus evaluated in terms of frequency-weighted and unweighted *rms* accelerations (a_{wc}, a_c), VDV, crest factors, SEAT, and VDVr, as described in section 3.3. The computed performance measures of the passive suspension seat model are summarized in Table 3.8 for the selected vehicular excitations. The

table also summarizes the measures corresponding to seat base excitation such as frequency-weighted and unweighted *rms* acceleration (a_{wb}, a_b), VDV_b, VDV_{wb}, CF_b, and CF_{wb}.

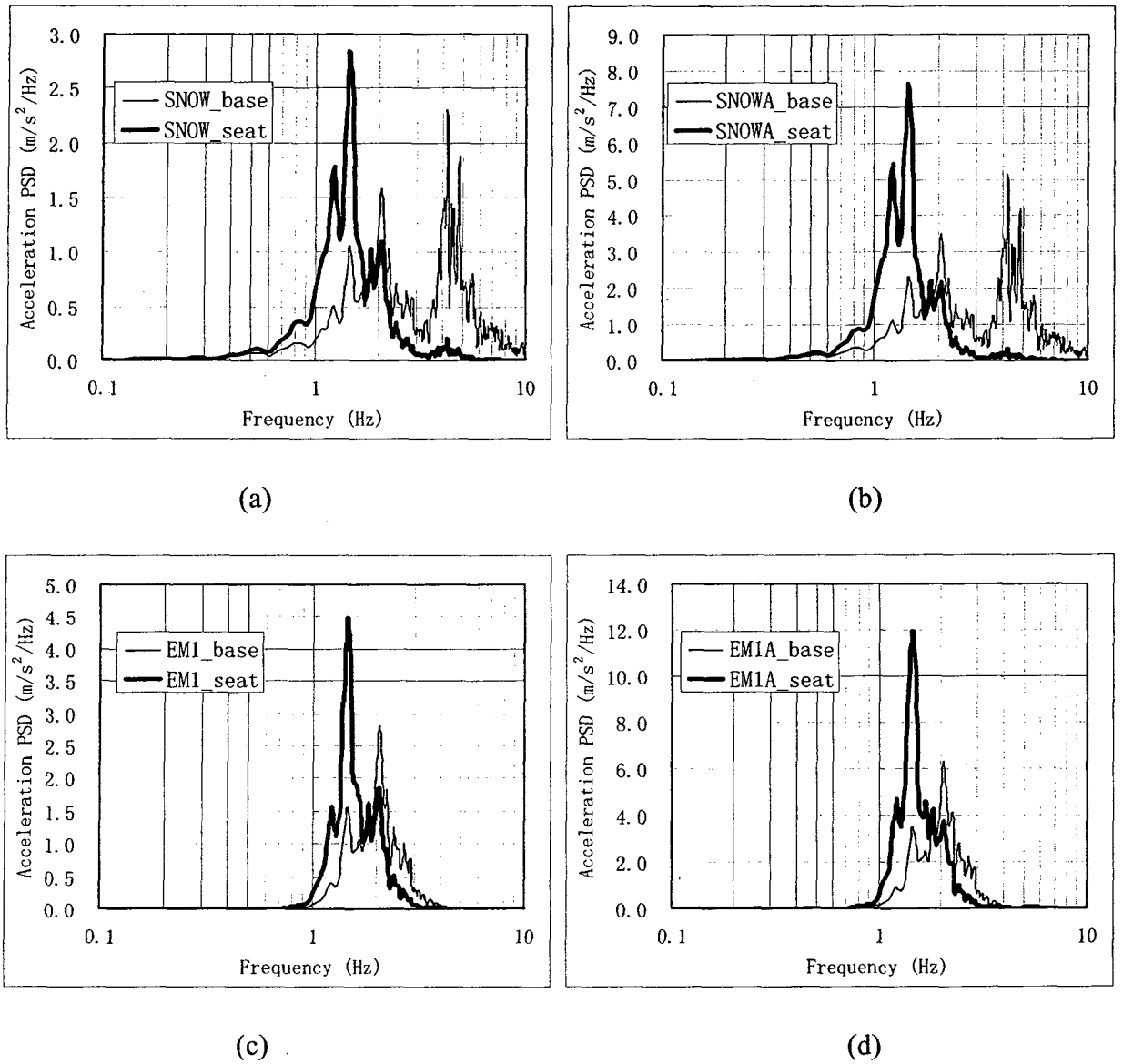

Figure 3.10: Comparison of response acceleration PSD and the excitation acceleration PSD: (a) SNOW, (b) SNOWA, (c) EM1, and (d) EM1A

The results reveal that the VDVr and the SEAT values are quite comparable under nominal vehicular inputs, which is attributed to the absence of end-stop impacts. These two measures, however, differ under amplified vehicular excitations, particularly for EM1A excitations, which

suggest the occurrence of end-stop impacts. The results further demonstrate that the frequency-weighted measures are considerably smaller than the corresponding unweighted values, particularly under BUS and EM1 excitations. This can be attributed to predominance of city bus and construction vehicle excitations at frequencies less or equal to *2Hz*. The predominance of snowplough vibration around *4.5Hz* yields somewhat comparable values of the frequency-weighted and unweighted *rms* acceleration and VDV at the seat base. The assessment of human exposure and suspension performance are mostly based on the frequency-weighted measures. The results also show that the seat amplitude transmissibility (SEAT) is close to unity under the EM1 and BUS excitations. This again is attributed to low frequency predominance of the excitations and low natural frequency of the suspension seat.

Table 3.8 Performance measures of the passive hydraulic suspension seat model

Excitation	BUS	BUSA	BUS2A	SNOW	SNOWA	EM1	EM1A
a_b	*0.85*	*1.27*	*1.69*	*2.26*	*3.38*	*1.49*	*2.24*
a_{wb}	*0.58*	*0.87*	*1.15*	*1.95*	*2.91*	*0.89*	*1.34*
a_c	*0.76*	*1.21*	*1.69*	*1.40*	*2.15*	*1.50*	*2.38*
a_{wc}	*0.40*	*0.61*	*0.85*	*0.80*	*1.19*	*0.80*	*1.26*
VDV_b	*3.73*	*5.60*	*7.46*	*10.11*	*15.09*	*6.55*	*9.82*
VDV_{wb}	*2.54*	*3.82*	*5.09*	*8.72*	*13.00*	*3.90*	*5.85*
VDV_c	*3.38*	*5.45*	*7.69*	*6.09*	*9.85*	*6.62*	*12.35*
VDV_{wc}	*1.65*	*2.61*	*3.69*	*3.31*	*5.14*	*3.31*	*6.42*
CF_b	*4.00*	*4.00*	*4.00*	*3.96*	*3.96*	*3.99*	*3.99*
CF_{wb}	*4.13*	*4.13*	*4.13*	*4.16*	*4.16*	*3.52*	*3.52*
CF_c	*3.71*	*3.74*	*3.77*	*3.71*	*5.87*	*3.52*	*7.45*
CF_{wc}	*3.31*	*3.50*	*3.48*	*2.98*	*5.49*	*3.45*	*7.83*
SEAT	*0.90*	*0.95*	*1.00*	*0.62*	*0.64*	*1.01*	*1.06*
$SEAT_w$	*0.70*	*0.71*	*0.73*	*0.41*	*0.41*	*0.89*	*0.94*
VDVr	*0.91*	*0.97*	*1.03*	*0.60*	*0.65*	*1.01*	*1.26*
$VDVr_w$	*0.65*	*0.68*	*0.73*	*0.38*	*0.40*	*0.85*	*1.10*

The SEAT values under SNOW excitations are in the order of only *0.6*, suggesting greater attenuation of vibration. This is clearly caused by effective attenuation of snowplough vibration in the vicinity of *4.5Hz*. The frequency-weighted SEAT measures of the suspension, however,

are considerably lower under the BUS and SNOW excitations, which again can be related to low frequency predominance of the BUS excitation and effective attenuation of high frequency components of the SNOW excitations. The $VDVr_w$ in most cases are also comparable since the predominant frequency of end-stop impacts is the suspension resonance frequency, which is significantly attenuated by the frequency-weighting filter. The VDVr, however, reflects the presence of end-stop impacts, thus, the end-stop impact performance assessment of a suspension seat should be based upon the VDVr, while the attenuation of continuous lower magnitude vibration may be adequately assessed using the SEATw.

3.4.3 Passive Suspension Seat Response to Transient Excitation

Abrupt discontinuities in road or terrain surfaces cause exponentially decaying oscillation of the vehicle mass around the vertical mode resonance frequency, which may yield transmission of high magnitude vibration to the seat/occupant mass. The magnitudes of transmitted vibration could be significantly higher when the vehicle resonance frequencies lie in the vicinity of the seat suspension resonance frequency, as in the case of a city bus. The transient excitations arising from a city bus may cause end-stop impacts under higher magnitudes of excitations. The suspension model responses to a transient excitation, defined in section 3.2.3, are evaluated to identify the energy required to initiate end-stop impacts [25]. The peak magnitude of the excitation was gradually increased until the occurrence of an end-stop impact. The simulation results revealed that a transient excitation of peak amplitude of $3.7m/s^2$ would cause an end-stop impact. Figure 3.11 illustrates the time-histories of displacement amplitude of the transient input and the acceleration of the seated mass, together with end-stop forces and relative suspension travel. The peak seat mass acceleration is approximately $7.5m/s^2$, which clearly shows significant amplification of the base acceleration. The peak relative displacement approaches or exceeds the

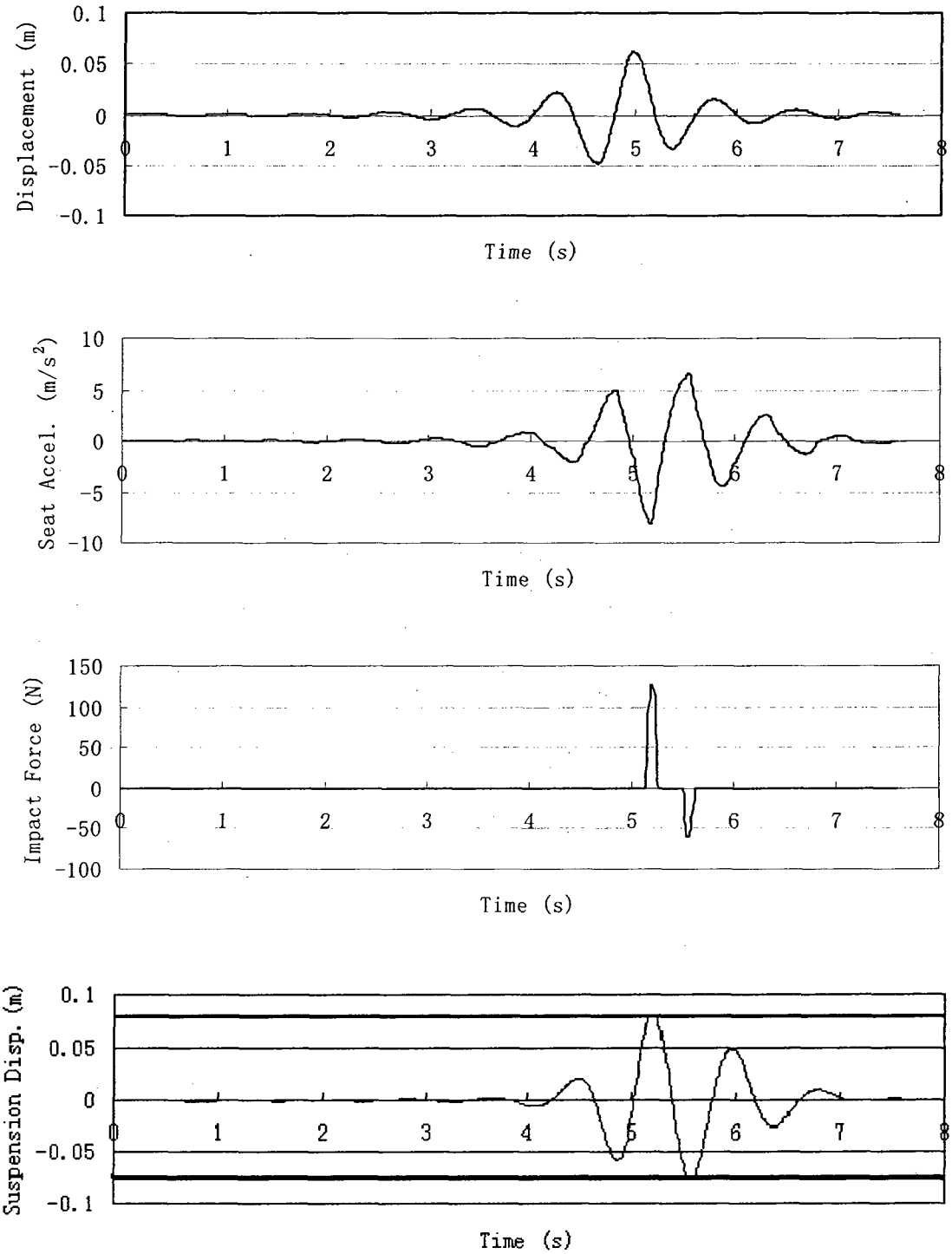

Figure 3.11: Transient base input displacement, seat acceleration, end-stop impact forces, and suspension relative displacement of the passive hydraulic suspension seat model under a transient input of *1.25Hz*

suspension travel near *5.2s*, which results in end-stop impact force. The results also show that the stronger impact occurred against the compression stop, since the corresponding suspension deflection was negative.

3.6 Summary

A kineto-dynamic model of the suspension seat was formulated upon consideration of contributions due to kinematics of suspension links and dynamics of the suspension components. A piecewise affine regression model of a MR damper was also proposed to predict damping force as a function of damper velocity and applied current. The validity of the damper and the passive suspension seat models was demonstrated under harmonic excitations. The performance characteristics of the passive suspension seat model were evaluated in terms of various frequency-weighted and unweighted measures such as *rms* seat acceleration, VDV, SEAT, and VDVr under different vehicular and transient excitations. Those measures are considered to serve as the reference values for assessment of semi-active suspension seat model in the subsequent chapter.

CHAPTER 4: PERFORMANCE ANALYSIS OF SUSPENSION SEAT SYSTEM USING CONTROLLED MAGNETO-RHEOLOGICAL DAMPER

4.1 Introduction

The behaviour and performance of the passive suspension seat model was investigated and validated in Chapter 3. The analysis showed that the passive suspension seat is effective at attenuating high frequency vibrations, while it generally amplifies the low frequency vibration of the bus and class one earthmoving vehicle. Moreover, the passive suspension resulted in occasional end-stop impacts under severe vehicle excitations. It has been suggested that both the vibration attenuation and frequency of end-stop impacts could be controlled by introducing semi-active MR damping [20,25,26]. A suspension seat with semi-actively controlled MR-damper was evaluated under transient and vehicular excitations in the laboratory [25]. The study showed that the MR-damper controller could eliminate the end-stop impacts even under most severe transient excitations, while the semi-active damper did not provide any improvement in attenuation of the vehicular excitations. The MR damper suspension model, presented in Chapter 2, is thus analyzed with integrated two stages of semi-active controllers. In the first stage, four different control schemes are synthesized for enhanced attenuation of low frequency vibration. The relative motion of the suspension is controlled in the second stage to reduce the frequency of end-stop impacts.

For continuous vibration attenuation, the sky-hook control scheme proposed by Karnopp et al. [89] has served as the primary benchmark for various semi-active control designs [18,20,21]. In this dissertation research, a sky-hook control is initially synthesized to assess its effectiveness in attenuating harmonic as well as random vehicular excitations. Owing to the considerable

challenges associated with implementation of the sky-hook controller, three alternate control schemes are synthesized for control of continuous vibration attenuation. The acceleration response characteristics of the suspension model with each controller are evaluated under harmonic, random vehicular and transient inputs. The performance characteristics of each controller are subsequently evaluated using frequency-weighted and unweighted *rms* acceleration, VDV, SEAT, and VDVr. The analyses are further performed with the two stages of the controllers to assess their effectiveness in enhancement of both the attenuation of continuous vibration and frequency of end-stop impacts.

4.2 Controller Synthesis

It is generally understood that the benefit of a semi-active damper mostly rely upon the controller design. A large number of semi-active damper control schemes for vehicular suspension systems have been proposed in literature [20,91,92,93,94,95,114]. The vast majority of these controllers have been based on the sky-hook control scheme proposed by Karnopp et al. [89] for control of continuous vibration. An 'on-off' sky-hook control scheme stipulates that in order for a semi-active suspension to achieve near active suspension performance, the damping must be turned 'on' when the damper force opposes the absolute velocity of the supported mass. The damping force should ideally be zero otherwise. Therefore, in the time domain, the switching function is determined by the product of the absolute velocity of the supported mass and the relative velocity between the supported mass and the input. The superior performances of the sky-hook control scheme have been demonstrated through simulations in many studies [20,104,112,115]. Owing to the requirement of measurement of the instantaneous absolute velocity of the supported mass, the implementation of the sky-hook scheme poses difficult challenges.

On the other hand, an end-stop impact control could be conveniently realized by implementing an 'on-off' control based on the instantaneous relative displacement of the suspension. Such a controller would switch the damper between 'low' and 'high' damping states based on the relative displacement between the supported mass and the input. The damper is set to 'low' states while the relative displacement is within a predefined range around the equilibrium position well-within the permissible suspension travel. The damper is set to 'high' state when the relative displacement approaches the suspension free travel in both the compression and rebound. The performance characteristics of such a controller could be further enhanced through consideration of the direction of the relative displacement apart from its magnitude. This may be realized by introducing a conditional function of the relative velocity and relative displacement indicating whether the suspension motion is toward or away from the equilibrium position. A higher damping would be desired only when the displacement magnitude approaches or exceeds the preset range and the suspension mass is moving away from the equilibrium position.

In this study, two stages of controller synthesis are considered to attain control of both the vibration attenuation and end-stop impacts. The synthesis of both first and second stage controllers are performed on a separate basis and combined to obtain the beneficial aspect of both. The first stage controllers are formulated on the basis of two control algorithm: (1) sky-hook algorithm, based on the absolute and relative velocities [20,21,89]; and (2) relative states feedback algorithm, based on directly measurable relative velocity and relative displacement [92,93]. Each algorithm is synthesized considering two current functions based on their respective states used in the switching algorithm.

4.2.1 Sky-Hook Control Algorithm: Current Proportional to the Absolute Velocity (SHAV)

The potential performance benefit of the sky-hook control scheme, proposed by Karnopp et al. [89], have been demonstrated in many studies involving simulations and laboratory evaluations [20,57,90,115]. The sky-hook synthesis suggests that the damping force is beneficial in attenuating continuous vibration only when it opposes the absolute velocity of the supported mass. The controller thus employs a damping switching condition base on the product of the absolute velocity of the supported mass and the relative velocity between the supported mass and the input (ground). It should be noted in this dissertation that the expression "sky-hook algorithm" refers only to the switching condition based on the product of the relative and absolute velocities; the term scheme is used to define the control algorithm combined with a specific current modulation function. For example, the sky-hook controller proposed by Karnopp et al [89] is referred by "sky-hook control algorithm: current proportional to absolute velocity" or "SHAV" control scheme.

Let i, G, z_c refer to controller current, controller gain, and switching function. The SHAV control scheme is synthesized to modulate the current in the following manner:

$$\begin{cases} i = 0 & -z_c = \dot{x}_s \dot{y}_s \le 0 \\ i = G|\dot{x}_s| & -z_c = \dot{x}_s \dot{y}_s > 0 \end{cases} \tag{4.1}$$

An absolute value function is applied to the absolute velocity to maintain the current positive. The above controller would yield discontinuity in the damper current and thus the force, which may cause high magnitude acceleration of the mass. In an attempt to eliminate such discontinuity, a modulation function, proposed by Wang [104], is applied to achieve continuous current modulation. The proposed modulation function M_c is expressed as:

$$M_c(\xi, z_c) = \frac{1}{2} + \left[-\frac{1}{\pi}(z_c \geq 0) \cup \frac{1}{\pi}(z_c < 0) \right] \left| \tan^{-1}(\xi, z_c) \right| \tag{4.2}$$

where ξ is a smoothing factor. It has been shown that a low value of ξ yields smooth current modulation with high current tracking error, while a higher value of ξ would yield lower tracking error with relatively greater discontinuities in the current [104] higher discontinuities in the current variation. Figure 4.1 illustrates the output of the current modulation function for different values of the switching function z_c, ranging from *-0.5* to *0.5*. Considering relatively small magnitude of the switching function in suspension seat applications, a higher value of ξ in the order of *1000* is used as an acceptable compromise between the low tracking error and smoothness of the function.

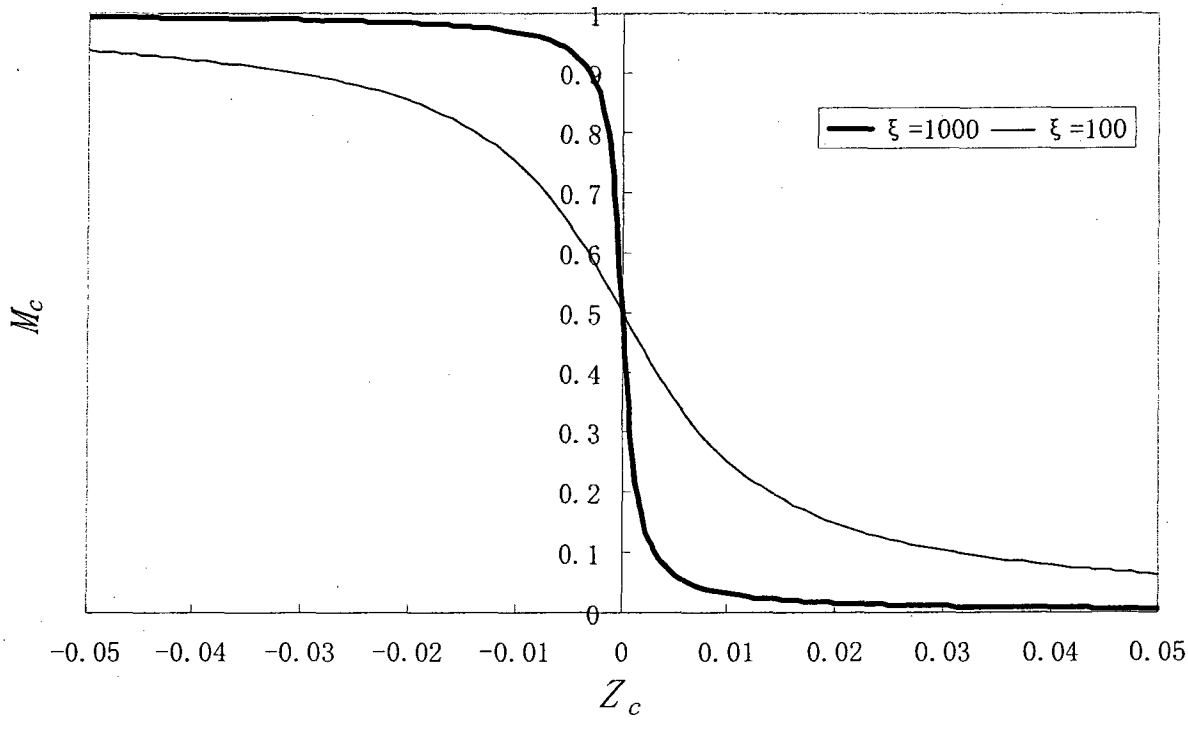

Figure 4.1: Current modulator function

The modified SHAV control scheme is realized by integrating the current modulation function, such that:

$$\begin{cases} i = 0 & -z_c = \dot{x}_s \dot{y}_s \le 0 \\ i = M_c(\xi, z_c) G |\dot{x}_s| & -z_c = \dot{x}_s \dot{y}_s > 0 \end{cases} \tag{4.3}$$

The current modulation function, however, is implemented only when the damper switched from 'off' to the 'on' state, since a sudden increase in damping force tends to cause high acceleration of the suspension mass, and may cause numerical instability.

4.2.2 Sky-Hook Algorithm: Current Proportional to the Relative Velocity (SHRV)

The limitation of the SHAV control scheme lies in its requirement of the absolute velocity. The absolute velocity, up until now, remains to be an estimated value in hardware implementation, which is mainly attributed to the lack of a reference, especially in vehicles and moving mechanism. Displacement and acceleration sensors have been employed to estimate the absolute velocity by differentiating and integrating the signals, respectively, or a combination of both. However, such measurements could introduce lag, noise, and drift, thereby reducing the effectiveness of the controller in real-time applications.

Alternatively, a sky-hook control scheme may be synthesized on the basis of the directly measurable relative velocity (SHRV). In this synthesis, the control current is varied in proportion to the relative velocity between the supported mass and the base. The control current thus approaches its maximum values, when the damper velocity approaches its maximum. The SHRV control scheme is thus formulated as:

$$\begin{cases} i = 0 & -z_c = \dot{x}_s \dot{y}_s \le 0 \\ i = M_c(\xi, z_c) G |\dot{y}_s| & -z_c = \dot{x}_s \dot{y}_s > 0 \end{cases} \quad (4.4)$$

The modulation function $M_c(\xi,z_c)$ is also introduced in the synthesis to ensure continuous current variations during switching. In the above controller, although the current is varied in proportion to the directly measurable relative velocity, it poses implementation challenges similar to the SHAV control scheme due to requirement of z_c that involve knowledge of instantaneous velocity of the mass.

4.2.3 Relative States Feedback Control Algorithm: Current Proportional to Relative Velocity (RSRV)

Rakheja et al. [92] proposed an alternate 'on-off' controller based on directly measurable relative displacement and relative velocity of the suspension. The algorithm is based on the principle of total force, sum of restoring and dissipative force components, transmitted to the supported mass. The transmitted force is small when the restoring and dissipative force components act in the opposite direction. The mass acceleration could be nullified when the damper force magnitude is identical to the spring force but in the opposite direction. The control algorithm switches to 'low' damping when the two force components tend to act in the same direction. The controller synthesis is formulated by integrating the modulation function to ensure smooth current modulation, such that:

$$\begin{cases} i = 0 & z_c = y_s \dot{y}_s \ge 0 \\ i = M_c(\xi, z_c) G |\dot{y}_s| & z_c = y_s \dot{y}_s < 0 \end{cases} \quad (4.5)$$

In the above synthesis, the condition function is the product of the relative velocity and relative displacement responses of the suspension, which are directly measurable. This control scheme is thus considered to be attractive for implementation. The current is modulated in

proportion to the instantaneous relative velocity response. Similarly to the SHRV control scheme, the current modulation as a function to the relative velocity allows the semi-active system to exploit the full potential of the damper bandwidth when maximum current is applied at maximum velocity.

4.2.4 Relative States Feedback Control Algorithm: Current Proportional to Relative Displacement (RSRD)

The RSRV control scheme based on the directly measurable states may also be implemented to modulate the current proportional to y_s (RSRD) instead of $\dot{y}_s$ (RSRV), such that:

$$\begin{cases} i = 0 & z_c = y_s \dot{y}_s \geq 0 \\ i = M_c(\xi, z_c) G |y_s| & z_c = y_s \dot{y}_s < 0 \end{cases} \tag{4.6}$$

The above synthesis yields high control current under high suspension deflection magnitudes. The magnitude of damping force may thus be significantly higher even when the velocity is small.

4.2.5 Stage Two Control: End-Stop Impacts Suppression

The low natural frequency suspension seats are known to transmit higher intensity vibration and shock to the occupant due to end-stop impacts under severe excitations arising from large discontinuities in the terrain. A second stage control is thus synthesized to limit the frequency of end-stop impacts under severe excitations. A second stage control based on relative displacement of the suspension was proposed by Ma [20], where the damper is set to yield maximum damping force as the suspension approaches its permissible travel limits. The proposed synthesis, however, did not consider the direction of suspension travel. An end-stop impact control is desirable only when the suspension is moving away from its equilibrium position.

The condition function employed in the relative states feedback algorithm, based on y_s and $\dot{y}_s$, also provides a measure of the direction of travel. A positive value of the condition function ($z_c = y_s \dot{y}_s > 0$) ensures the suspension motion away from the equilibrium position. A controller synthesis is thus formulated to yield maximum control current (i_{max}) when y_s exceeds a preset suspension deflection and when the motion is away from the equilibrium position ($z_c > 0$), such that:

$$i_t = \begin{cases} i_{\max}; & |y_s| \geq y_{stop} \quad \text{and} \quad y_s \dot{y}_s > 0 \\ i; & otherwise \end{cases} \tag{4.7}$$

The preset limit may be defined as a portion of the suspension free travel with respect to its mid-position, such that: $y_{stop} = \eta d$, where $\eta < 1$ is a constant. The second stage controller is synthesized in conjunction with the first-stage controller to achieve attenuation of continuous vibration together with the control of end-stop impacts. The second-stage control thus reverts to the control derived from stage 1 control in its 'off' state.

4.3 Response Characteristics of the Semi-Active Suspension Seat (Stage One Controls)

The suspension seat model coupled with four different first-stage control schemes are evaluated under harmonic, selected random vehicular, and transient excitations. While the performance characteristics under harmonic and vehicular excitations are evaluated for the suspension seat model with first-stage control schemes only, the responses to transient excitations are attained with both stage controls, individually and combined. Excitations identical to those presented in section 3 were employed in order to compare the potential benefits of the controlled MR damper over the passive hydraulic damper in the suspension seat.

4.3.1 Harmonic Excitations

The response characteristics of the semi-active suspension seat models are evaluated in terms of acceleration transmissibility in the *0.5* to *10Hz* range. Figure 4.2 illustrates the frequency response characteristics of the semi-active suspension models with selected controller gains ranging from *1* to *10* for SHAV, SHRV, and RSRV control schemes, and from *10* to *200* for RSRD control scheme. Higher controller gains were omitted due to saturation of the response, which may be attributed to the saturation of the damping force. The results show that the SHAV controller yields the best overall acceleration transmissibility attenuation over the entire *0.5* to *10Hz* range. The transmissibility responses peak near *1.2*, *1.25*, *1.3*, and *1.3Hz*, respectively for the suspension models employing SHAV, SHRV, RSRV, and RSRD control schemes.

In the case of the SHAV controller, an increase in the controller gain tends to shift the attenuation frequency to the left from *1.75Hz* (G = *1,2*) to *1.6Hz* (G = *5,9*). The resonance frequency also shifts to the left from *1.3Hz* (G = *1* and *2*) to *1.1Hz* (G = *5* and *9*). A very small and negligible discrepancy can be observed near *2.1Hz*. It can be concluded that the current gain does not affect the transmissibility beyond *1.9Hz*.

In the case of the SHRV controller, the peak magnitudes transmissibility is higher than those attained with the SHAV controller. Furthermore, the attenuation frequencies shift to the right with increase in the controller gain from *1.85Hz* (G = *1* and *2*) to *2Hz* (G = *5* and *9*). However, the resonance frequency still shifts to the left from *1.3Hz* (G = *1* and *2*) to *1.1Hz* (G = *5 and 9*). Unlike the SHAV control scheme, the SHRV control scheme yields poor vibration attenuation performance under a higher gain until about *5Hz*. This effect is similar to that of the passive damping. Larger discrepancies are thus evident from the inflection point at *1.75Hz* to the converging point at *5.5Hz*. The difference in the response due to different gains is at its largest

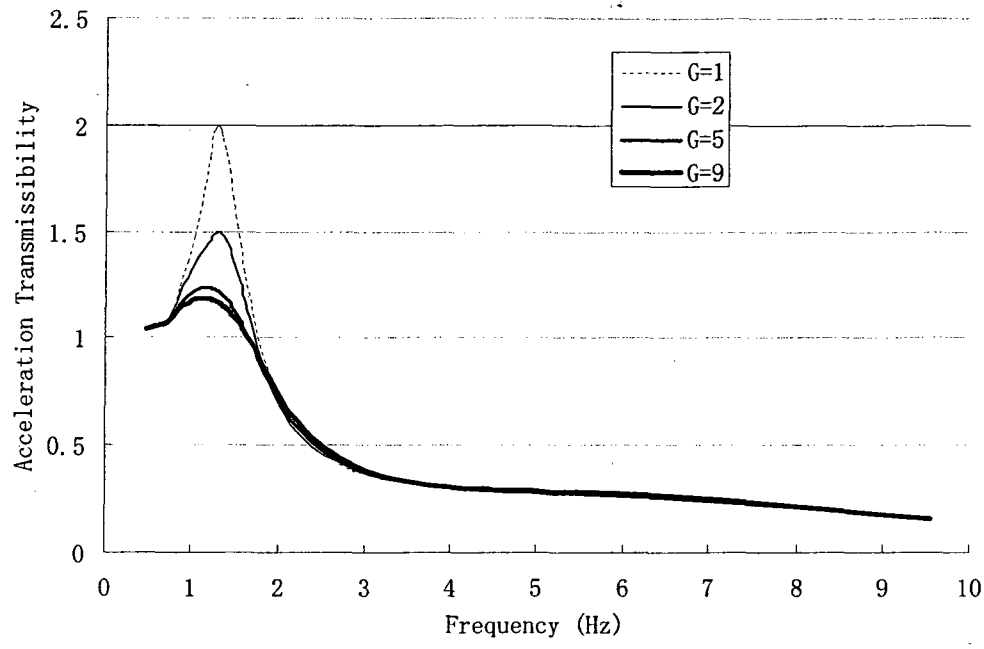

(a)

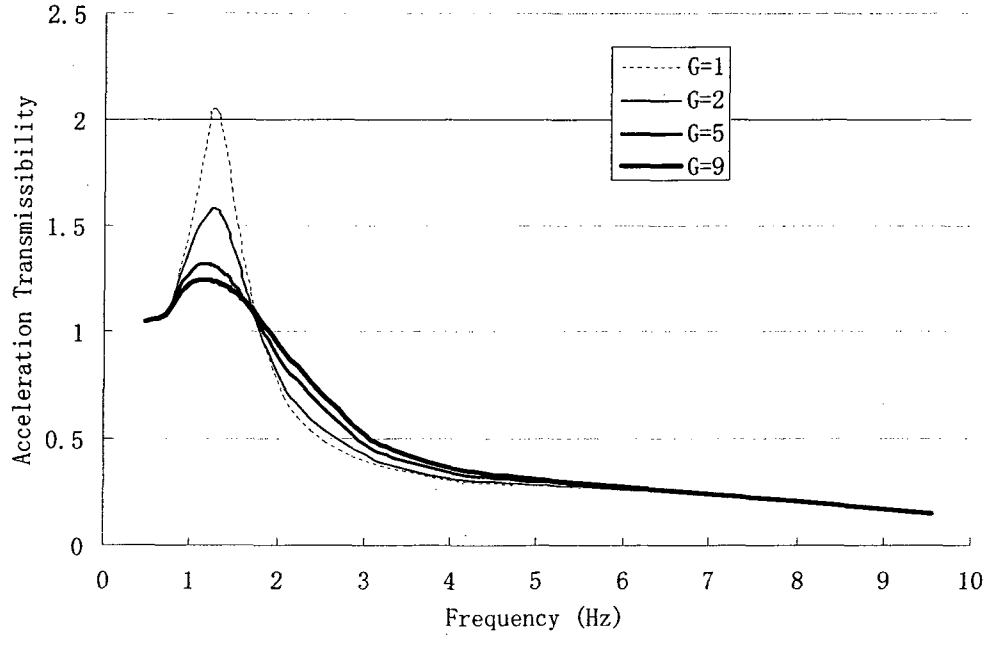

(b)

Figure 4.2: Acceleration transmissibility response characteristics of the semi-active suspension seat models for different control gains: (a) SHAV; (b) SHRV; (c) RSRV; and (d) RSRD (Continued)

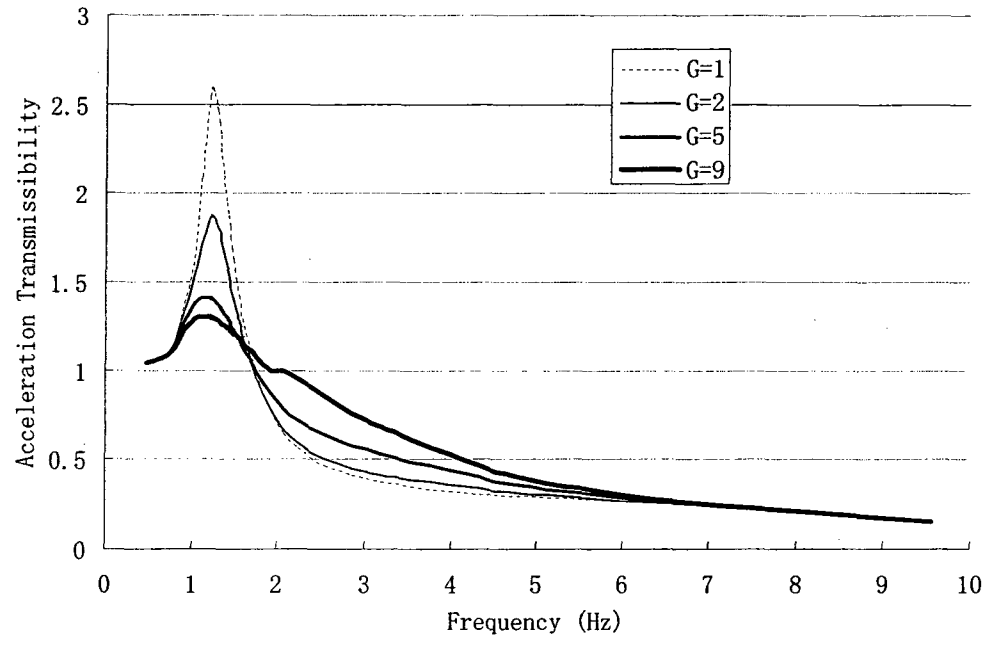

(c)

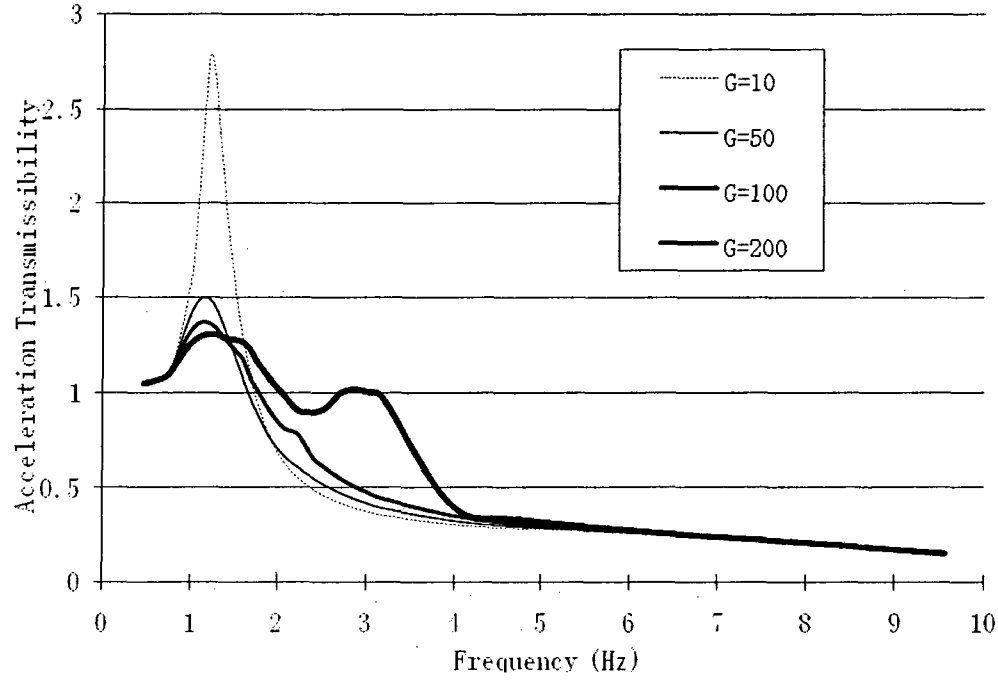

(d)

Figure 4.2: Acceleration transmissibility response characteristics of the semi-active suspension seat models for different control gains: (a) SHAV; (b) SHRV; (c) RSRV; and (d) RSRD

around *2.4Hz*. It can be concluded that this control scheme exhibits the behaviour of a passive damper (an increase in control gain leads to decrease in peak amplitude with increase in the post resonance amplitude), but the effect is greatly diminished beyond *5.5Hz*. Almost linear decrease in transmissibility is observed with frequency beyond *6Hz*.

The responses of the suspension seat model with RSRV control scheme, exhibit relatively higher peak magnitudes, which are up to *1.25* times those of the model with the SHAV control scheme, irrespective of the current gains. The vibration attenuation frequency is near *1.75Hz* for $G = 1, 2,$ and *5* and ranges from *1.9* to *2.2Hz* for $G = 9$. The stagnation of the transmissibility in the latter frequency range indicates the presence of a second resonance frequency of the two-DOF model and presence of an overdamped mode. The differences in the transmissibility magnitudes corresponding to high controller gains approach as high as *0.4* at *2.4Hz*, which is quite considerable. However, the converging frequency remains at *6Hz*, as observed for the model with SHRV control scheme.

Finally, in the case of the RSRD controller, the results demonstrate considerably higher peak magnitude corresponding to a low gain of *10*, while the peak responses under higher gains are either lower or comparable to those observed for other control schemes. The peak magnitude decreases from *2.75* ($G = 1$) to *1.5* ($G = 2$), while the peak transmissibility occurs at *1.3Hz*. The responses corresponding to gains *10* and *50* exhibit an inflection point near *1.95Hz*, while those with gains of *100* and *200* show an inflection point near *1.45Hz*. The resonance frequency (*1.2Hz* for $G = 10$; *1.15Hz* for $G = 50$; and *1.1Hz* for $G = 100$) decreases slightly with gain increasing from *10* to *100* but increases to *1.25Hz* for $G = 200$. This higher gain causes the overdamped

suspension mode, where the fundamental peak occurs at a slightly higher frequency. The higher gain of *100* and *200* yield a secondary peak near *2.2Hz* and around *3.2Hz*, respectively. All the responses, however, tend converge at *4Hz*, yielding a nearly linear decrease in transmissibility with frequency.

In summary, the SHAV control scheme yields the best harmonic excitation transmissibility performance. The SHRV control scheme is very comparable to the SHAV control scheme in terms of performance. The RSRV control scheme, however, shows higher peak amplitude and higher post resonance amplitude. The RSRD control scheme reveals a distinct secondary peak at higher controller gains and higher peak response at lower controller gains. Considering the implementation challenges associated with the SHAV and SHRV control schemes, the RSRV control scheme may be considered meritorious.

4.3.2 Random Vehicular Excitations

The response characteristics of the semi-active suspension seat models coupled with different first-stage control schemes are evaluated under selected random vehicular excitations. The responses are evaluated for different controller gains similar to those used under harmonic excitations, and are presented in terms of seat acceleration PSD. The responses are also compared with those of the passive suspension model to illustrate potential benefits of the proposed semi-active controllers. The responses are illustrated only up to *3Hz*, since these were observed to be very small at frequencies above *3Hz*. SNOWA excitations make an exception. Figures 4.3 to 4.6 show the acceleration PSD responses of the semi-active seat suspension models function under BUS, BUS2A, SNOWA, and EM1A excitations for the SHAV, SHRV, RSRV, and RSRD control schemes, respectively. The results suggest that the passive suspension

seat generally performs better or similar to the semi-active suspension seats when a low controller gain ($G = 1$) is implemented using sky-hook algorithm controls, but the passive case

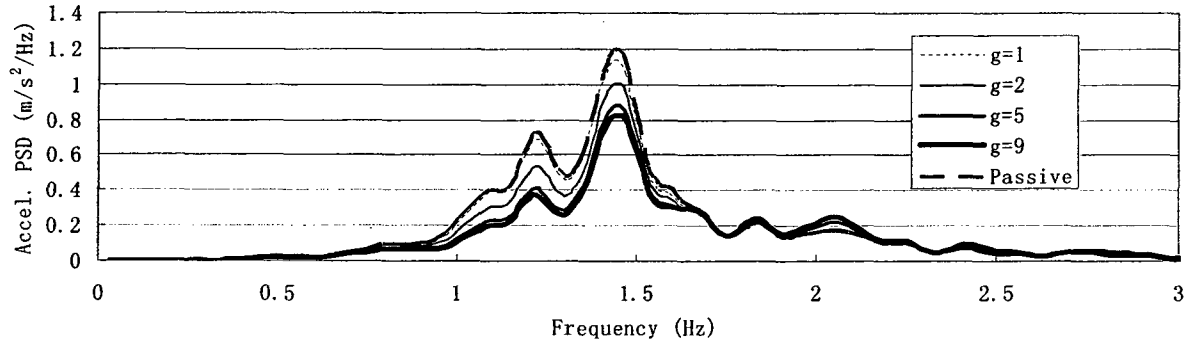

(a)

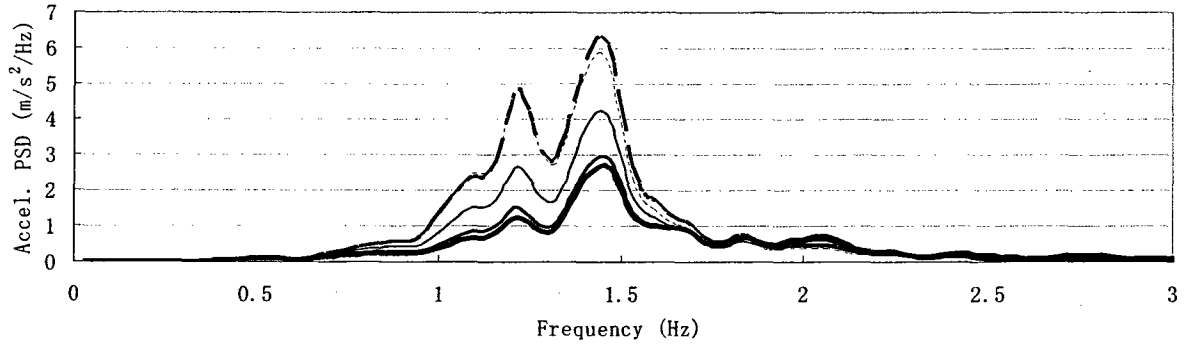

(b)

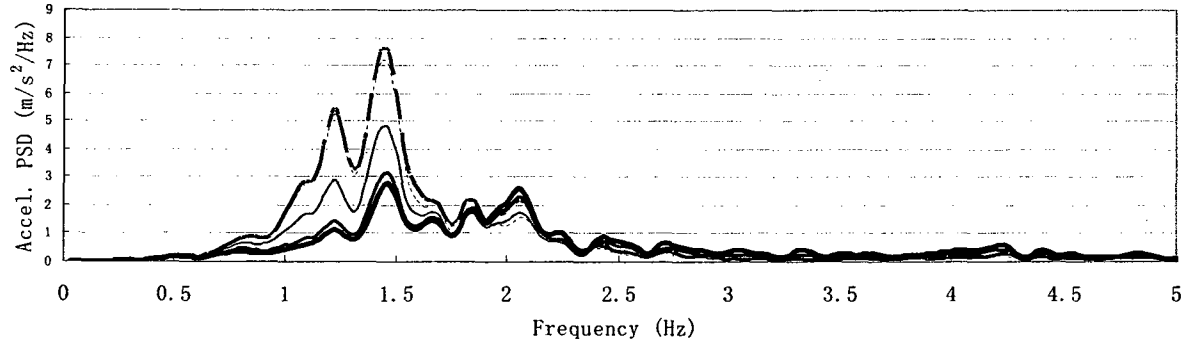

(c)

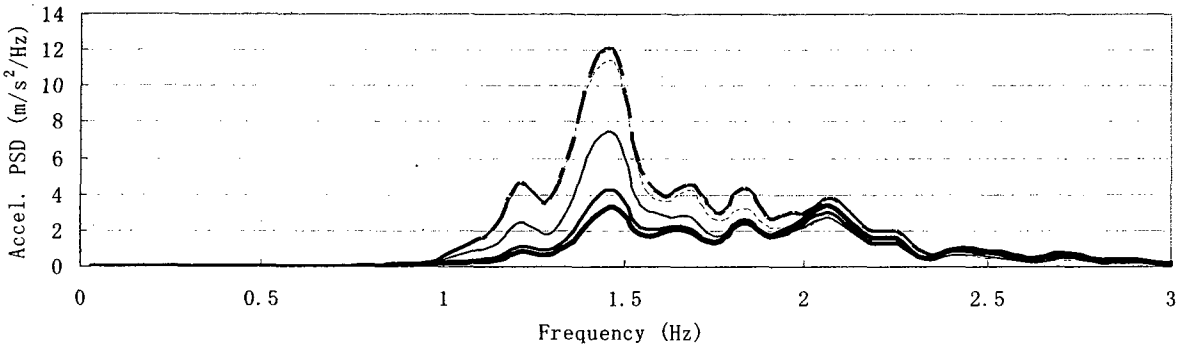

(d)

Figure 4.3: Comparisons of acceleration PSD responses of the semi-active suspension seat model employing the SHAV controller under different vehicular excitations: (a) BUS; (b) BUS2A; (c) SNOWA; and (d) EM1A

outperforms the relative states feedback algorithm controls at low controller gain ($G = 1$ or $G = 10$).

The acceleration PSD of the semi-active suspension seat model using SHAV control scheme is governed by a general trend, where an increase in the current control gain yields lower resonance peak amplitude, irrespective of the excitation considered. This control scheme also revealed lower peak transmissibility response to BUS and BUS2A excitations, while a higher controller gain yields lower response at lower frequencies, it does not deteriorate the vibration isolation performance, as observed in the transmissibility response. The suspension seat effectively reduces the peak transmissibility at resonance frequency of the BUS and BUS2A excitations. A higher gain ($G = 9$) yields a small peak, although negligible, near *2.2Hz* under EM1A and SNOWA excitations, which is more significant under SNOWA excitation. The SHAV control scheme, however, effectively attenuates the predominant peak of the SNOWA excitation near *4Hz*. The lower controller gain also resulted in occasional end-stop impacts under BUS2A, EM1A, and SNOWA excitations, as observed for the passive suspension seat model. The end-stop impacts, however, were entirely eliminated under higher controller gains

The acceleration PSD of the semi-active suspension seat model with the SHRV control scheme (Figure 4.4) exhibits trends similar to those with the SHAV control scheme. An increase in the controller gain yields considerable reductions in the resonance peak magnitudes. The SHRV control scheme, however, yields slightly higher vibration transmission in the isolation range compared to the SHAV control scheme. This is particularly evident in response to SNOWA and EM1A excitations.

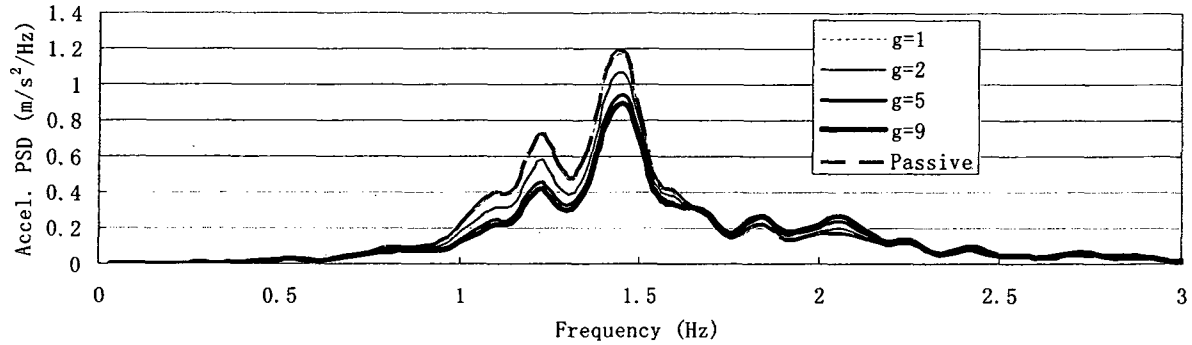

(a)

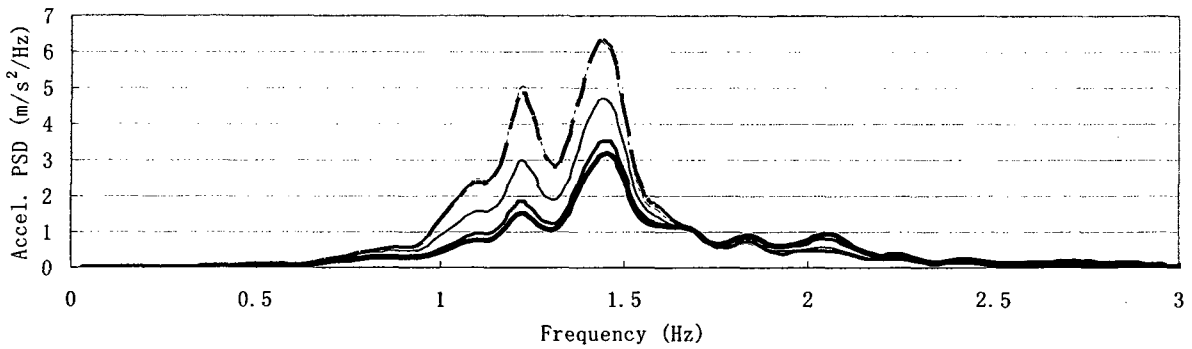

(b)

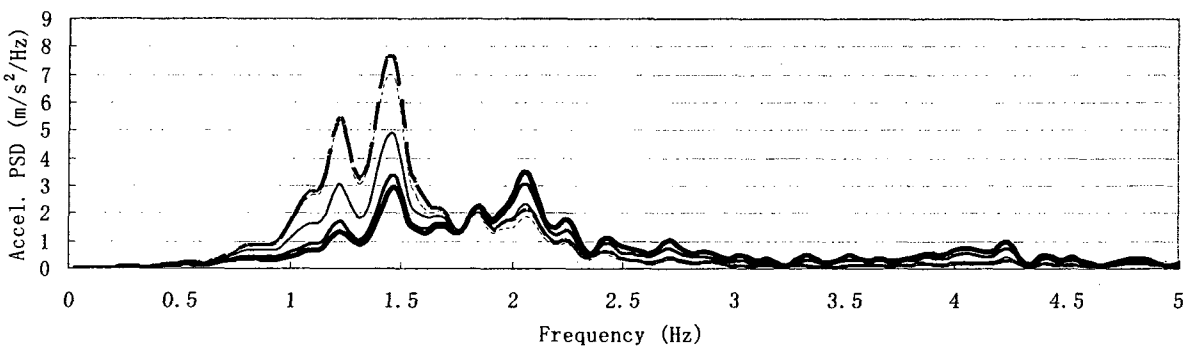

(c)

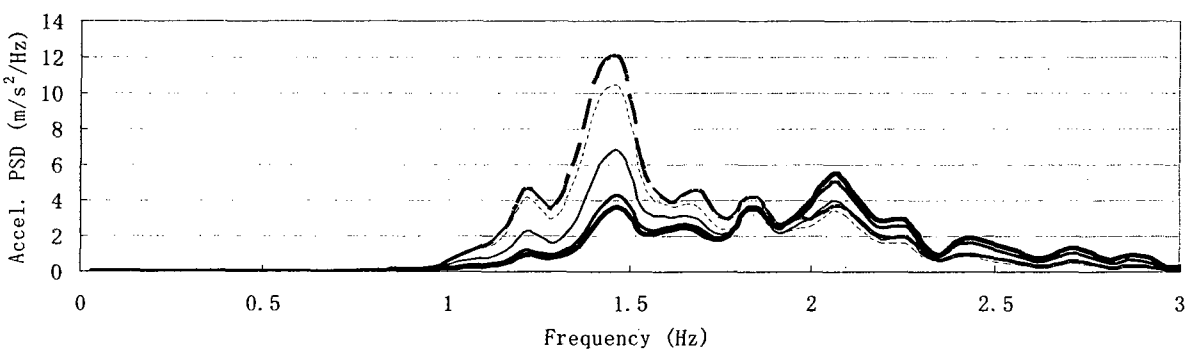

(d)

Figure 4.4: Comparisons of acceleration PSD responses of the semi-active suspension seat model employing the SHRV controller under different vehicular excitations: (a) BUS; (b) BUS2A; (c) SNOWA; and (d) EM1A

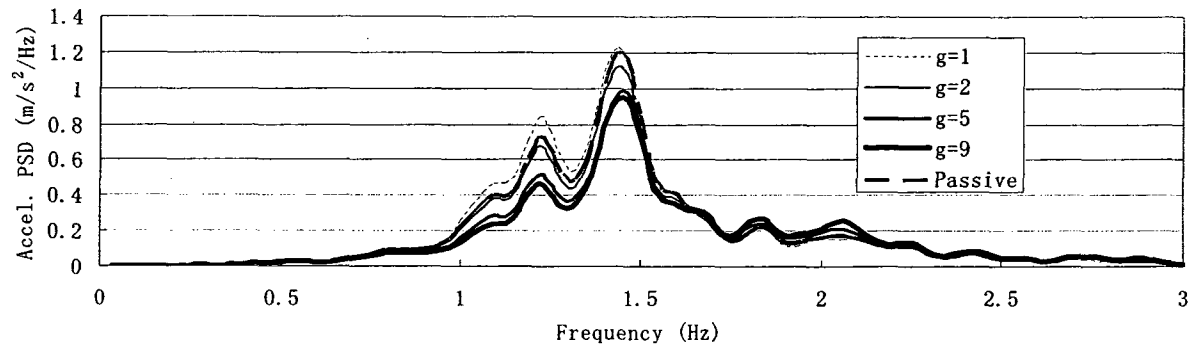

(a)

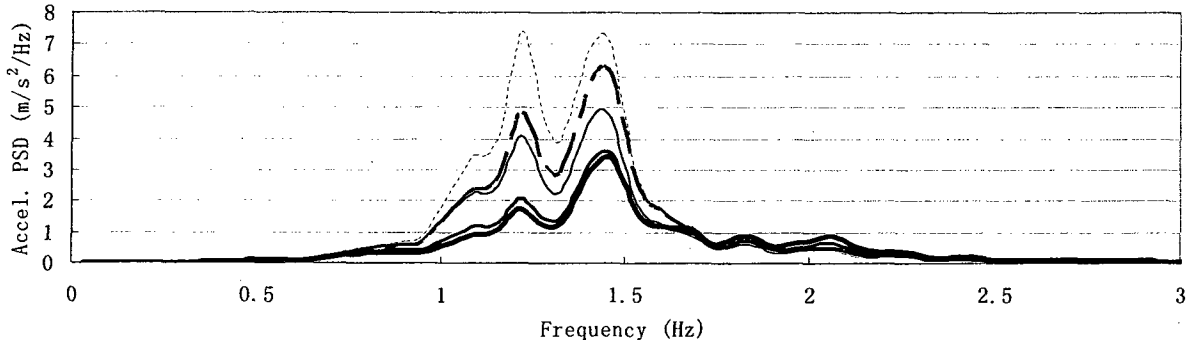

(b)

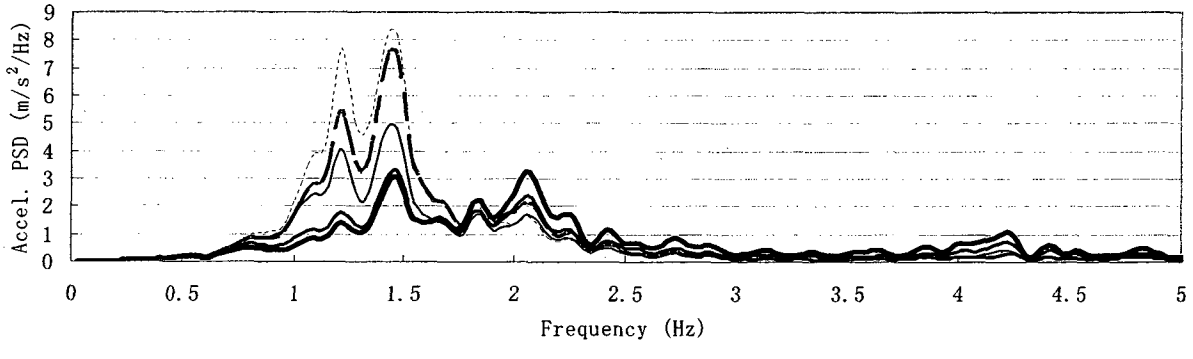

(c)

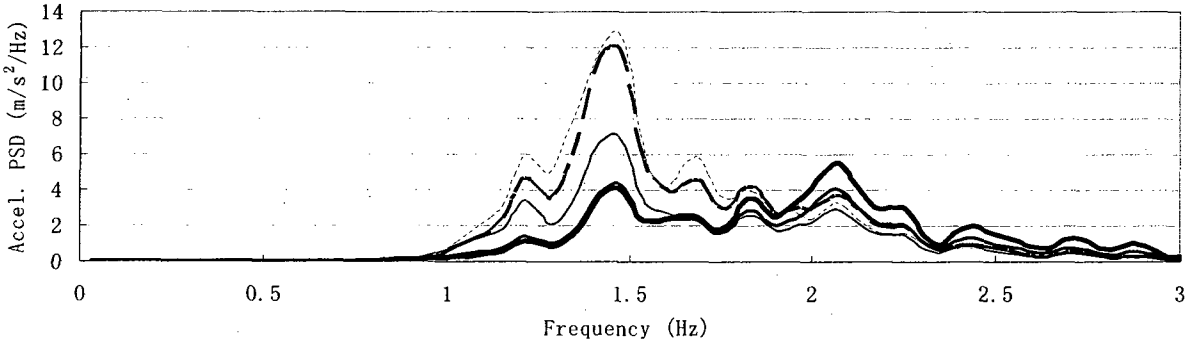

(d)

Figure 4.5: Comparisons of acceleration PSD responses of the semi-active suspension seat model employing the RSRV controller under different vehicular excitations: (a) BUS; (b) BUS2A; (c) SNOWA; and (d) EM1A

The acceleration PSD responses of the semi-active suspension seat model with the RSRV control scheme, shown in Figure 4.5, are also greater than those of the model with the SHAV control scheme. This control scheme yields approximately *10%* higher response than the SHAV control scheme and is similar to the SHRV control scheme, with the exception of the low controller gain ($G = 1$). The responses with low controller gain ($G = 1$) tends to be greater than those of the passive suspension, irrespective of the type of excitation, which is attributable to lower damping and thereby more frequency end-stop impacts. The results also show that an increase in controller gain helps to suppress the low frequency vibration, as observed in case of SHAV and SHRV control schemes. A higher gain, however, emphasize secondary peaks in the isolation region (near *2.2Hz* under EM1A and near *4.2Hz* under SNOWA excitation). The RSRV controller seems to perform best under the BUS and BUS2A signals, where the predominant excitation frequency is close to the suspension resonance frequency, while the higher frequency components are very small.

The response characteristics of the model with the RSRD control scheme exhibit trends similar to those with the RSRV controls scheme, as seen in Figure 4.6. The RSRD control scheme yields significantly higher response corresponding to low controller gain ($G = 10$) leading to more frequency end-stop impacts. Its performance under higher gains and BUS2A, SNOWA, and EM1A excitations, however, is slightly superior to that of the seat with RSRV controller. The responses to the SNOWA and EM1A excitations are quite comparable to those of the SHRV control scheme.

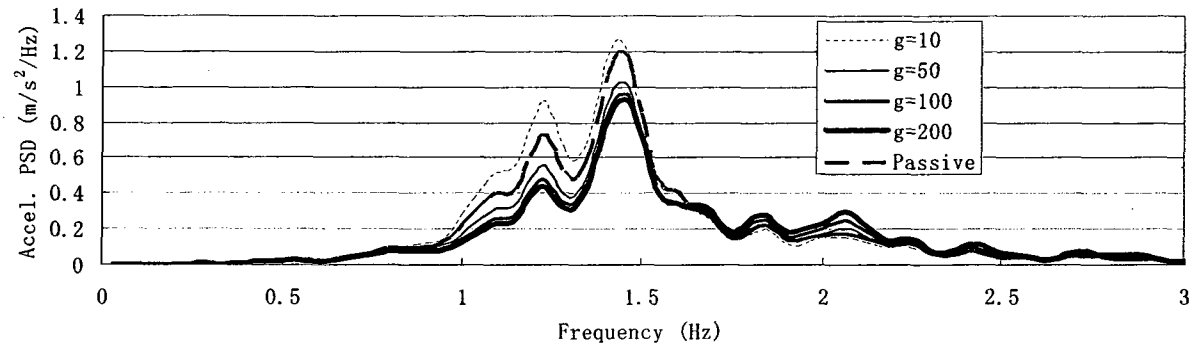

(a)

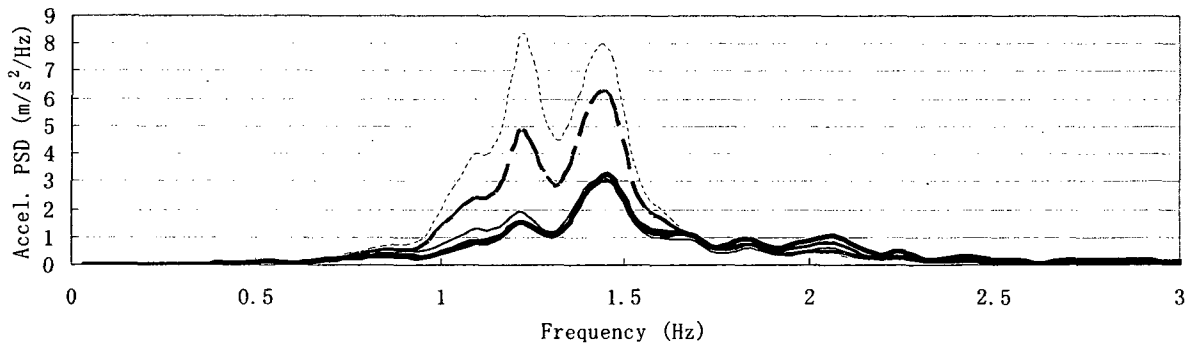

(b)

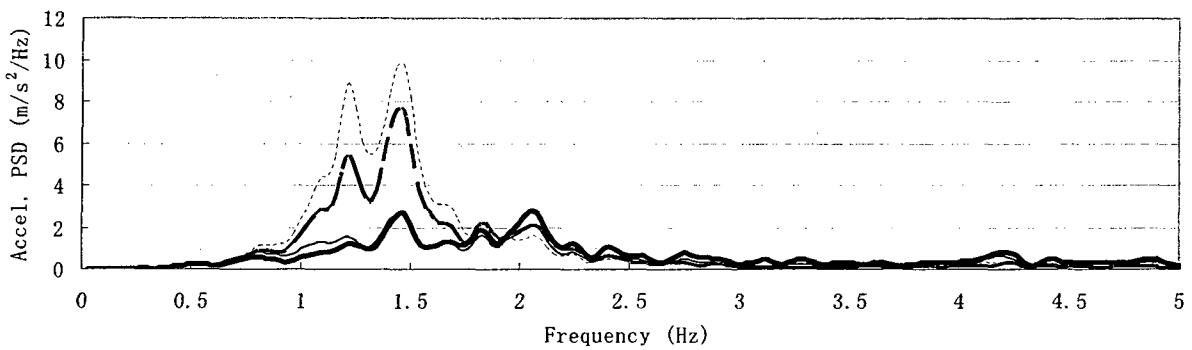

(c)

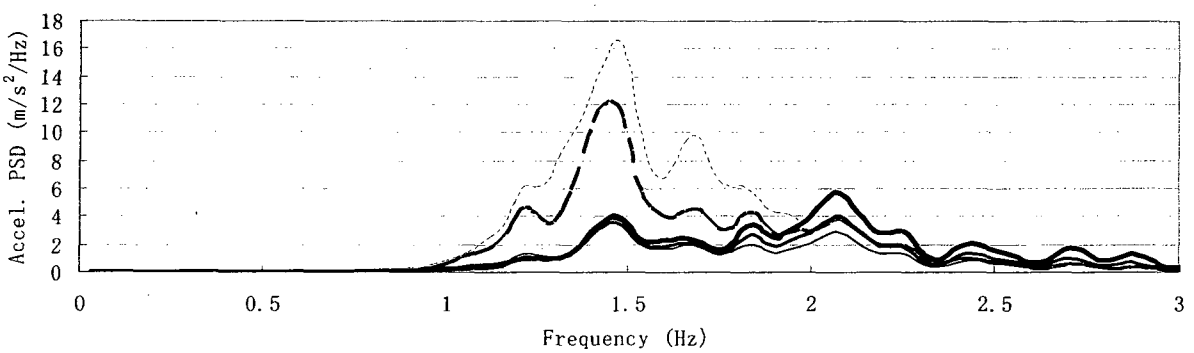

(d)

Figure 4.6: Comparisons of acceleration PSD responses of the semi-active suspension seat model employing the RSRD controller under different vehicular excitations: (a) BUS; (b) BUS2A; (c) SNOWA; and (d) EM1A

4.3.3 Transient Response

The performance potentials of the semi-active suspension seat models with different first-stage control schemes are further investigated under a transient input. The responses are evaluated in terms of occupant mass acceleration, suspension relative deflection, end-stop force and variations in the control current. The transient excitation was synthesized as described in section 3.2.3, to yield peak displacement of *75mm* and predominant frequency of *1.25Hz*. The peak acceleration due to this excitation was obtained as $3.7m/s^2$ Owing to the high magnitudes of the states under the transient excitation, the controller gains were limited to $G = 1, 2, and\ 5$ except for RSRD control scheme, where these were taken as *20*, *40*, and *100*. The time-histories of the responses of the suspension models with SHAV, SHRV, RSRV, and RSRD control schemes are presented in Figure 4.7 to 4.10, respectively. The figures also show the responses of the passive suspension in order to assess the relative potential benefits of the semi-active suspensions.

The results suggest saturation of the transient response at relatively lower controller gains for all of the control schemes. The effect on the seat acceleration can be generally characterized by two peaks instead of a single peak (clipping). This is attributed to relatively higher current due to high magnitude of the states, and thereby greater damping force. This would contribute to an overdamped mode and thus greater coupling between the suspension and occupant masses. This phenomenon is most apparent in the case of SHAV and RSRD control schemes. Furthermore, a saturation of control current (*2A*) is observed for the RSRD control scheme, which further confirms the higher suspension damping, overdamped suspension mass mode, and relatively greater contributions of the cushion/occupant mode. The results show the presence of end-stop impacts in all cases with low control gains, while the magnitudes of impact forces tend to be

lower in case of SHAV and SHRV control schemes. The peak end-stop force occurs when suspension relative deflection exceeds the permissible travel (shown by bold lines). These occur at instants when control current is close to zero, for all the control schemes, except for the RSRD where the control current is proportional to the relative displacement. The occurrence of end-stop impacts can be eliminated with a higher control gain, as observed from the results. Alternatively, the occurrence of such end-stop impacts can also be eliminated by introducing the second stage controller, which imposes maximum current when the suspension deflection exceeds a preset value.

From the seat acceleration time histories, it can be seen that the sky-hook control algorithms, at a low controller gain ($G = 1$), perform as well as the passive suspension; while the relative states feedback algorithms yield nearly twice the peak acceleration response. The effect is further supported by the high magnitudes of the end-stop impact forces observed in the relative states feedback control algorithms. The peak impact forces corresponding to lower gains are nearly 1.5 times those observed for the passive suspension model.

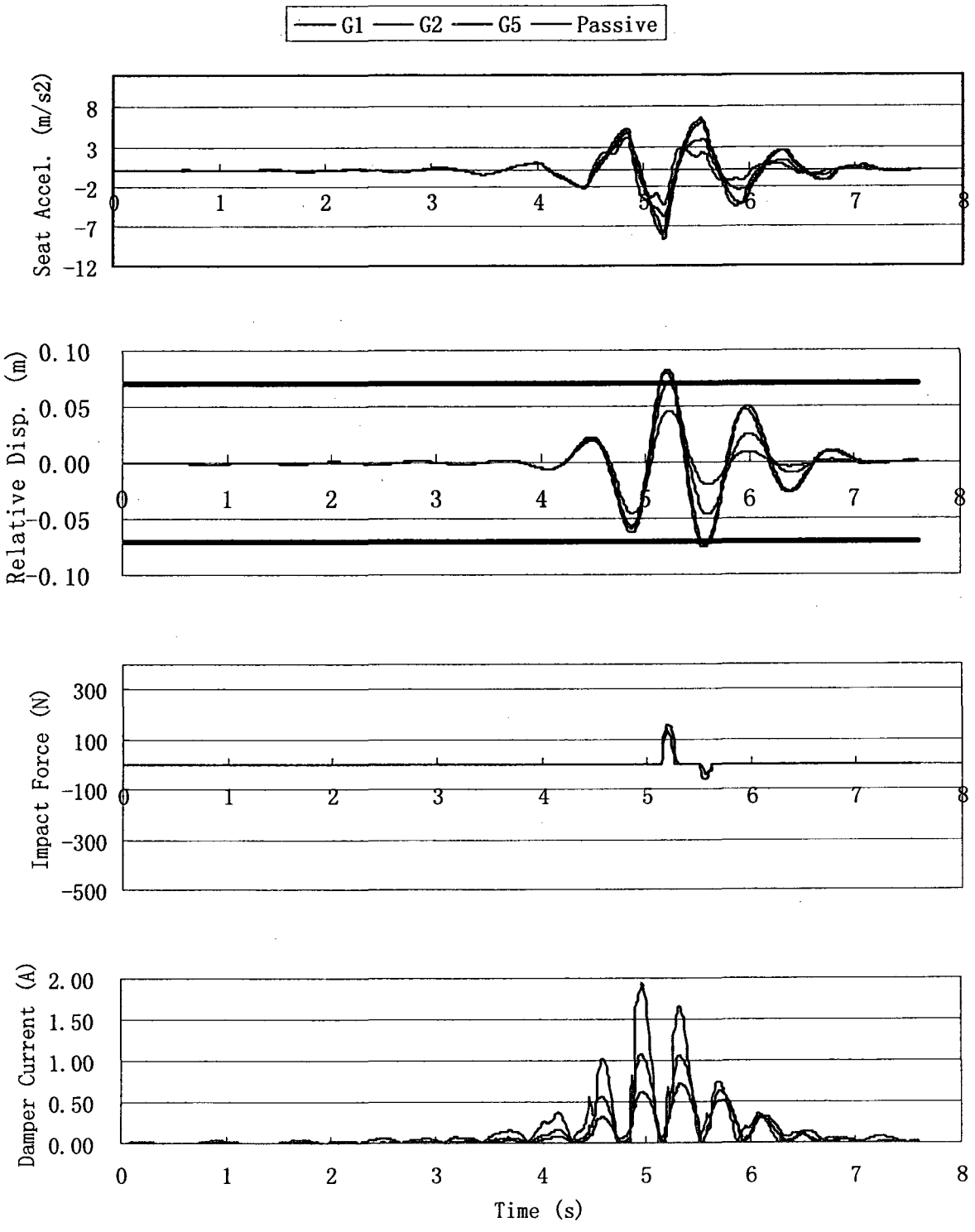

Figure 4.7: Comparison of transient responses of semi-active suspension seat using SHAV controller with current setting $G = 1, 2, 5$ and passive suspension seat

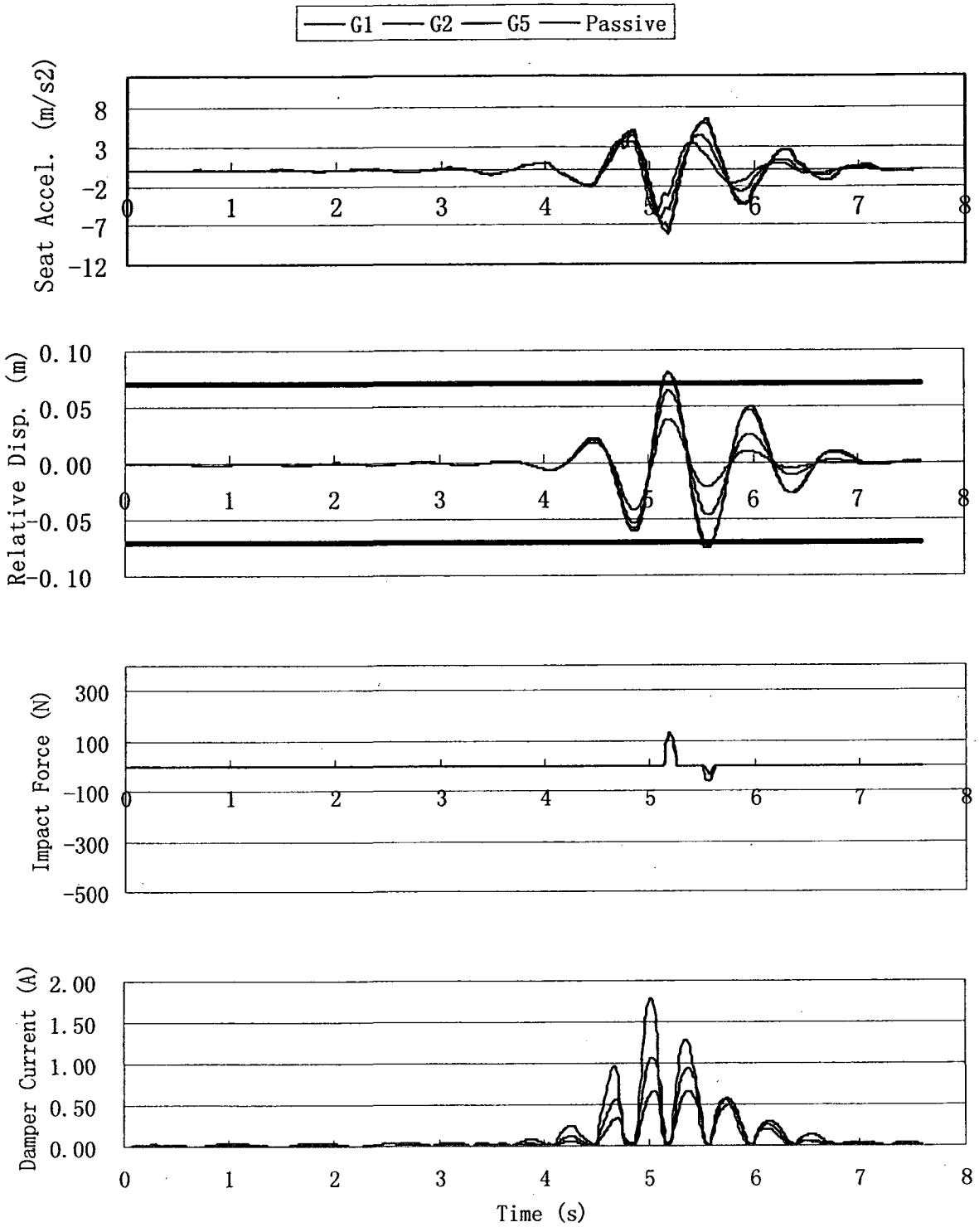

Figure 4.8: Comparison of transient responses of semi-active suspension seat using SHRV controller with current setting $G = 1, 2, 5$ and passive suspension seat

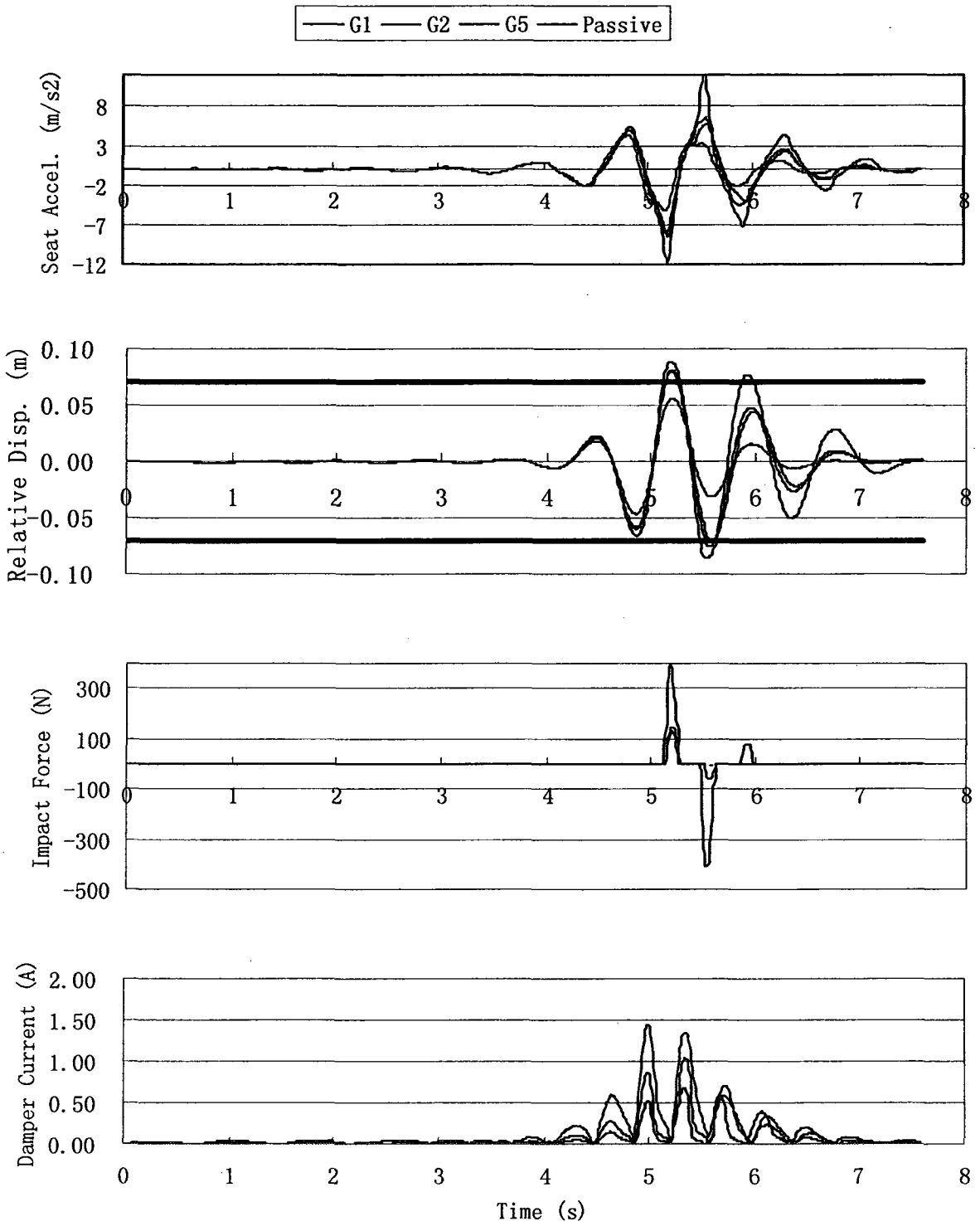

Figure 4.9: Comparison of transient responses of semi-active suspension seat using RSRV controller with current setting $G = 1, 2, 5$ and passive suspension seat

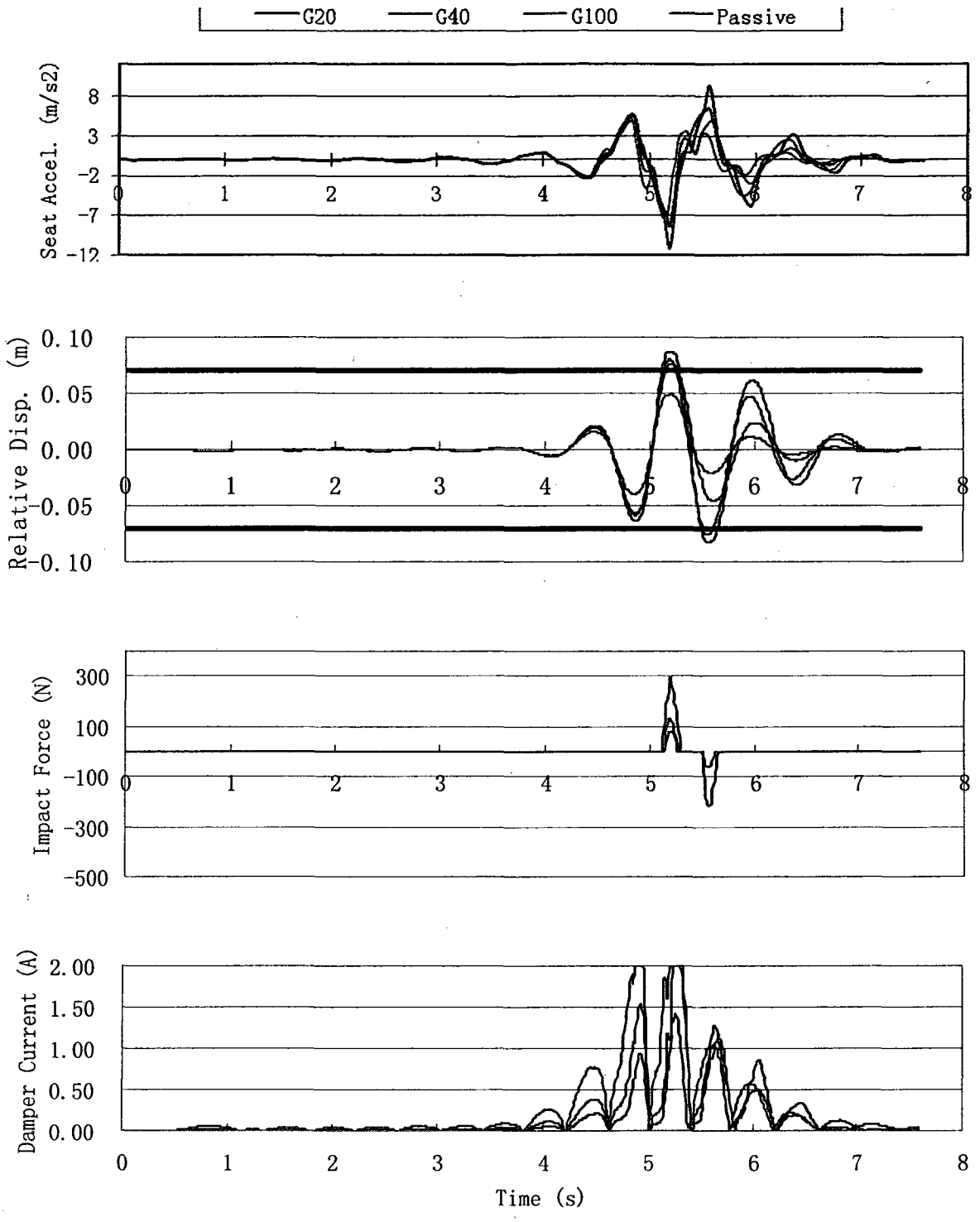

Figure 4.10: Comparison of transient responses of semi-active suspension seat using RSRD controller with current setting *G = 20, 40, 100* (*G1*, *G2*, *G5*) and passive suspension seat

4.4 Performance Evaluation of Semi-Active Suspension Seat

The responses of the semi-active suspension seat models employing the proposed current controllers are subsequently evaluated to assess their relative performance using the measures described in section 3.3 In order to evaluated the proposed first stage controllers, a single suitable gain is identified for random vehicular excitation. For this purpose, the frequency-weighted and unweighted *rms* acceleration and VDV of each combination of selected vehicular excitation and controller are initially obtained for different controller gains. The computed responses are subsequently applied to derive frequency-weighted and unweighted SEAT and VDVr as a function of the controller gain. The results are subsequently used to identify a suitable controller gain for each controller and vehicular excitation combination.

Figure 4.11 to 4.13 illustrate the variations in the unweighted and frequency-weighted SEAT and VDVr for different controller gains of each controller corresponding to BUS2A, SNOWA, and EM1A excitations, respectively. The appropriate controller gains are taken as those leading to lowest SEATw (continuous vibration attenuation) and VDVr (end-stop impacts) values. Furthermore, the gains were selected for both the nominal and amplified vehicular excitations based on the amplified excitations, which yielded enhanced attenuation of continuous vibration and end-stop impacts.

The results show a general trend for the SHAV control scheme yielding lowest performance values (best) and RSRD control scheme yielding highest performance values (worst). The general trend for all results is a rapid drop in performance values with controller gain increasing from a low value (G = *1* and *2*), and only small increase or saturated performance values with further increase in gains.

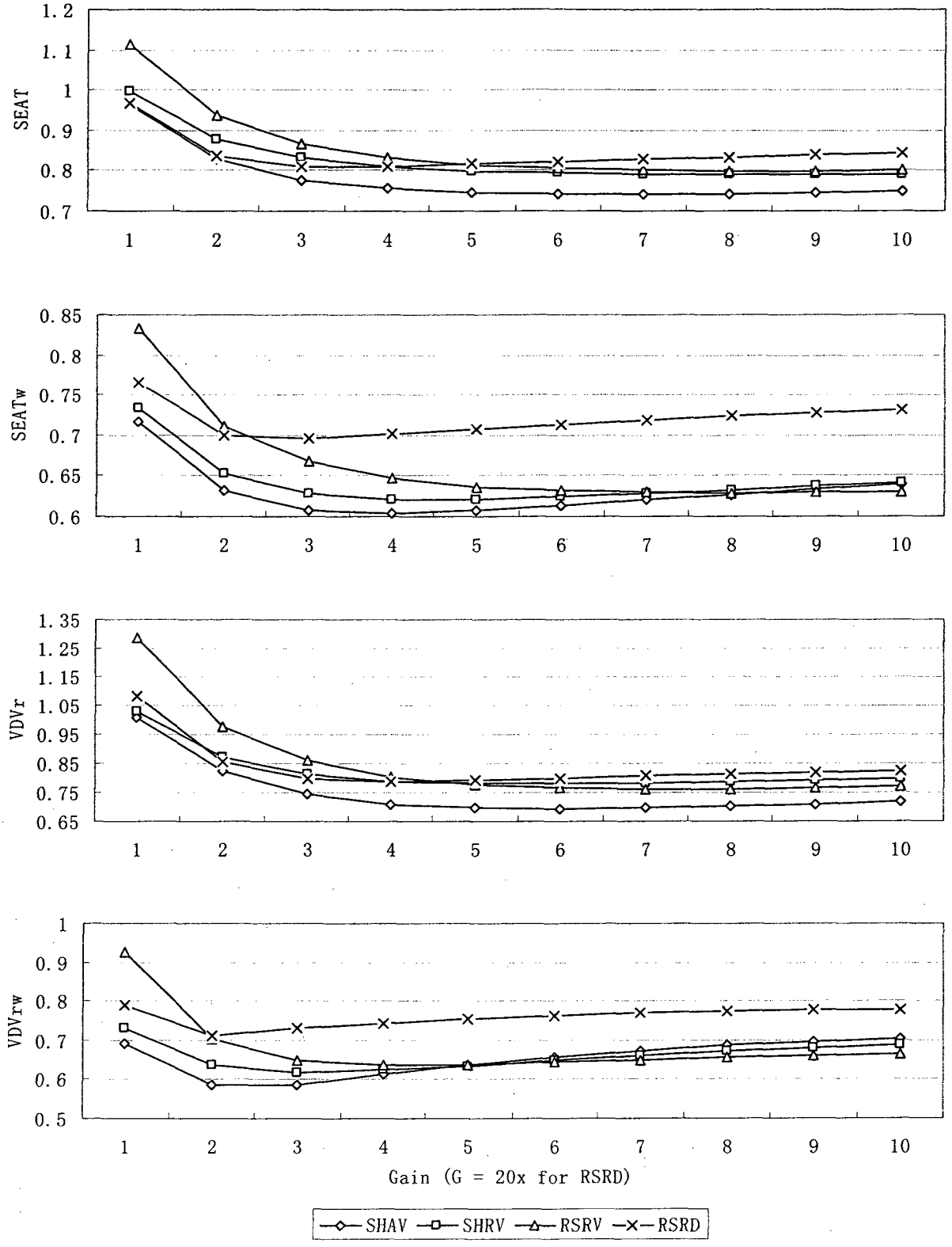

Figure 4.11: Comparisons of performance measures of proposed semi-active suspension seat controllers as a function of the controller gain under BUS2A excitation

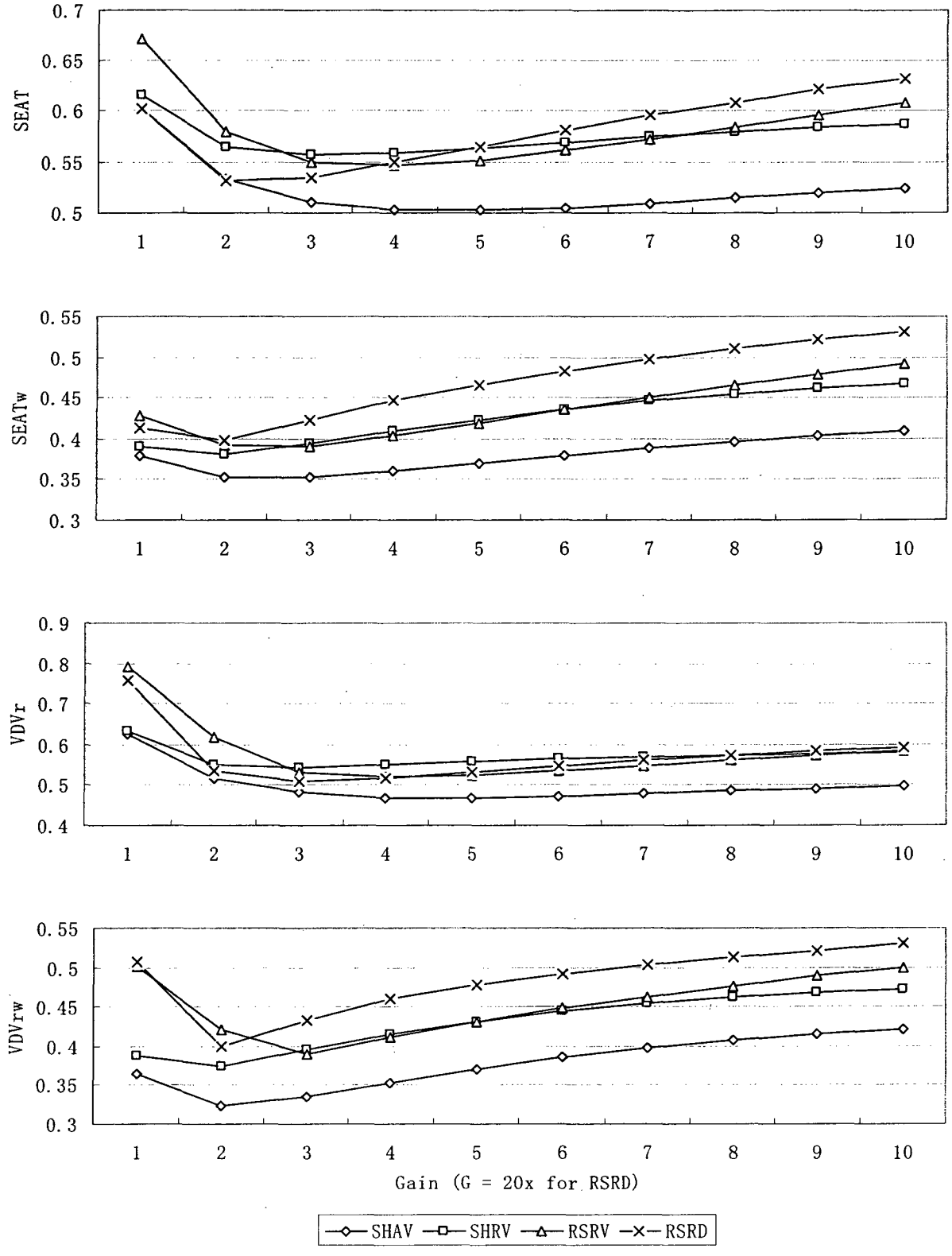

Figure 4.12: Comparisons of performance measures of proposed semi-active suspension seat controllers as a function of the controller gain under SNOWA excitation

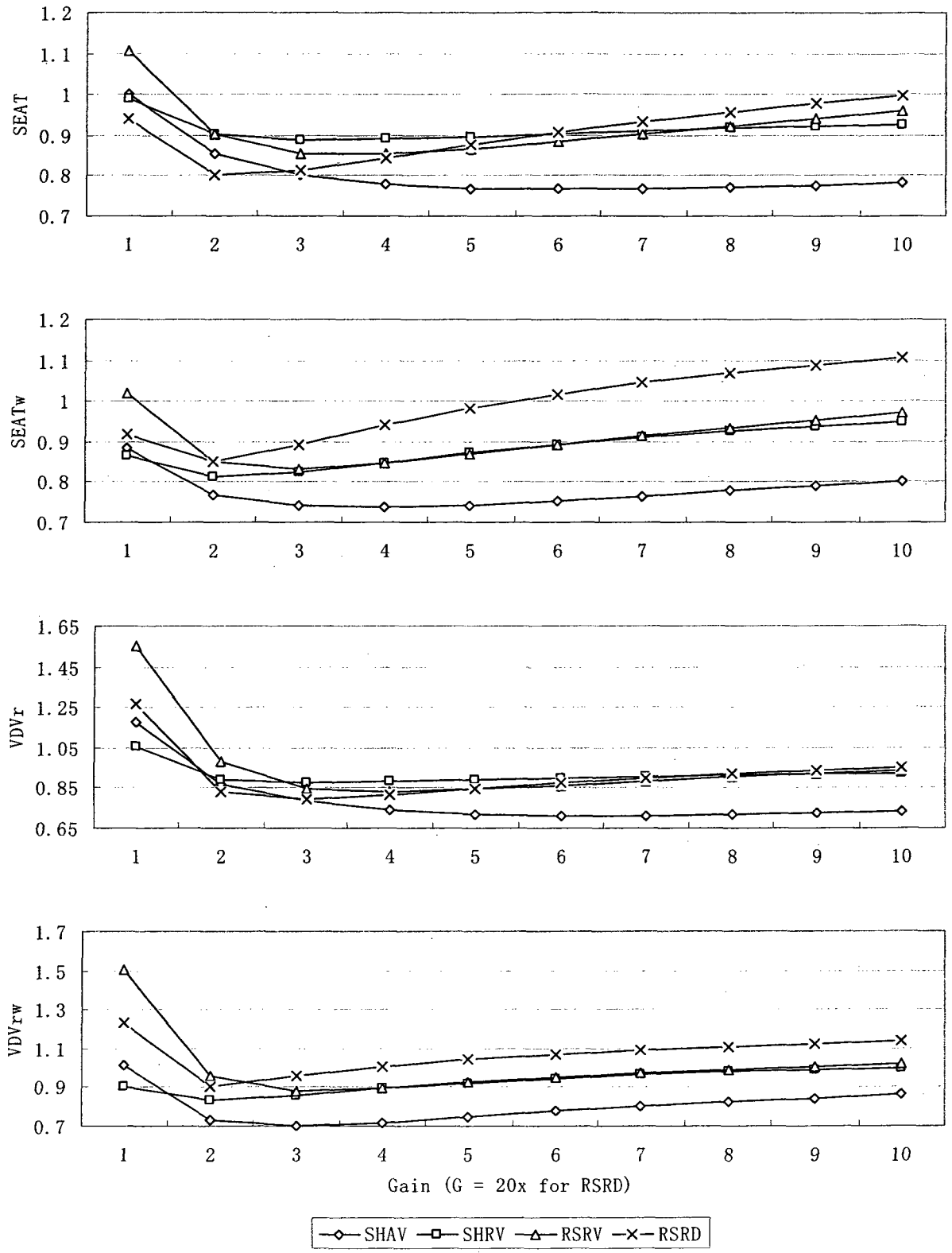

Figure 4.13: Comparisons of performance measures of proposed semi-active suspension seat controllers as a function of the controller gain under EM1A excitation

Under the BUS2A excitation, the RSRV control scheme shows the worst performance with a low controller gain (SEAT = *1.1*; SEATw = *0.83*; VDVr = *1.26*; and VDVrw = *0.92*). The suspension seat with other controllers exhibit comparable values at lower gains (SEAT = 1.0; SEATw = 0.74; VDVr = 1.05; and VDVrw = 0.75). The frequency-weighted performance values of the RSRD control scheme indicate a steady increase in values from $G = 40$, where both frequency-weighted values remain above *0.7*. The other control schemes, however, result in those measured as low as *0.65*. Furthermore, the frequency-weighted values suggest that lower gains, around *3* to *4* are beneficial, whereas unweighted measures suggest desirable gains up to *8*, although the saturation is generally observed near *4*.

Under the SNOWA excitation, all results seem to indicate that a low gain of *2* to *4* yields the best performance. A further increase in the gain yields increase in all performance values, particularly for the weighted measures. The results also reveal that the two sky-hook and relative states feedback control algorithms yield comparable responses corresponding to the low gains. The responses of each of the control schemes within those groups exhibit considerable deviation near $G = 2$, while the performances of the SHRV and RSRV control scheme then to converge at higher gains. This is attributed to their identical current modulation. Overall, the performance values of the semi-active suspension under SNOWA excitation are significantly better than those attained under BUS2A excitation, which is mainly due to the relatively higher frequency of the SNOWA excitation.

Under the EM1A excitation, the RSRD control scheme yields the lowest value of SEAT until $G = 40$, which increases steadily with further increase in the gain. The SHAV and SHRV control schemes yield similar SEAT values corresponding to low gain ($G = 1$), but diverge to below *0.8* and *0.92*, respectively, under $G = 10$. The RSRV control scheme, on the other hand, yields a

relatively higher SEAT value of *1.1*, corresponding to $G = 1$, but converges to that of the SHRV control scheme for $G = 2$. This convergence is also shown in the SEATw value at $G = 3$. The RSRD control scheme performs poorly in terms of the frequency-weighted measures, while the SHAV control scheme maintains its overall superiority.

The selection of the controller gain was based on the SEATw (representing continuous vibration attenuation) and the VDVr (representing shock motions) measures of the semi-active suspension seat under BUS2A, SNOWA, and EM1A excitations. The average of all gains yielding the lowest SEATw and VDVr for each combination of controller and selected inputs are computed and summarized in Table 4.1. As an example, the SEATw and VDVr performance measures of the SHAV control scheme attained under the BUS2A excitation were lowest corresponding to $G = 4$ and $G = 6$, respectively. An average gain of *5* is thus selected for subsequent relative performance analyses. For the SHRV control scheme, the lowest SEATw and VDVr were obtained for $G = 4$ and *5* and $G = 6$, respectively, leading to an average gain of *5.25*. RSRV control scheme resulted in lowest SEATw and VDVr measures corresponding to gain of $G = 7$ and *8* and $G = 9$, respectively, leading to an average gain of *7.5*. In the similar fashion, lowest SEATw and VDVr of the RSRD control scheme were obtained for $G = 60$ and $G = 80$, respectively, which resulted in an average of *70*.

Table 4.1 Selected controller gains for each control scheme corresponding to BUS, SNOW, and EM1 classes vehicular excitations

	BUS class	SNOW class	EM1 class
SHAV	5	4	5.5
SHRV	5.25	2.5	2.5
RSRV	7.5	3.5	3.5
RSRD	70	50	50

The relative performance characteristics of the proposed control schemes were subsequently evaluated under each vehicular excitation using the average gains identified in Table 4.1. The performance measures of the control schemes, evaluated in terms of SEAT, SEATw, VDVr, and VDVrw measures are presented in Figure 4.14 to 4.16 for the BUS, SNOW and EM1 class excitations, respectively. The results showed that the SHAV control scheme generally yielded the best performance, irrespective of the vehicular excitation. The superior performance of the SHAV control scheme is particularly evident for the unweighted SEAT and VDVr measures. The frequency-weighted performance measures of the passive suspension seat are also comparable to those of the semi-active suspension seat under most of the excitation, except for more severe low frequency excitations, namely BUS2A, and EM1A, which tend to cause end-stop impacts. This is mostly attributed to the frequency contents of the w_k weighting filter, which exhibits most significant attenuation of vibration below *4Hz* and above *10Hz* [37]. The low frequency suspension design yields predominant vibration in the vicinity of its resonance frequency, which are effectively suppressed by the weighting filter. The poor relative performance of the passive suspension becomes evident when unweighted SEAT and VDVr measures are considered. The results clearly show that all the proposed control schemes with selected gains yield considerable performance gain over the passive suspension. These are particularly evident in VDVr under the amplified vehicular excitations.

The performance values of the semi-active suspension seat models under BUS class excitations reveal that the SHAV is definitively the best control scheme, which yields beneficial reductions in both the SEATw and the VDVr measures, while the RSRD control scheme yields the highest weighted performance measures. The SHAV control scheme yields reductions in the order of *18%* in the SEATw and *32%* in the VDVr measures, compared to the passive

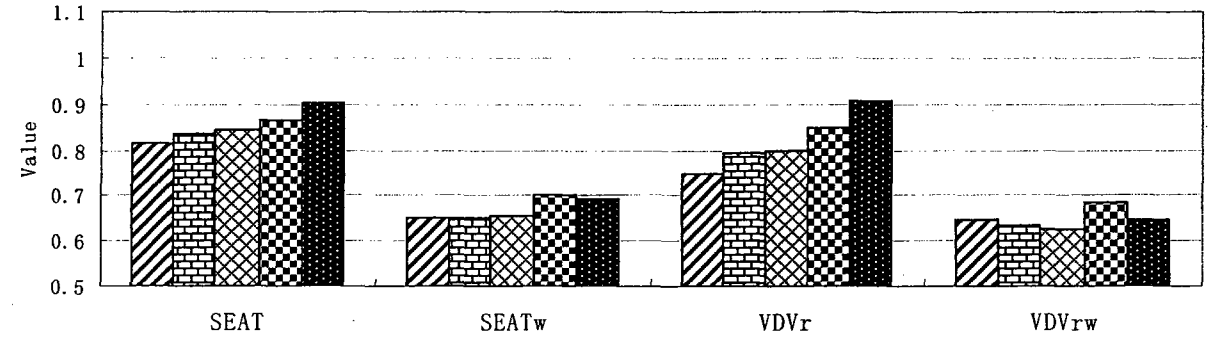

(a)

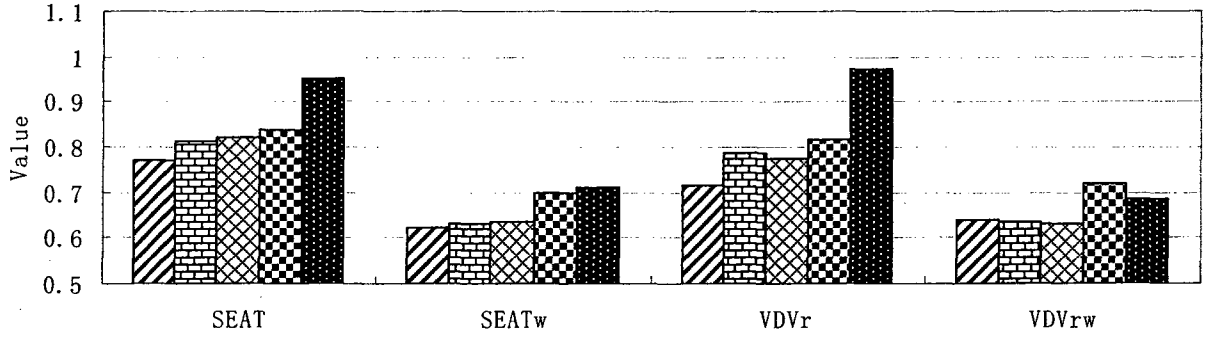

(b)

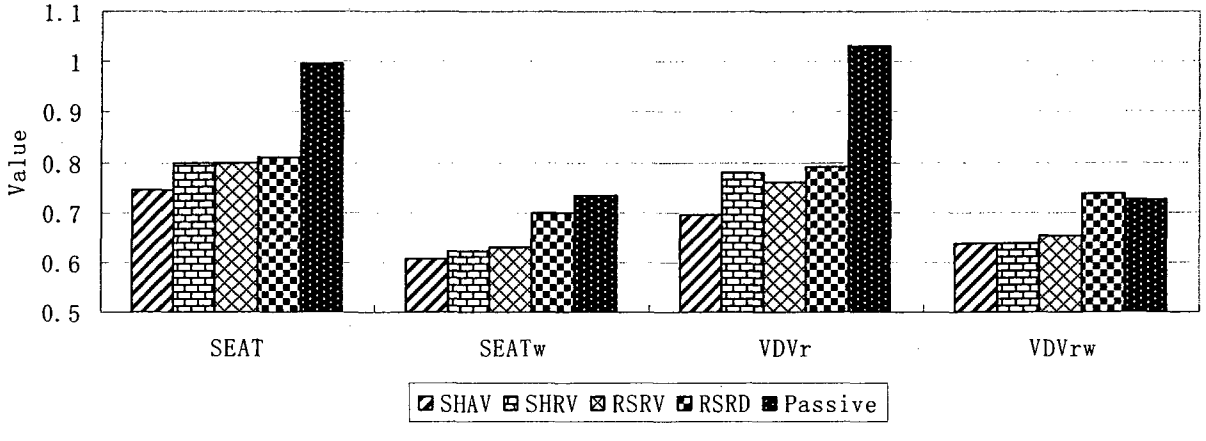

(c)

Figure 4.14: Comparisons of performance measures of the passive and semi-active suspension seat model employing proposed control schemes with selected gains subject to BUS class excitations: (a) BUS; (b) BUSA; and (c) BUS2A

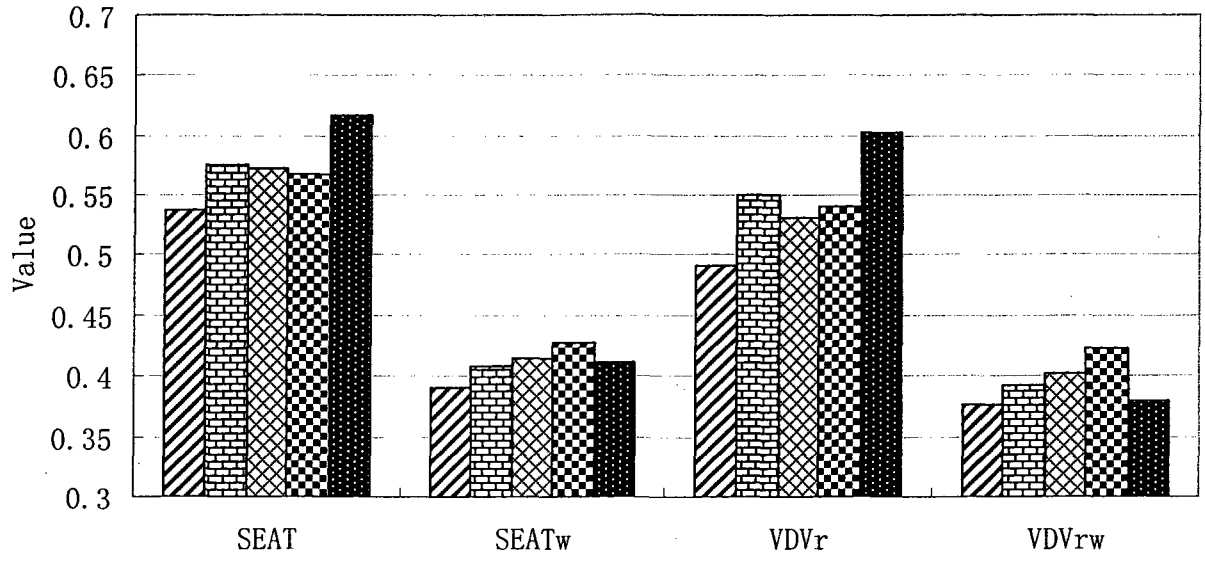

(a)

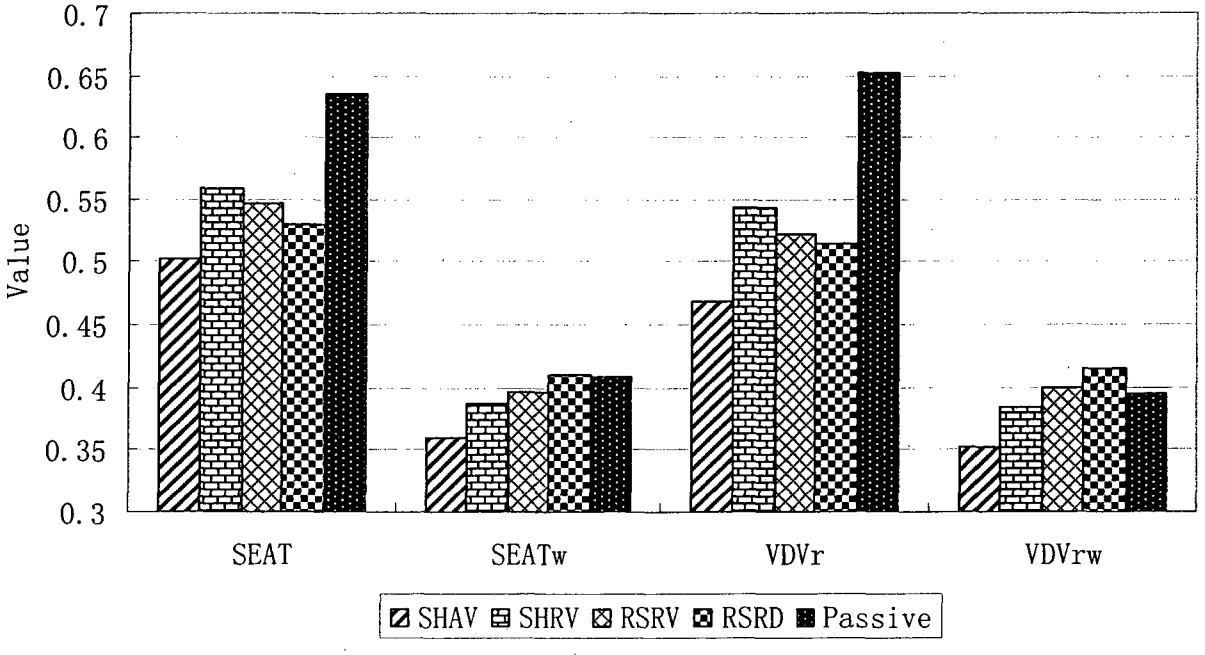

(b)

Figure 4.15: Comparisons of performance measures of the passive and semi-active suspension seat model employing proposed control schemes with selected gains subject to SNOW class excitations: (a) SNOW and (b) SNOWA

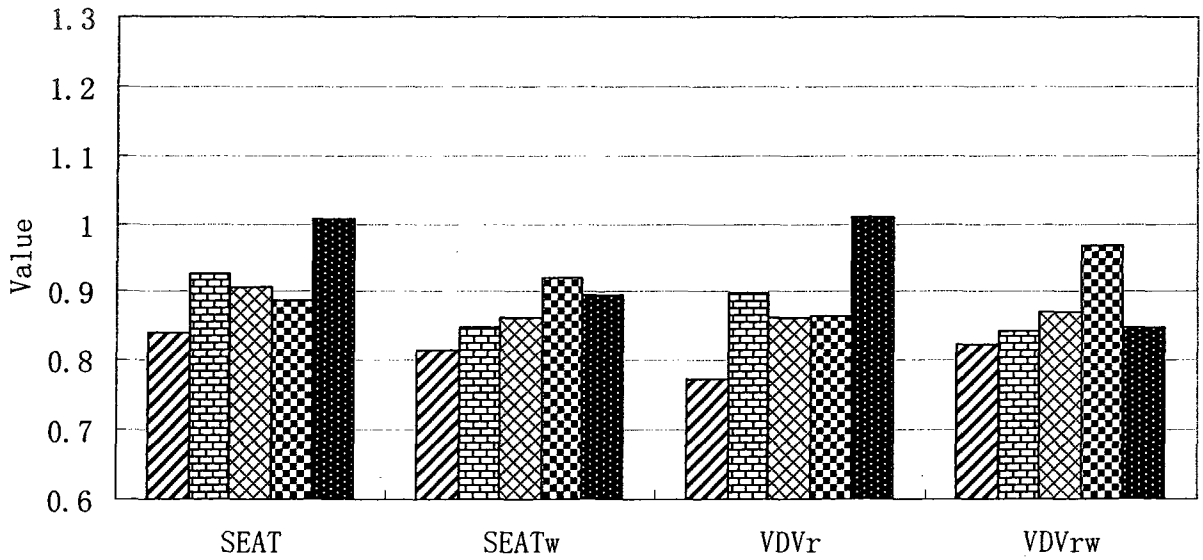

(a)

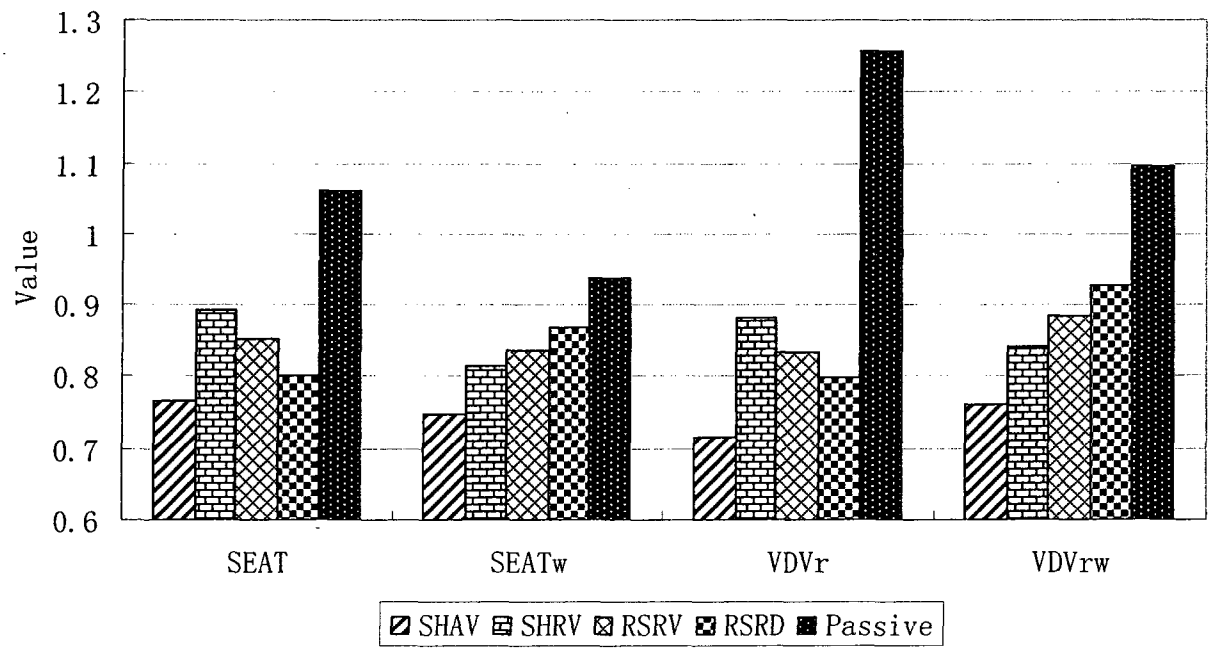

(b)

Figure 4.16: Comparisons of performance measures of the passive and semi-active suspension seat model employing proposed control schemes with selected gains subject to EM1 class excitations: (a) EM1 and (b) EM1A

suspension under the BUS2A excitation. For the RSRV control scheme, the respective reductions are in the order of *15%* and *25%*. The results further reveal that the VDVr measures are slightly lower than the SEAT value for the semi-active suspension seat, while the results for the passive suspension seat exhibit opposite trends. This can be attributed to the end-stop impacts which only occurred for the passive suspension seat. The results for the SNOW class excitations again show the superior performance of the SHAV control scheme, which yields reductions of *12%* and *28%* in the SEATw and VDVr measures, respectively, compared to the passive suspension under the SNOWA excitation. The performance gains of the RSRV control scheme, on the other hand, are only *5%* in SEATw measures and *20%* in VDVr measures. These results suggest that the proposed control schemes also limit the end-stop impacts apart from attenuating continuous vibration. The performance values under EM1 class excitations show relatively greater improvements in both the SEATw and VDVr measures, which is mainly attributed to the high excitation amplitudes with predominant frequency near the resonance frequency of the suspension seat. The greater performance gain is thus mostly related to the end-stop impact suppression. The SHAV control scheme yields reductions of approximately *20%* in SEATw measures and *42%* in VDVr measures, compared to the passive suspension. For the RSRV control scheme, the respective reductions are *11%* and 34%.

In summary, the proposed semi-active suspension seat could yield considerable performance benefits compared to the passive suspension seat in both continuous vibration attenuation and end-stop impact suppression. The type of excitation greatly affects the performance in view of the continuous vibration attenuation, while the end-stop suppression performance gains are most significant under all the amplified excitations. In the case of the SNOW class excitation, the results suggest relatively smaller performance gains of the semi-active suspension due to high

frequency contents of excitation, which are effectively attenuated by a passive suspension. The semi-active controllers, however, yield effective suppression of end-stop impacts. In this case, a first-stage controller alone could be sufficient to achieve end-stop impacts suppression. The performance measures under the BUS class excitations suggest that both the SHAV and RSRV control scheme can achieve reasonable improvements in continuous vibration attenuation, while providing greater end-stop impact suppression. The results due to EM1 class excitations suggest that the semi-active suspension is definitively beneficial. However, unless the SHAV control scheme can be implemented, a second stage controller combined with a low constant damping scheme and an even lower (less than *1.3Hz*) seat resonance frequency could achieve better results since the dominant frequency of the input is around *2Hz*.

4.5 Performance Evaluation of the Second Stage Controller

The suspension effectiveness in supressing the end-stop impacts could be further enhanced by introducing the second-stage controller described in section 4.2.5. The performance characteristics of the semi-active suspension model employing both stages of control are thus evaluated under transient excitations. The analyses, however, are limited to only RSRV first-stage controller. The choice of this controller is attributed to two primary factors. First, the RSRV control scheme is considered to be practically implementable. Second, the end-stop impact supression performance of the RSRV control scheme needs to be enhanced since the damping force is generated in proportion to the relative velocity. The RSRD controller provides effective end-stop impacts supression since the damping force is generated in proportion to the relative displacement. The second-stage controller was introduced by selecting $y_{stop} = 0.05m$, while the gain of the RSRV control scheme was set as to *5*. The end-stop impact performance of the semi-active suspension emplying first-stage (RSRV) controller only were initially evaluated

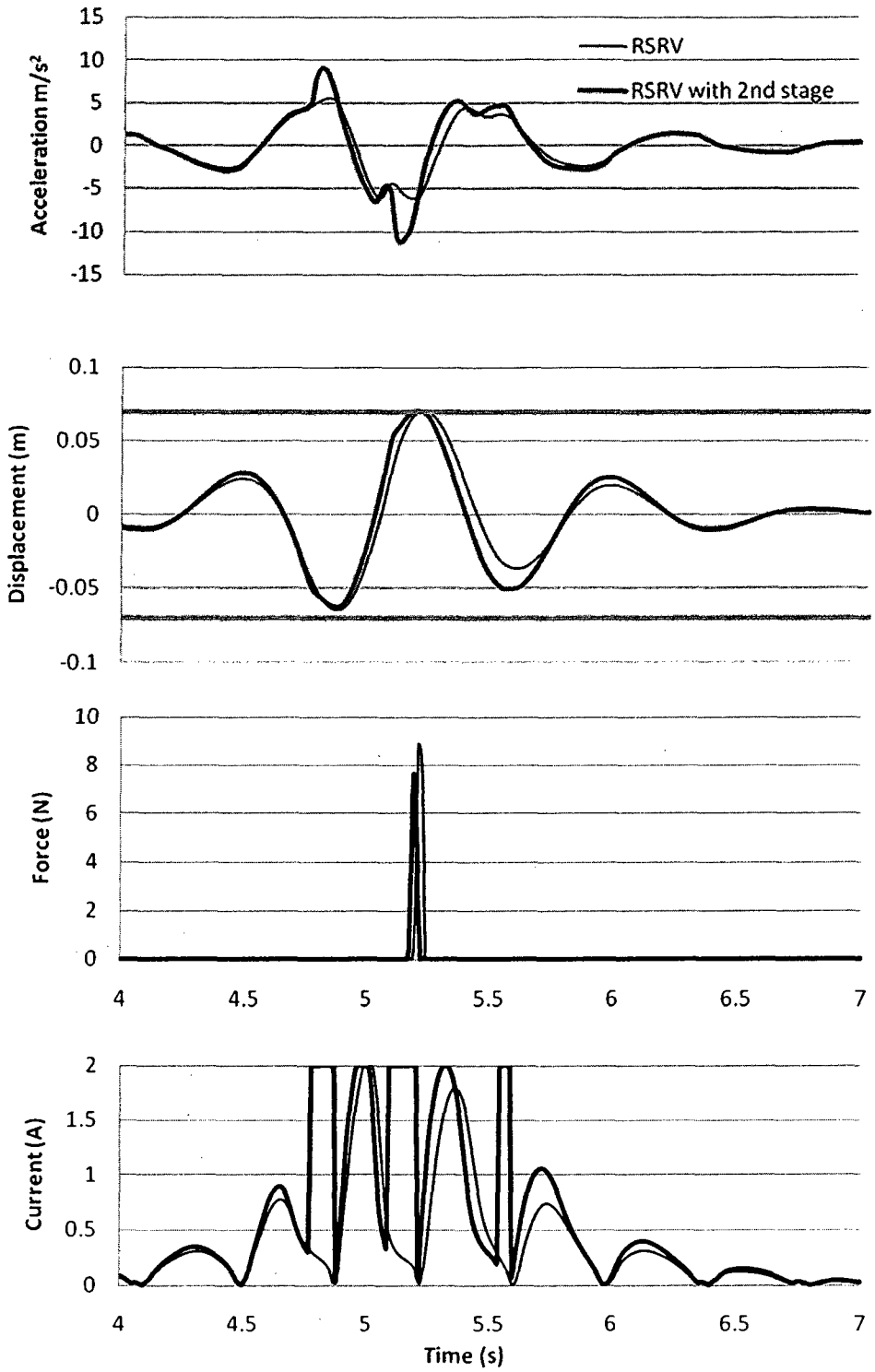

Figure 4.17: Comparison of transient response of semi-active suspension seat model using RSRV control scheme with and without combination of the second-stage controller

under the *1.25Hz* transient excitation with peak excitation displacement of *89mm*. The two stages combined controller was subsequently evaluated using the same transient excitation. The peak excitation magnitude was gradually increased until an end-stop impact was observed. The results revealed presence of an impact under the *99mm* excitation for the two stage combined controller. This difference is attributable to the integration of the second-stage controller, which attempts to limit the suspension displacement to $\pm 5cm$. Figure 4.17 shows the transient response of the RSRV control scheme alone and the combined two stages controller. The suspension employing both stages of control, however, exceeds the free travel ($\pm$7cm), as seen in Figure 4.17, which is attributed to saturation of the damping force corresponding to higher control current. A damper design capable of generating higher damping force may help realize suprerior end-stop impact performance. Figure 4.17 also illustrates the relative displacement and impact force responses together with variation in the control current. It can be concluded that the integration of the second-stage controller increases the RSRV control scheme transient performance by *11%*.

4.6 Summary

In order to increase the vibration attenuation and end-stop impacts suppression performances of the passive hydraulic suspension seat, four first-stage (continuous vibration) and one second-stage (impact motion suppression) controllers were synthesized. The first-stage control schemes, comprised of the SHAV, SHRV, RSRV, and RSRD demonstrated, through simulations, a reduction in continuous vibration transmissibility by *10* to *20%* and a reduction of impact motions by up to *35%*. The results further showed that the two stage combined controller (RSRV with additional position control) allowed an additional *25%* increase in excitation magnitude prior to reach end-stop impacts.

CHAPTER 5: HARDWARE-IN-THE-LOOP (HIL) SIMULATIONS OF THE MAGNETO-RHEOLOGICALLY DAMPED SUSPENSION SEAT

5.1 Introduction

In order to further verify the results of the simulations, the suspension seat model together with the proposed RSRV control scheme was evaluated in the laboratory using the Hardware-in-the-Loop (HIL) platform. The HIL method consists of simulating the entire system model in the simulation software while replacing the target or non-linear element by the real component. The HIL technique has been employed effectively for analysis of various non-linear components, such as suspension tuning and semi-active controller designs [20,21,116,117,118]. Hansselman [116] has summarized the HIL test techniques with the hardware requirements and various capabilities of the HIL real-time simulations. The HIL technique has certain physical limitations and hardware delay issues. Considering the coupling between the active or target component responses and the input motion generation, the system experience instabilities and pose safety risks under extreme conditions. Consequently, shock motions must be avoided in such evaluations. This chapter describes the HIL test procedure and presents the HIL simulation results for the semi-active suspension seat model employing the RSRV control scheme synthesized in Chapter 4.

5.2 An Introduction to Hardware-in-the-Loop (HIL)

Hardware-in-the-loop test techniques have been evolving for efficient design and evaluations of a subsystem or a component while retaining the primary coupling effects of the overall system. The technique is ideally suited for nonlinear subsystems that pose complex modeling

challenges and for controller tuning in an interactive manner. The method was initially developed to allow efficient testing and evaluations of nonlinear components without implementing the entire system [116]. In this study, an HIL test platform was developed using the DS1104 board by Dspace together with a MR damper, developed by Lord Corporation. The damper was installed on the same characterization test bench shown in Figure 2.1. The damper is interceded between a hydraulic cylinder and a fixed inertial beam through a load cell. The hydraulic cylinder is controlled by an MTS 407 hydraulic controller, which also monitors signals, namely the damper force, damper velocity, and damper displacement. An interface between the hardware MR damper and the seat suspension model without the damper, developed in MATLAB Simulink environment, was constructed using the ControlDesk software. The interface consist of a I/O board installed inside a desktop computer, which allows the connection with an I/O box comprising multi-channel digital to analog (DAC) and analog to digital (ADC) signal converters. The ControlDesk software, operating within the I/O ensemble, is linked with the MATLAB Simulink real-time toolbox.

A damper current modulator is integrated between the I/O board and the damper hardware. Figure 5.1 illustrates the HIL simulation scheme. A linear velocity transducer (LVT) and a linear variable different transformer (LVDT) were installed on the shaft of the hydraulic cylinder in order to record the velocity and displacement off the damper, respectively. The displacement signal is also fed back into the servo controller to realize the actuator deflection equal to the suspension relative displacement response derived in the ControlDesk platform. Several hardware settings are of extreme importance prior to the experimentation. The damper must be initially compressed by *25.4mm* to its mid height prior to application of an input excitation. The span of the hydraulic actuator must be set to a safe range, through the servo-controller. For the

MR damper considered in the study the safety range was set to *15.24mm*. The total stroke was thus limited at *30.48mm* to prevent bottoming or topping of the MR damper. Furthermore, the damper current generated from the controller (i_{max}) was limited to *2A* to ensure its safe operation.

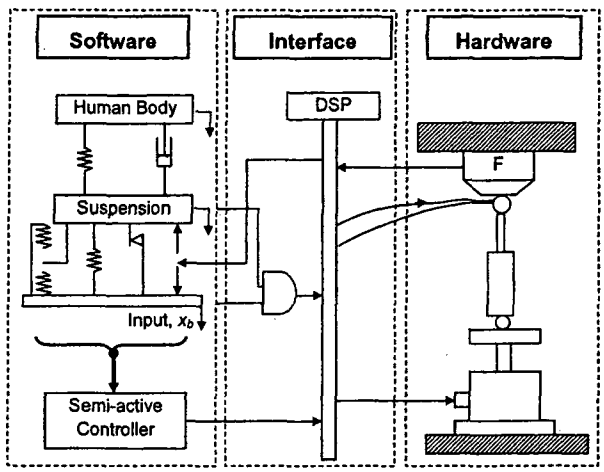

Figure 5.1: Hardware-in-the-loop schematics [20]

5.3 Input for HIL Experiment

The HIL simulation using the candidate MR damper was performed in conjunction with the semi-active suspension seat model employing the RSRV control scheme. In order to verify the simulation responses, the HIL evaluations were conducted under harmonic and random vehicular excitations as described in section 3.2.1 and 3.2.2, respectively. The responses to harmonic inputs were evaluated at various discrete frequencies (*6, 7, 8, 9, 10, 11, 12, 13, 15, 20, 30,* and *40rad/s*), while the magnitudes were identical to those described in section 3.2.1. The responses to random vehicular excitations were evaluated using a repeated signal (*128s*). Due to the occurrence of large magnitude displacement in the random vehicular excitations, the BUS, SNOW, and EM1 excitations were halved and referred to as BUSR, SNOWR, and EM1R. These signals are recorded using Simulink, and then repeated indefinitely through the ControlDesk software for consistency between the different tests. The responses were recorded for *128s* over

their respective cyclic excitations. The transient excitations were also omitted due to the same safety reasons.

5.4 HIL Experimental Results

The HIL experimental results of the semi-active suspension seat using RSRV control scheme under harmonic and vehicular excitation were evaluated in terms of the acceleration transmissibility and the occupant mass acceleration PSD, respectively. The response of the semi-active suspension seat to harmonic inputs (Figure 5.2) related characteristics similar to those observed in the simulation results presented in Figure 4.2 (c): (1) attenuation of the resonance frequency transmissibility magnitude with increasing control gain; and (2) increase in transmissibility magnitude with increasing controller gain in the *2* to *5Hz* range. The frequency response characteristics of the semi-active suspension employing RSRV control scheme are also compared with those of the passive suspension model in Figure 5.2.The comparison suggest that the semi-active suspension seat could yield a reduction of around *20%* in the resonant transmissibility corresponding to $G = 6$. A further increase in the controller gain resulted in saturation of the peak transmissibility magnitude. Furthermore, the resonance frequency of the semi-active suspension seat shifted towards the right with increasing controller gain as observed in the simulation results (Figure 4.2 (c)). The results further showed an increase in the frequency at which attenuation begins with increase in the controller gain. The vibration isolation is attained at frequencies above *2Hz* for $G = 2$ and above *2.4Hz* for $G = 6$.

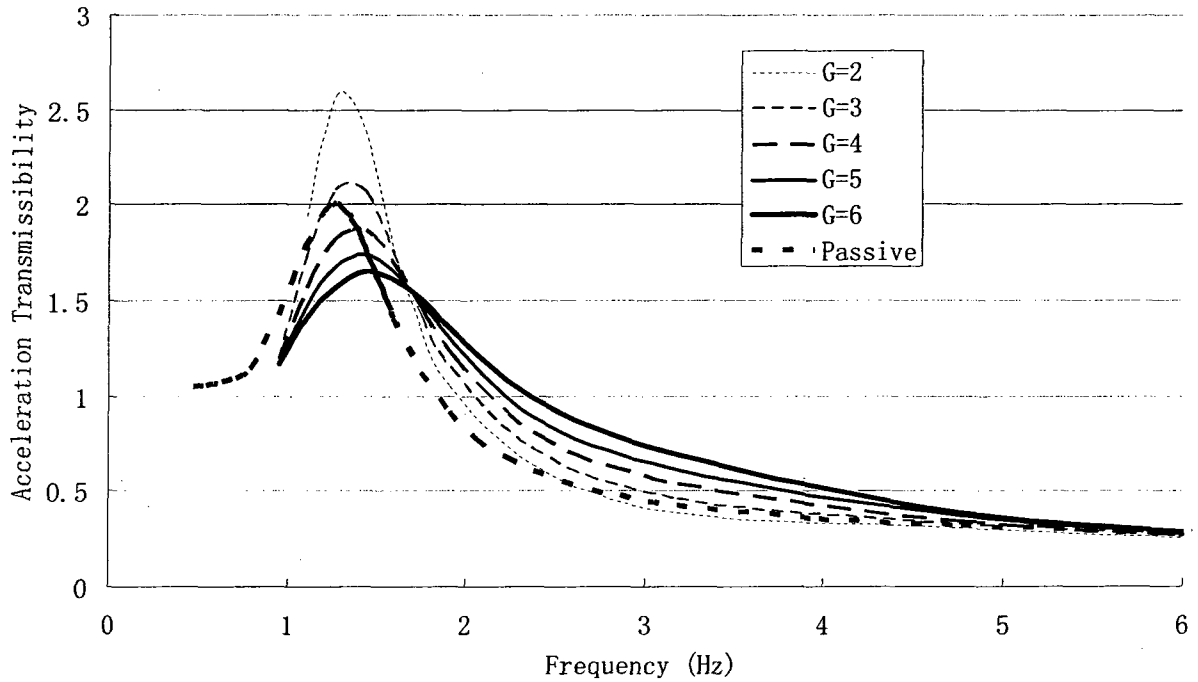

Figure 5.2: Comparisons of HIL acceleration transmissibility responses of the semi-active suspension seat model employing RSRV controller with the simulation results for the passive hydraulic suspension seat model.

Figure 5.3 illustrates the acceleration PSD responses of the HIL semi-active suspension seat model employing the RSRV control scheme subject to BUSR, SNOWR, and EM1R excitations with the acceleration PSD responses of the passive suspension seat model at *50%* magnitude. The figure illustrates the results attained for different controller gains, ranging from *1* to *9*. The results reveal that three distinct peaks are detected near *1.45Hz* with the passive seat resonance peak sitting on top of *1.45Hz*. As the controller gain increased, a reduction of the peak magnitude of the main resonance peak is observed in the case of the SNOWR and EM1R excitations. The two smaller peaks around *1.5Hz*, however, is increased as a compromise. The response PSD behaves in the opposite way for the BUSR excitations as if the data should be labelled $G = 9, 5, 2$, and *1*. However, the peak near *2.1Hz* indicates that the data was properly labelled; only the damper effect is reversed in this case.

The acceleration PSD response of the HIL semi-active suspension seat model to BUSR excitations reveals low resonance magnitude for the main resonance peak at *1.45Hz* with higher compromises for the secondary resonance peaks at *1.25Hz* and *1.6Hz*. However, it should be noted that the real resonance peak of the suspension seat model was located at *1.25Hz*, which exhibits a reduction in magnitude while the controller gain was increased. The resonance peak located at *1.45Hz* could be the second peak observed in the simulation results, which is formed under overdamped conditions. Similar phenomenon could be observed at *1.8Hz* and *2.1Hz*. However, the peak at *1.6Hz* exhibited the exact same trend as the *1.25Hz* peak. These behaviours could be attributted to the effect due to a small excitation amplitude (half of the nominal random excitation amplitude), which requires the damper to operate more often in the pre-yield range thus yielding higher damping coefficients. Furthermore, since the damper was operating more frequently in the pre-yield range, the hysteresis effect could also become a more dominant source of error.

The acceleration PSD response of the HIL semi-active suspension seat model to SNOWR excitations reveals also three distinct peaks near *1.45Hz*. The trend, however, is reversed from the responses to BUSR excitations. At low controller gain ($G = 1$). The peak magnitude is higher than the peak magnitude of the passive model. As the controller gain was increased, both the *1.25* and *1.45Hz* peaks diminished by compromising the *1.6Hz* peak, which saturated at a magnitude of $0.9m/s^2/Hz$ from $G = 2$. Peaks in the *2* to *2.6Hz* range showed an increase in magnitudes at higher control currents ($G = 5$ and 9).

The acceleration PSD response of the HIL semi-active suspension seat model to EM1R excitations reveals also three distinct peaks near *1.45Hz*. The first peak, near *1.25Hz* is of higher magnitude at low controller gain ($G = 1$) than the passive model peak magnitude. The peak

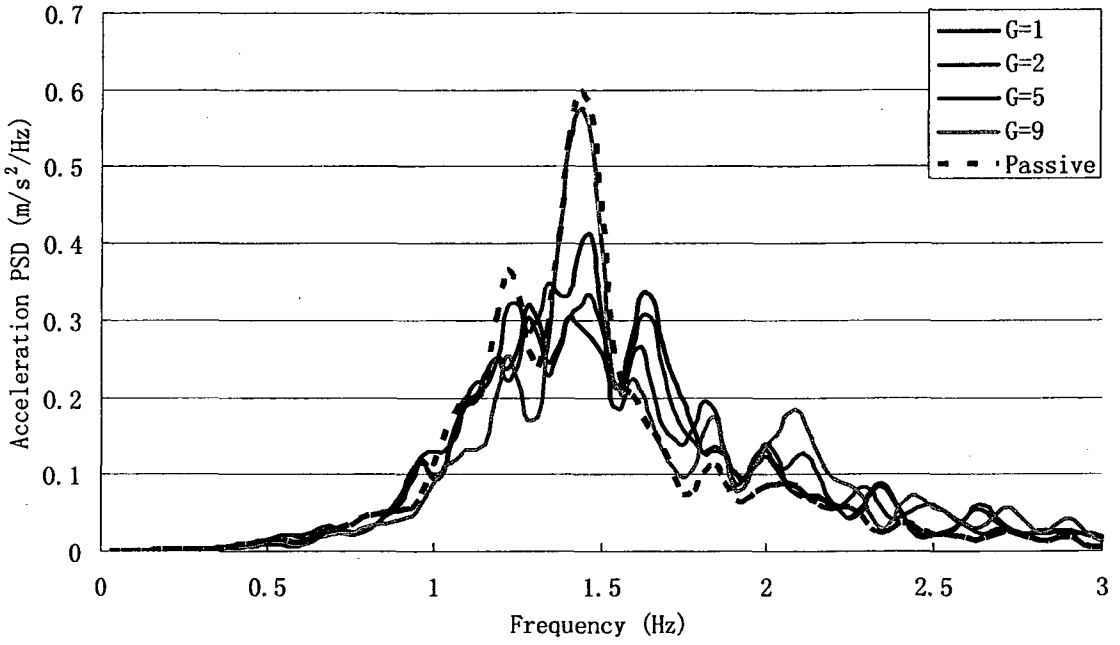

(a)

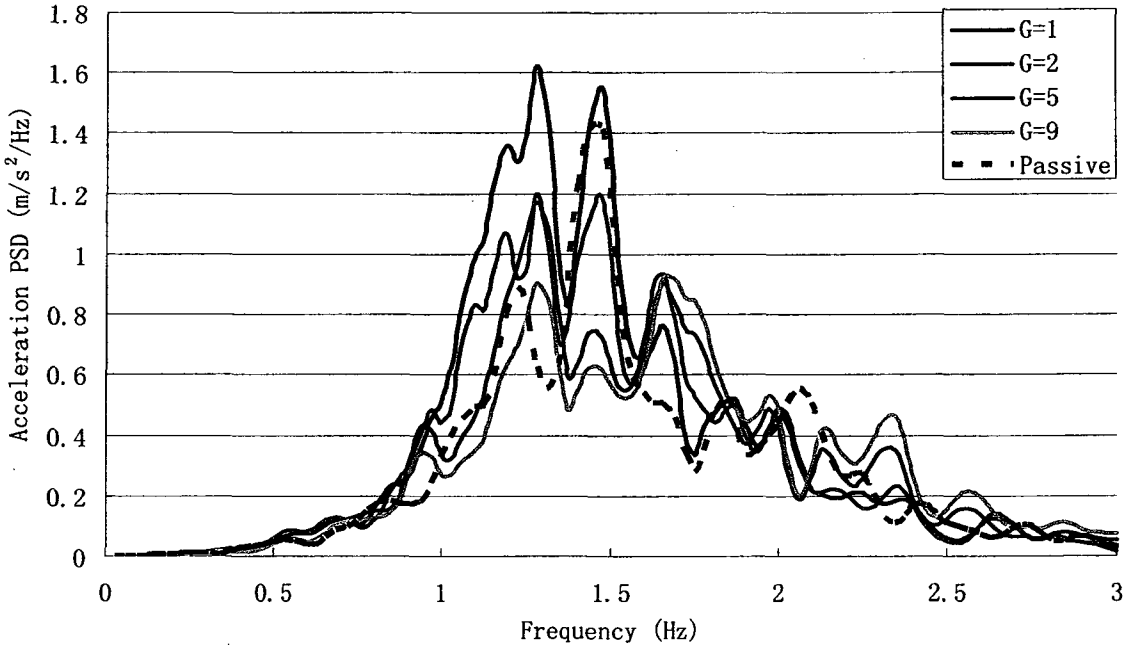

(b)

Figure 5.3: Comparison of HIL simulation results of the PSD functions of the suspension seat model response to the (a) BUSR, (b) SNOWR, and (c) EM1R inputs (continued)

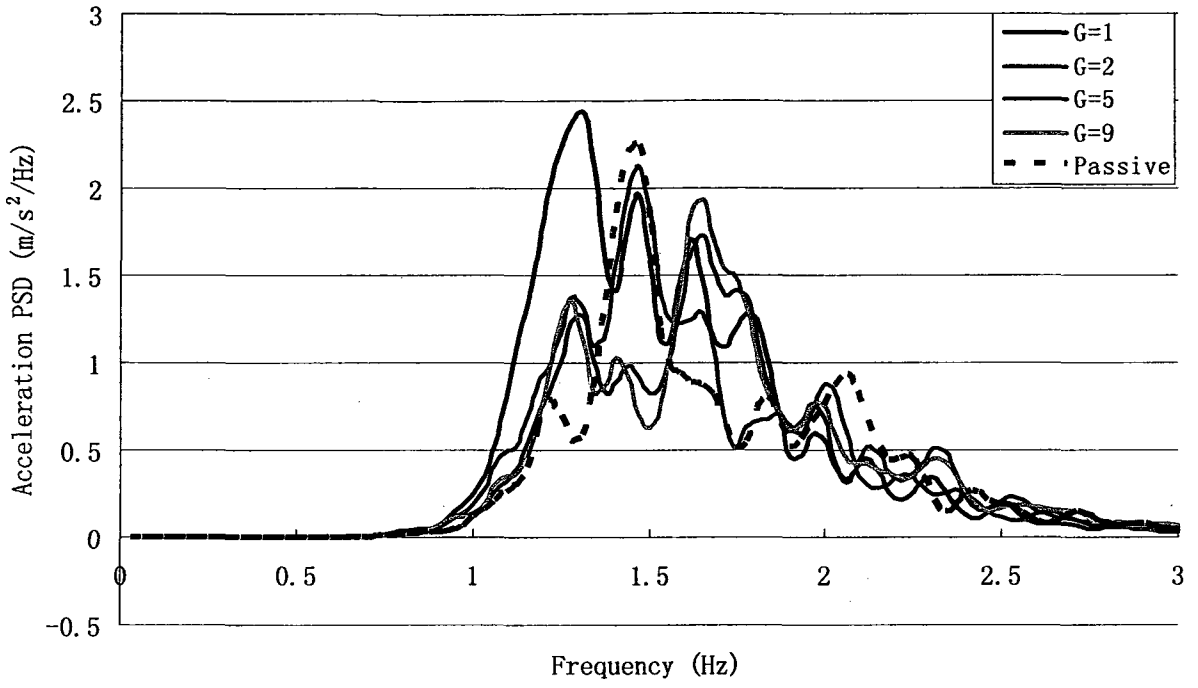

(c)

Figure 5.3: Comparison of HIL simulation results of the PSD functions of the suspension seat model response to the (a) BUSR, (b) SNOWR, and (c) EM1R inputs

immediately saturates near *1.25m/s²/Hz*, for *G = 2, 5,* and *9*, at around half the magnitude when *G = 1*. The similar phenomenon is observed for the second peak around *1.45Hz*. The peaks magnitudes corresponding to *G = 1* was just below *2m/s²/Hz* and corresponding to *G = 2* was right above *2m/s²/Hz*. The peaks corresponding to *G = 5* and *9* saturated at around *1m/s²/Hz*. The third peak, near *1.6Hz* suggests that a magnitude reduction occurred from *G = 1* to *2*. The magnitude then increased corresponding to *G = 5* and *9*. It suggests that perhaps a better gain is available between *G = 2* and *5*. The peak near *2Hz* showed better attenuation than the passive suspension seat model.

The performance measures of the HIL semi-active suspension seat equipped with RSRV control scheme are computed and shown in Figure 5.4. The results revealed higher performance

measures for the semi-active suspension seat model. The overall trend is characterized by a decrease in performance measures with increasing controller gain. A few exceptions were observed at high controller gains ($G = 9$) for SNOWR and EM1R excitations, where an increase in performance values were observed. The passive suspension model simulation performed better than the HIL semi-active suspension model in most cases; nevertheless, the performance measures were very comparable between HIL and non-HIL simulations. The lower performance indicated by the HIL simulations may be attributed to several factors that were not considered in non-HIL simulations such as: damper hysteresis (accentuated by reducing the excitations magnitudes), hardware delays, measurement drifts, and current overshoot.

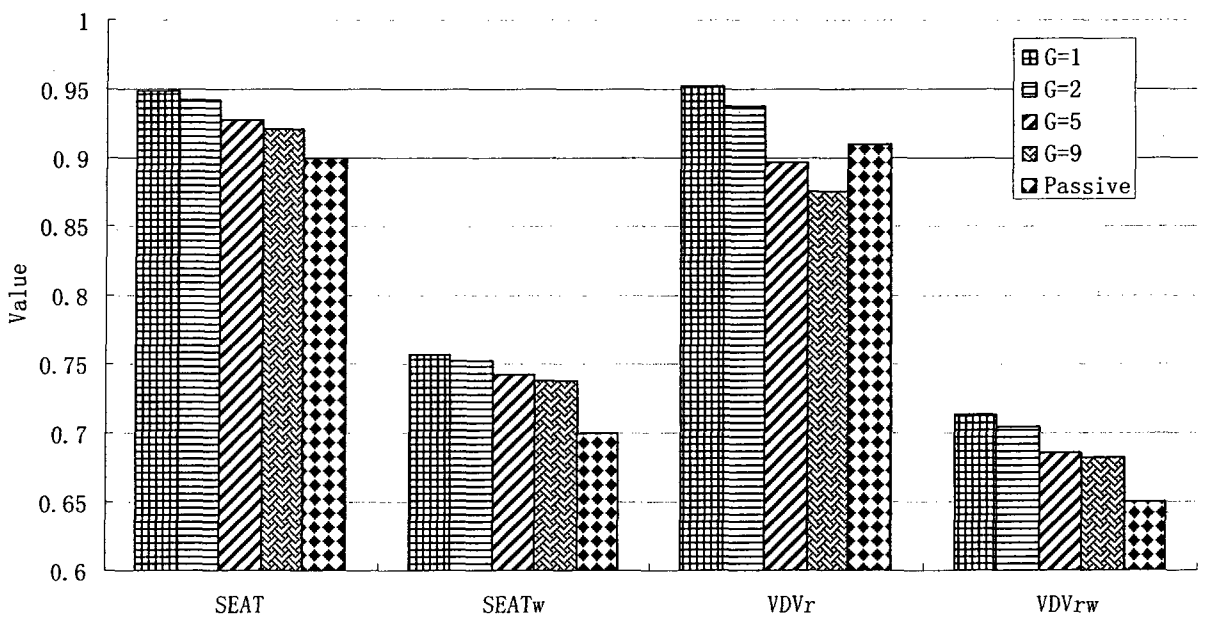

(a)

Figure 5.4: Comparisons of performance measures of the HIL semi-active suspension seat model and the passive suspension seat model under selected vehicular excitations: (a) BUSR; (b) SNOWR; and (c) EM1R inputs (continued)

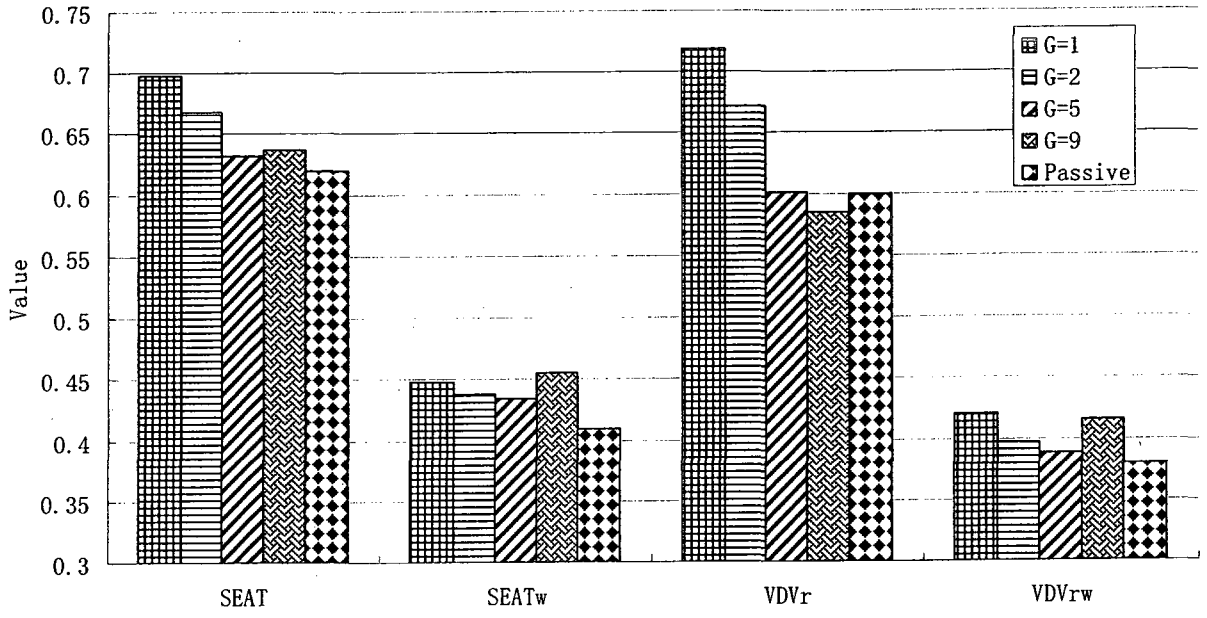

(b)

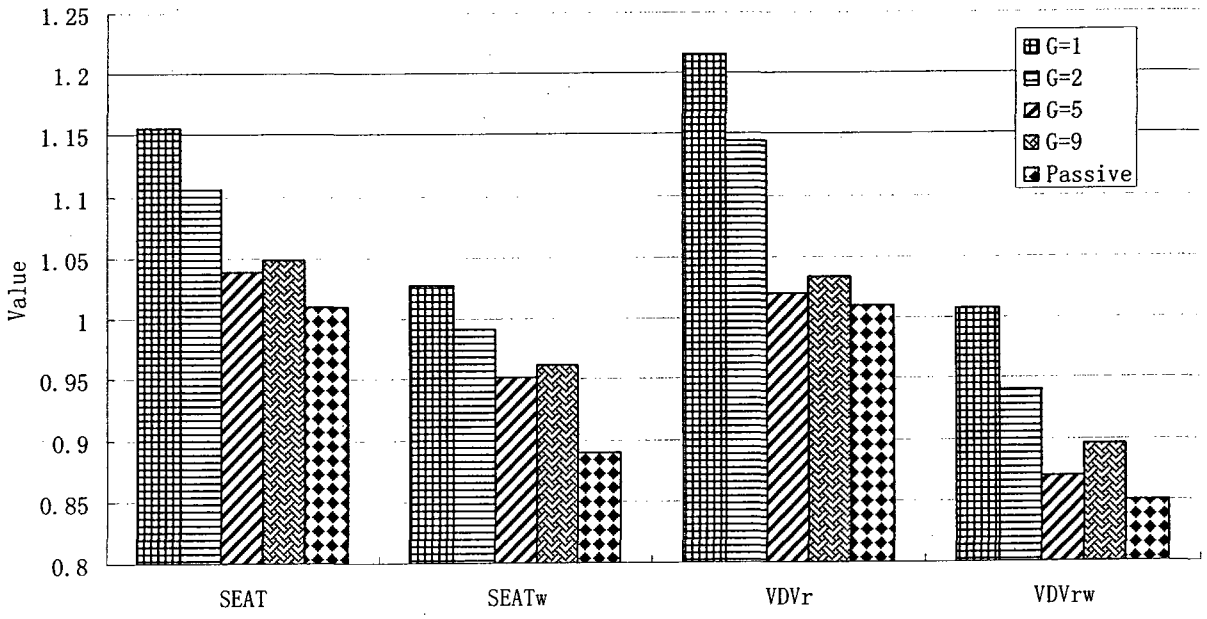

(c)

Figure 5.4: Comparisons of performance measures of the HIL semi-active suspension seat model and the passive suspension seat model under selected vehicular excitations: (a) BUSR; (b) SNOWR; and (c) EM1R inputs

It was demonstrated by Ma [20], through laboratory experiment, that the hysteresis of the MR damper was negligible when implemented in applications. However, in this study, the HIL simulations random vehicle excitations are halved in order to provide a safety margin to the hardware equipments and component. The hysteresis of the MR damper, which occurs mostly in the pre-yield range, thus contributes to increase the error between the MR damper model and the MR damper characteristics. In additional, the hardware used for HIL simulations may have contributed to some of the lack of performance, shown by the performance measures, due to hardware delays. In order to reduce the amount of shocks introduced into the MR damper from the hydraulic compressor, the hydraulic controller, which controls the hydraulic compression via a PID controller, was set to a lower differential coefficient and a higher integral coefficient in order to provide a smoother motion to the damper and less noise and drifts in the load cell signal. The setting may thus have created some lag between the time the displacement signal was sent to the hardware and the time the force signal was collected and converted into digital signal inside the simulation. Finally, it was observed during the HIL simulations that if the current has been brought up to a high value (>1.25), the measured current overshot in the negative range after it was turned off by the controller. Such overshoot would certainly increase the damping force more than it is required.

Due to these unaccounted factors, the performance of the HIL semi-active suspension seat model simulation did not provide a positive feedback in respect to the non-HIL simulation results. The trends observed in the non-HIL simulations were, however, observed in the HIL simulation. This shows good consistency in the HIL simulations.

5.5 Summary

Chapter 5 overviewed the experimental setup, procedures, and results of the hardware-in-the-loop (HIL) experiment. A candidate MR damper was used in the HIL simulation of the semi-active suspension model equipped with the RSRV control scheme proposed in Chapter 4. The responses were analyzed under harmonic excitations and reduced selected random vehicular excitations (both at *50%* of nominal excitation magnitudes).

The trends generally agreed with the non-HIL simulations, but the magnitudes of the transmissibility and acceleration PSD of the responses are slightly higher. The performance values also showed higher magnitude transmissibility compared to the passive suspension seat model. Several factors in hardware experimentation may be at the source of lower performances.

CHAPTER 6: CONCLUSIONS

6.1 Major Highlights and Contributions

Occupational vehicle drivers are exposed to continuous vibrations and shock motions for extended periods of time on a daily basis. The use of suspension seat to attenuate such motions between the vehicle cab and the driver is of utmost importance. Suspension seats designed with low natural frequencies are employed in off-road and road vehicles to control the transmission of vibration to the seated occupant. The low natural frequency suspension seat with limited free travel, however, yields end-stop impacts resulting shock motions of the occupant. This dissertation research investigated a MR semi-active suspension seat to achieve control of both the continuous vibration and shock motion. The results showed that improvements in both continuous vibration and shock motions attenuations can be achieved using a semi-active suspension.

The dissertation research mainly focused on three aspects of the semi-active suspension system: the modeling of a MR damper and its validations; the modeling of a non-linear suspension seat incorporating its kinematics and its validations; and synthesis of a two stages controller for the MR damper. A generalized model describing the force velocity function of the MR damper was developed through linear regression analysis of the experimental data. The damper model was validated using data obtained from the damper test bench over a wide range of applied currents. A two degree-of-freedom model of the suspension seat was developed, which comprised non-linearity due to the linkage kinematics and the damper orientation. The effectiveness of the suspension seat model was demonstrated through comparisons of the simulation results with the available measured data.

Four different MR damper first stage controllers were proposed based on the sky-hook and the relative states feedback control algorithms. The relative states feedback current proportional to relative displacement was rejected due to its poor performance. The relative states feedback current proportional to relative velocity control scheme was further evaluated using the hardware-in-the-loop technique, owing to the control scheme's greater practical implementation potentials. A second-stage controller was further proposed and evaluated for limiting for limiting the end-stop impacts.

6.2 Major Conclusions

Following major conclusions could be drawn from the simulation and experimental results attained in the course of the dissertation research.

1. The magneto-rheological (MR) damper model proposed, which was based on a bi-linear extension of the bi-viscous damper model, was simple to implement into simulations. The addition of the third order polynomial function for the pre-yield range, in order to make the damper model continuously differentiable, reduced the amount of chattering in simulations. The model, although neglected the hysteresis of the MR damper characteristics provided a great precision of the mean force-velocity characteristics up to *0.75A*. Beyond such current setting, the damper model over estimated the actual damping force due to the non-linearity of the force-current characteristics. The damper force-current characteristics diminished rapidly past *0.75A* thus making the *0* to *0.75A* range most useful.
2. The proposed two-DOF suspension seat model for both passive and semi-active suspension seat contained the non-linearity of the candidate suspension seat. The results showed that under the same types of vehicular excitations, the proposed passive suspension seat model had less end-stop impacts than a previous model of the same seat proposed by Ma [20]. The model also showed that end-stop impacts occurred more frequently using the MR damper at zero control current. The seat equipped with the MR damper was thus considered unsafe under controller failure situations.
3. The performance of a suspension seat in attenuating continuous vibration and in suppression of end-stop impacts was enhanced by integrating a two-stage controller, where the second stage controller base on relative displacement feedback reduced the end-stop impacts. The SHAV control scheme demonstrated the best performance followed by SHRV and RSRV at equal standing, and finally RSRD. Increases in vibration attenuations by up to *30%* depending on the type of inputs were attained using the various first-stage controllers. The

second-stage controller, in combination with the RSRV control scheme, could further provide up to *11%* under extreme transient excitations.

4. Further attempts to validate the RSRV control scheme using hardware-in-the-loop (HIL) technique did not yield positive results. The various HIL simulations of the RSRV control scheme demonstrated worse performance than the passive suspension seat model simulations. The difference could be attributed to several aspects that were not considered during non-HIL simulations: damper hysteresis, hardware component delays, measurement inaccuracy, and current modulator overshoot.

6.2 Research Limitations and Future Works

A forward step was achieved in the control of suspension seats, however, more investigation are still required prior to commercialization of a semi-active suspension seats. This thesis addressed part of the application requirements of a semi-active suspension seat; however, several limitations have not been addressed. The damper model, which is based on regression of measured values, is only precise up to *0.75A*. The suspension seat model is derived based on a single suspension seat design and cannot be applied to other suspension seats. Furthermore, the position of the damper does not allow the damper to exert sufficient amount of equivalent damping when zero current is applied through the damper. The HIL simulations, although practical and cost effective, has limitations such as hardware delays. Three future work propositions are described as follow to remedy the limitations:

1. The damper technology can be further enhanced if the damping force can be increased and the current operating range widened. Currently, available *2in* stroke MR damper operate from *0* to *2A* with a useful bandwidth of *0.75A*. If the total operating range of the damper can be double, it is safe to assume that a working range up to *1.5A* can be achieved using similar designs.
2. A parameter study can be performed using the proposed suspension seat model. The damper angle can be rearranged to obtain better non-linearity. Currently, most suspension seats are designed with passive damper characteristics in mind, semi-active suspension seats are only available by replacing the passive damper by an MR or ER damper, which results in must lower damping force when the control current or voltage is off for various reasons, for instance controller failure. Under such circumstances, it was shown in Chapter 3 that the suspension seat will hit the elastic end-stops with an increased frequency, thus the

emplacement of the damper shoudl be carefully studied and the seat should be designed with a MR damper in mind.

3. An HIL simulation can be performed by implementing the entire seat on a seat shaker while the controller is simulated using the ControlDesk software. Such setup allows the experimentation of the entire seat as well as the performance assessment of end-stop impacts.

REFERENCES

1. Griffin, M.J., "Handbook of Human Vibration", Academic Press Limited, London, 1990.
2. Boileau, P.-É., Rakheja, S., Lin, P.J., "A combined seat suspension-vehicle driver model for estimating the exposure to whole-body vehicular vibration and shock", *International J. of Vehicle Design, Heavy Vehicle Systems*, 4(2-4): 244-265.
3. Corbridge, C., "Vertical vibration transmission through a seat: effects of vibration input, subjects' postures and subjects' physical characteristics", *The UK informal Group Meeting on Human Response to Vibration*, Royal Military College of Science, Shrivenham, England, 21 – 22 September, 1987.
4. Thakurta, K., Koester, D., Bush, N., Bachle, S., "Evaluating short and long term seating comfort", *International Congress and Exposition*, Detroit, Machigan, February 27 – March 2, SAE Paper No. 950144, 1995.
5. Griffin, M.J., "Discomfort from feeling vehicle vibration", *Vehicle System Dynamics, Vol. 45, 679 – 698, 2007.*
6. Eger, T., Grenier, S., Salmoni, A., "Whole-body vibration exposure experienced by mining equipment operators", *Proceedings of Fifth Canadian Rural Health Research Society Conference and the Fourth International Rural Nurses Congress*, Sudbury, ON, Canada, 2004.
7. Ahmadian, M., Marjoram, R.H., "Effects of passive and semi-active suspensions on body and wheel hop control", *Journal of Commercial Vehicles*, 98: 596 – 604, 1998.
8. Rakheja, S., Ahmed, A.K.W., Yang, X., Guerette, C., "Optimal suspension damping for improved driver- and road-friendliness of urban buses", *Proceedings of the SAE International Truck & Bus Meeting*, Detroit, USA, November, 1999.
9. Cebon, D., "Handbook of vehicle-road interaction", ISBN 9026515545, Copyright © 1999 Swets & Zeitlinger B.V., Lisse, the Netherlands, 1999.
10. Boileau, P.-É., Rakheja, S., "Charactérisation de l'environnement vibratoire dans différentes catégories de catégories de véhicules : industriels, utilitaires et de transport urbain", *Institut de recherche en santé et sécurité du travail (IRSST) report*, R-242, 162, 2000.
11. Tchernychouk, V., "Objective assessment of static and dynamic seats under vehicular vibration", Master's Thesis, Concordia University, Montreal, 1990.
12. Suggs, C.W., Abrams, C.F., Stikeleather, L.F., "Application of a damped spring-mass human vibration simulator in vibration testing of vehicle seats", *Ergonomics*, 12: 79 – 90, 1969.

13. Gunston, T.P., Rebelle, J., Griffin, M.J., "A comparison of two methods of simulating seat suspension dynamic performance", *Journal of Sound and Vibration*, 278(1 – 2): 117 – 134, 2004.

14. Lewis, C.H., Griffin, M.J., "Evaluating the vibration isolation of soft seat cushions using an active anthropodynamic dummy", *Journal of Sound and Vibration*, 253(1): 295 – 311, 2002.

15. Perisse, J., Jezequel, L., "An original feedback control with a reversible electromechanical actuator used as an active isolation system for a seat suspension. Part I: theoretical study", *Vehicle System Dynamics*, 24: 305 – 331, 2000.

16. Perisse, J., Jezequel, L., "An original feedback control with a reversible electromechanical actuator used as an active isolation system for a seat suspension. Part II: experimental study", *Vehicle System Dynamics*, 24: 381 – 399, 2000.

17. Thompson, A.G., "Optimal and suboptimal linear active suspensions for road vehicles", *Vehicle System Dynamics*, 13: 61 – 72, 1984.

18. Margolis, D.L., "Procedure for comparing passive, active and semi-active approaches to vibration isolation", *Journal of the Franklin Institute*, 315(4): 225 – 238, 1983.

19. Rabinow, J., "The magnetic fluid clutch", *AIEE Transaction*, 67: 1308 – 1315, 1948.

20. Ma, X.Q., "Dynamic characterization of a magneto-rheological fluid damper and synthesis of a semi-active suspension seat", Ph.D. Dissertation, Concordia University, Montreal, Canada, 2006.

21. Choi, S.-B., Lee, B.-K., Nam, M.-H., Cheong, C.-C., "Control and response characteristics of a magneto-rheological fluid damper for passenger vehicles", *Smart Materials and Structures 2000, Proceedings of SPIE*, 3985: 438 – 443, 2000.

22. Yokoyama, M., Hedrick, J.K. Toyama, S., "A model following sliding mode controller for semi-active suspension systems with MR dampers", *Proceedings of the American Control Conference*, 4: 2652 – 2657, 2001.

23. Liao, W.H., Wang, D.H., "Semi-active vibration control of train suspension systems via magneto-rheological dampers", *Journal of Intelligent Material Systems and Structures*, 14(3): 161 – 172, 2003.

24. Guo, D.L., Hu, H.Y., and Yi, J.Q., "Neural network control for a semi-active vehicle suspension with amagneto-rheological damper", *Journal of Vibration and Control*, 10(3): 461 – 471, 2004.

25. McManus, S.J., St. Clair, K.A., Boileau, P.-É., Rakheja, S., « Evaluation of the vibration and shock attenuation performance of a semi-active magneto-rheological fluid damper", *Journal of sound and Vibration*, 253(1): 313 – 327, 2002.

26. Gunston, T., "An investigation of suspension seat damping using a theoretical model", *Proceedings of the 35th UK Group Meeting on Human Responses toVibration*, Southampton, England, September, pp. 207 – 219, 2000.

27. Rakheja, S., boileau, P.-É., Wang, Z., "Performance analysis of suspension seats under high magnitude vibration excitations: Part II: design parameters study", *Journal of Low Frequency Noise, Vibration and Active Control*, 23(1): 7 – 26, 2004.

28. Allen, G.R., "A critical look at biodynamic modeling in relation to specifications for human tolerance of vibration and shock", *AGARD Conference Proceedings*, Paris, France, 6 – 10 November, No. 253, Paper A25 – 5, pp. 519, 1979.

29. International Organization for Standardization, "Mechanical vibration and shock-range of idealized values to characterize seated-body biodynamic response under vertical vibration", ISO 5982, 2001.

30. Renae, B.C., Carnahan, T., Rachel, T.-C., Crump, R., et al., "User perspectives on seat design", *International Truck and Bus Meeting and Exposition*, Winston-Salem, North Carolina, 13 – 15 November, SAE no. 952679, 1995.

31. Rebelle, J., "Development of a numerical model of seat suspension to optimize the end-stop buffers", *Proceedings of the 35th UK Group Meeting on Human Responses to Vibration*, Southampton, England, September, pp. 221 – 238, 2000.

32. Rakheja, S., "Computer-aided dynamic analysis and optimal design of suspension systems for off-road tractors", Ph.D. Thesis, Concordia University, Montreal, Canada, 1983.

33. Pare, C.A., "Experimental evaluation of semi-active magnto-rheological suspensions for passenger vehicles", M.Sc. Thesis, Virginia Polytechnic Institute and State University, Blacksburg, Virginia, 1998.

34. Wu, X., "Study of drive-seat interactions and enhancement of vehicular ride vibration environment", Ph.D. Thesis, Concordia University, Montreal, Canada, 1998.

35. Boileau, P.-É., "A study of secondary suspension and human driver response to whole-body vehicular vibration and shock", Ph.D. Thesis, Concordia University, Montreal, Canada, 1995.

36. Rakheja, S., Afework, Y., Sankar, S., "An analytical and experimental investigation of the driver-seat-suspension system", *Vehicle System Dynamics*, 23: 501 – 524, 1994.

37. International Organization for standardization, "Evaluation of human exposure to whole-body vibration – part I: General requirements", ISO 2631/1, 1997.

38. International Organization of Standardization, "Earth-moving Machinery – Laboratory Evaluation of Operator Seat Vibration", ISO 7096, 2000.

39. Rakheja, S., Boileau, P.-É., Wang, Z., Politis, H., "Performance analysis of suspension seats under high magnitude vibration excitations: Part 1: Model development and validation", *Journal of Low Frequency Noise, Vibration and Active Control*, 22(4): 225 – 252, 2003.

40. Ebe, K., "Effect of composition of polyurethane foam on the vibration transmissibility of automotive seat", *The UK informal Group Meeting on Human Response to Vibration*, Ministry of Defense, Farnborough, Hampshire, England, 20 – 22 September, 1993.

41. Wu, X., Griffin, M.J., "The influence of end-stop buffer characteristics on the severity of suspension seat end-stop impacts", *Journal of Sound and Vibration*, 215(4): 989 – 996, 1998.

42. Wu, X., Griffin, M.J., "A semi-active control policy to reduce the occurrence and severity of end-stop impacts in a suspension seat with an electrorheological fluid damper", *Journal of Sound and Vibration*, 203: 781 – 793, 1997.

43. Ng, D., Cassar, T., Gross, C.M., "Evaluation of an intelligent seat system", *Applied Ergonomics*, 26(2): 109 – 116, 1995.

44. Hilyard, N.C., Collier, P., Care, C.M., "Dynamic mechanical behavior of flexible foam cushion materials and its influence on ride comfort", *The UK informal group Meeting on Human Response to Vibration*, the National Institute of Agricultural Engineering, Silsoe, Bedfordshire, England, 14 – 16 September, 1983.

45. Ebe, K., Griffin, M.J., "Effect of polyurethane foam on dynamic sitting comfort", *International Noise 94*, Pacifico Yokohama, Japan, 29 – 31 August, 1994.

46. Ebe, K., "Effect of thickness on static and dynamic characteristics of polyurethane foams", *The UK informal Group Meeting on Human Response to Vibration*, ISVR, University of Southampton, Southampton, England, 17 – 19 September, 1997.

47. Smith, S.D., "the effect of military aircraft seat cushion on human vibration response", *The UK information Group Meeting on Human Response to Vibration*, The Institute of Naval Medicine, Alverstoke, Gosport, Hants, England, 19 – 21 September, 1994.

48. Rakheja, S., Mandapuram S., Dong R.G., "Energy Absorption of Seated Occupants Exposed to Horizontal Vibration and Role of Back Support Condition", *Industrial Health*, vol. 46(6) pp. 550 – 566, 2008.

49. Pranesh, A., Rakheja, S., Dumont, R., "Analysis of biodynamic responses of a seated body under vertical vibration", *Revue Internationale sur l'Ingénierie des Risques Industriels*, Vol.1, No.2, 2008.

50. Crosby, M., Karnopp, D.C., "The active damper – a new concept for shock and vibration control", *Shock Vibration Bulletin*, Part H, Washington D.C., 1973.

51. Guclu, R., "Active control of seat vibrations of a vehicle model using various suspension alternatives", *Turkish Journal of Engineering, Environment and Science*, 27: 361 – 373, 2003.

52. Hrovat, D., Margolis, D.L., Hubbard, M., "An approach toward the optimal semi-active suspension", *Journal of Dynamic Systems, Measurement and Control*, 110(3): 288 – 296, 1988.

53. Carlson, J.D., "The promise of controllable fluids", *Proceedings of Actuator 94*, AXON Technologic consult GmbH, pp. 266 – 270, 1994.

54. Carlson, J.D., Weiss, K.D., "A growing attraction to magnetic fluids", *Machine Design*, August, pp. 61 – 64, 1994.

55. Carlson, J.D., Catanzarite, D.M., St Clair, K.A., "Commercial magneto-rheological fluid devices", *Proceedings of the 5th International Conference on ER fluids, MR fluids, and Associated Technologies*, University of Sheffield, Sheffield, UK, 1995.

56. Thomas Lord Research Center, Lord Corporation, "Designing with MR fluids", Engineering Note, 1999.

57. Choi, S.-B., Lee, B.-K., Nam, M.-H., Cheong, C.-C., "Vibration control of a MR seat damper for commercial vehicles", *Smart Structures and Materials 2000, Proceedings of SPIE*, 3985: 491 – 496, 2000.

58. Chrzan, M.J., Carlson, J.D., "MR fluid spong devices and their use in vibration control of washing machines", *International Society of Optical Engineering (SPIE)*, 4331: 379 – 378, 2001.

59. Carlson, J.D., "Implementation of semi-active control using magneto-rheological fluids", *Mechatronic system, Proceedings Volume from IFAC Conference*, Germany, pp. 973 – 978, 2000.

60. Dyke, S.J., Spencer Jr. B.F., Sain, M.K., Carlson, J.D., "An experimental study of MR dampers for seismic protection", *smart Materials and Structures*, 7: 693 – 703, 1998.

61. Carlson, J.D., Catanzarite, D.M., St Clair, K.A., "commercial magneto-rheological fluid devices", *5th International Conference on ER, MR Suspensions Associated Technologies*, Sheffield, England, 1995.

62. Bouc, R., "Solution périodique de l'équation de la ferro-resonance avec hysteresis". *Comptes Rendus Académiques Hebdomadaires Séances*, A263, pp. 497 – 499, 1966.

63. Bouc, R., "Forced vibration of mechanical system with hysteresis", *Proceedings of the 4th Conference on Nonlinear Oscillation*, Prague, Czechoslovakia, 1967.

64. Shames, I.H., cozzarelli, F.A., "Elastic and Inelastic Stress Analysis", Taylor and Francis Inc. ISBN 1560326867, 1997.

65. Wang, E.R., Ma, X.Q., Rakheja S., Su, C.-Y., "A general model of a magneto-rheological controllable damper", *9th conference of sound and vibration*, Orlando, USA, 2002.

66. Stanway, R., Sproston, J.D., El-wahed, A.K., "Application of electrorheological fluids in vibration control: a survey", *Smart Materials and Structures*, 5(4): 464 – 482, 1996.

67. Spencer, B.F., Dyke, D.J., Sain, K.M., Carlson, J.D., "Phenomenological model of a magneto-rheological damper", *Journal of Engineering Mechanic*, ASCE, 123(3): 230 – 238, 1997.

68. Kamath, G.M., Wereley, N., "Nonlinear viscoelastic-plastic mechanism-based model of an electrorheological damper", *Journal of Guidance, Control and Dynamics*, 20(6): 1125 – 1132, 1997.

69. Choi, S.B., Lee, S.K.A., "Hysteresis model for the field-dependent damping force of a magneto-rheological damper", *Journal of Sound and Vibration*, 245(2): 375 – 383, 2001.

70. Phillips, R.W., "Engineering applications of fluids with a variable yield stress", Ph.D. Thesis, Mechanical Engineering, University Berkeley, California, USA, 1969.

71. Prager, W., "Introduction to Mechanics of Continua", Ginn and Company, New York, ISBN 0486438090, 1961.

72. Li, W.H., Yao, g.Z., Chen G., Yeo, S.H., Yap, F.F., "Testing and steady state modeling of a linear MR damper under sinusoidal loading", *Smart Materials and Structures*, 9: 95 – 102, 2000.

73. Pang, L., Kamath, G.M., Wereley, N.M., "dynamic characterization and analysis of magnetorheological damper behavior", *SPIE Conference on Passive Damping and Isolation*, 1 – 5 March, San Diego, California, 3327: 284 – 302, 1998.

74. Ma, X.Q., Wang, E.R., Rakheja, S., Su, C.Y., "Modeling hysteretic characteristics of MR-fluid damper and model validation", *41st IEEE Conference on Decision and Control*, December 10 – 13, Las Vegas, Nevada, USA, pp. 1675 – 1680, 2002.

75. Leva, A., Piroddi, L., "NARX-based technique for the modeling of magneto-rheological damping devices", *Smart Materials and Structures*, 11: 79 – 88, 2002.

76. Tao, G., Kokotovie, P.V., "Adaptive control of plants with unknown hysteresis", *IEEE Transactions on Automatic Control*, 40(2): 200 – 212, 1995.

77. Su, C.-Y., Stepanenko, Y., Svoboda, J., Leung, T.P., "Robust adaptive control of a class of nonlinear systems with unknown backlash-like hysteresis", *IEEE Transactions on Automatic Control*, 45(12): 2427 – 2431, 2000.

78. Khalil, H., "Nonlinear System", Prentice Hall, Inc., Upper Saddle River, NJ, ISBN 07458, 2002.

79. Grimm, E.A., Huff, G.J., Wilson, J.N., "An active seat suspension for off-road vehicles", *Symposium on computers, electronics and Control*, 3: 265, 1974.

80. Stein, G.J., Ballo, I., "Active vibration control system for the driver's seat for off-road vehicles", *vehicle System dynamics*, 20: 57 – 78, 1991.

81. Wu, J.D., Chen, R.J., "application of an active controller for reducing small-amplitude vertical vibration in a vehicle seat", *Journal of Sound and Vibration*, 274: 939 – 951, 2004.

82. Bouazara, M., Richard, M.J., Rakheja, S., "Safety and comfort analysis of a 3-D vehicle model with optimal non-linear active seat suspension", *Journal of Terramechanics*, 43: 97 – 118, 2006.

83. Choi, Y.T., Wereley, N.M., "Mitigation of biodynamic response to vibratory and blast-induced shock loads using magneto-rheological seat suspension", *2003 ASME International Mechanical Engineering Congress*, November, Washington D.C., USA, 2003.

84. Getpreecharsawas, J., Lyshevski, S.E., "Modeling and analysis of flexible beams with surface-mounted PZT actuators", *Proceedings of the 41st IEEE Conference on Decision and Control*, Las Vegas, Nevada, USA, 2002.

85. Gong, J.Q., Guo, L., Lee, H.S., Yao, B., "Modeling and cancellation of pivot nonlinearity in hard disk drive", *Proceedings of the American Control Conference*, Anchorage, AK, USA, 2002.

86. Tan, K.K., Lee, T.H., Zhou, H.X., "Micro-positioning of linear piezoelectric motors based on a learning nonlinear PID controller", *IEEE/ASME Transaction , Mechatron*, 6: 428 – 436, 2001.

87. Tan, X.B., Baras, J.S., "Modeling and control of a magnetoastrictive actuator", *Proceedings of the 41st IEEE Conference on Decision and Control*, Las Vegas, Nevada, USA, 2002.

88. Smith, R.C., Salapaka, M.V., Hatch, A., Smith, J., De, T., "Model development and inverse compensator design for high speed nonpositioning", *Proceedings of the 41st IEEE Conference on Decision and Control*, Las Vegas, USA, pp. 3652 – 3657, 2002.

89. Karnopp, D.C., Crosby, M.J., Harwood, R.A., "Vibration controlling semi-active generators", *Journal of Engineering for Industries*, 96(2): 619 – 626, 1974.

90. Wang, E.R., Ma, X.Q., Rakheja, S., Su, C. – Y., "Semi-active control of vehicle vibration with MR-dampers", *Proceedings of the 42nd IEEE Conference on Decision and Control*, 2003

91. Krasnicki, E.J., "The Experimental Performance of an "On-Off" active damper", *Shock and Vibration Bulletin*, 1981

92. Rakheja, S., Sankar, S., "Effectiveness of on-off damper in isolating dynamic systems", *Shock and Vibration Bulletin*, Vol. 57, pp. 146-156, 1986.

93. Alandy, J., Sankar, S., "A new conception semi-active vibration isolation" , Translations of the ASME, *Journal of Mechanisms, Transmissions and Automation in Design*, vol. 109, pp. 242-247, 1987.

94. Wu, X.M., Wang, J.Y., Sturk, M., Russell, D.L., "Simulation and experimental study of a semi-active suspension with an electrorheological damper", *International Journal of Modern Physics,* vol. B8, pp 2987-3003, 1994.

95. Decker, H., Schramn, W., "An Optimized Approach to Suspension Control", *SAE Paper*, no. 900661, 1990.

96. Wereley, N.M., Pang, L., Kamath, G.M., "Idealized hysteresis modeling of electro-rheological and magneto-rhelogical dampers", *Journal of Intelligent Material Systems and Structures*, 9: 642 – 649, 1998.

97. Mclellan, N., "On the development of a real-time embedded digital controller for heavy truck semi-active suspensions", M.Sc. Thesis, Virginia Polytechnic Institute and State University, Blacksburg, Virginia, USA, 1998.

98. Ballo, I., "Power requirement of active vibration control systems", *Vehicle System Dynamics*, 24(9): 683 – 694, 1995.

99. Carlson, J.D., Sproston, J.L., "Controllable fluids in 2000 – status of ER and MR fluid technology", *7th International Conference on New Actuator*, 19 – 21 June, Bermen, Germany, pp. 126 – 130, 2000.

100. Dixon, J.C., "The shock absorber handbook", SAE Internation Publisher, ISBN 0768000505, 1999.

101. Besinger, F.H., Cebon, D., Cole, D.J., "Damper models for heavy vehicle ride dynamics", *Vehicle System Dynamics*, 24(1): 35, 1995.

102. Dyke, S.J., Spencer Jr., B.F., Sain, M.D., Carlson, J.D., "Seismic response reduction using magnetorheological dampers", *Proceedings of IFAC 13th Triennial World Congress*, San Francisco, USA, pp. 145 – 150, 1996.

103. Wang, E.R., Ma, X.Q., Rakheja, S., Su, C.-Y., "Modeling hysterestic characteristics of a MR-fluid damper", *Proceedings of the Institute of Mechanical Engineers, Part D: Journal of Automobile Engineering*, 217: 537 – 550, 2002.

104. Wang, E.R., "Syntheses and analyses of semi-action control algorithms for a magneto-rheological damper for vehicle suspensions", Ph.D. Dissertation, Concordia University, Canada, 2005.

105. Wu, X., Rakheja, S., Boileau, P.-É., "Dynamic performance of suspension seats under vehicular vibration and shock excitations", *Transactions of SAE, Passenger Car Journal*, 108(6): 2398 – 2410, 1999.

106. Politis, H., Rakheja, S., Juras, D., Boileau, P.-É., Boutin, J., "Limits of application of human body dynamics in assessing vibration comfort of seats", *SAE 2003 World Congress and Exhibition, Session: Human Factors in Seating Comfort*, Detroit, MI, USA, SAE paper No. 2003 – 01 – 0953, 2003.

107.Coermann, R.R., "The mechanical impedance of the human body in sitting and standing position at low frequencies", *Human Factors*, pp. 227 – 253, 1962.

108.Gunston, T.P., "Two methods of simulating a suspension seat cushion", *Proceedings of the 37th UK Conference on Human Responses to Vibration*, Loughborough University, 18 – 20 September, 2002.

109.Patten, W.N., Pang, J., "Validation of a nonlinear automotive seat cushion vibration model", *Vehicle Systems Dynamics*, 30: 55 – 68, 1998.

110.Milliken, W.F., Milliken D.L., "Race Car Vehicle Dynamics", SAE, PA, USA, ISBN 1560915269, 1995.

111. Society of Automotive Engineer J1051, 1988

112.Choi, S.B., Nam, M.-H., Lee, B.-K., "Vibration Control of a MR Seat Damper for Commercial Vehicles", *Jounrnal of Intelligent Material Systems and Structures,* vol .11, 2000.

113.Park, C., Jeon, D., "Semiactive Vibration Control of a Smart Seat with an MR Fluid Damper Considering Its Time Delay", *Journal of Intelligent Material Systems and Structures*, vol. 13, 2002.

114.Nguyen, Q.-H., Choi, S.-B., "Optimal Design of MR Shock Absorber and Application to Vehicle Suspension", *Smart Materials and Structures,* vol. 11, pp. 11, 2009.

115.Han, Y.M., Nam, M.H., Han, S.S., Lee, H.G., Choi, S.B., "Vibration Control Evaluation of a Commercial Vehicle Featuring MR Seat Damper", *Journal of Intelligent Material Systems and Structures,* vol. 13, 2002.

116.Hanselmann, H., "Hardware-in-the-loop simulation as a standard approach for development, cost optimization and production test", *SAE paper* No. 930207, 1993.

117.Krohm, H., "Hardware-in-the-loop simulation for an electronic clutch management system, *SAE paper*, No. 950420, 1995.

118.Hwang, S., Heo, S., Kim, H., Lee, K., "Vehicle dynamic analysis and evaluation of continuously controlled semi-active suspension using hardware-in-the-loop simulation", *vehicle System Dynamics,* 27(5-6): 423-434, 1997.